

Evidence of a sharp multi-modal distribution in the relative position of the highest Riemann Siegel Z function analogue peaks of 5 periodic 1st degree L-functions and Davenport Heilbronn functions, along the critical line in the piecewise intervals

$$[N^2 \cdot \frac{2\pi}{5}, (N+1)^2 \cdot \frac{2\pi}{5}), N \in \mathbb{Z}.$$

John Martin

January 2, 2026

DRAFT Executive Summary

Analysis of the distribution of the extreme Riemann Siegel Z function peaks on the critical line ($s = 1/2 + I \cdot t$) for the two 5-periodic 1st degree Dirichlet L-functions $L(\chi_5(3, \cdot), s)$, $L(\chi_5(2, \cdot), s)$ and their Davenport-Heilbronn function counterparts $f_1(s)$ and $f_2(s)$ with the most extreme peak in each piecewise interval $[N^2 \cdot \frac{2\pi}{5}, (N+1)^2 \cdot \frac{2\pi}{5})$ obtained for $N=\{0,3000\}$ is investigated as a function of its transformed co-ordinate $\sqrt{\frac{t \cdot 5}{2\pi}} - \left\lfloor \sqrt{\frac{t \cdot 5}{2\pi}} \right\rfloor$ value into the rescaled interval [0,1) for each $N \bmod 5$ value. A multi-modal density distribution for the relative positions of the extreme peaks is observed which varies across the four 5-periodic functions. One possible explanation for the relative positions of the modes in the density distribution is presented arising from a heuristic approximation of the indefinite integral of the Riemann Siegel Z function analogues using the tapered finite Dirichlet Series sum. In particular, the indefinite integral approximation of finite Dirichlet Series sum exhibits piecewise behaviour on the critical line with clear mesoscale features that consistently have the steepest curvature in the interval $[N^2 \cdot \frac{2\pi}{5}, (N+1)^2 \cdot \frac{2\pi}{5})$. Of further interest, the indefinite integral approximation exhibits consistent growth of $(\frac{t \cdot 5}{2\pi})^{0.25}$ on the critical line for the investigated t intervals and there are mesoscale differences for the piecewise intervals between three different Dirichlet Series sum approaches to the indefinite integral approximation, the zeroth order Riemann Siegel formula Dirichlet Series sum, and the tapered Dirichlet Series sum results truncated at the first quiescent region ($\lfloor (\frac{t}{\pi})^{(d=1)} \cdot (N_C = 5) \rfloor$) and second quiescent region ($\lfloor \sqrt{(\frac{t}{2\pi})^{(d=1)} \cdot (N_C = 5)} \rfloor$) respectively for these first degree functions with conductor value $N_C = 5$.

Introduction

In this paper, the distribution of the extreme Riemann Siegel Z function analogue peaks on the critical line ($s = 1/2 + I \cdot t$) for the two 5-periodic 1st degree Dirichlet L-functions $L(\chi_5(3, \cdot), s)$, $L(\chi_5(2, \cdot), s)$ [1] and their Davenport-Heilbronn function counterparts $f_1(s)$ and $f_2(s)$ [2-4] within each piecewise interval $[N^2 \cdot \frac{2\pi}{5}, (N+1)^2 \cdot \frac{2\pi}{5})$ for $N=\{0,3000\}$ is investigated as a function of its transformed co-ordinate $\sqrt{\frac{t \cdot 5}{2\pi}} - \left\lfloor \sqrt{\frac{t \cdot 5}{2\pi}} \right\rfloor$ value.

Every largest Riemann Siegel Z function analogue peak of the (four) 5 periodic 1st degree L-functions and Davenport Heilbronn functions in each successive $[N^2 \cdot \frac{2\pi}{5}, (N+1)^2 \cdot \frac{2\pi}{5}), N \in \mathbb{Z}$ piecewise interval, for $N=\{0-3000\}$ was identified using a grid search. To save time with the grid search (i) at the lowest imaginary

co-ordinate values the standard (high precision Pari-gp [5]) L-functions were used, (ii) at moderately low imaginary co-ordinate values the tapered Dirichlet Series with truncation at the second quiescent region was employed and (iii) at the highest imaginary co-ordinate values a spectrally filtered finite Euler Product estimate truncated at the first quiescent was obtained followed by confirmation of the extreme peak height (typically accurate to <1e-2) using tapered Dirichlet Series with truncation at the first quiescent region.

It can be seen in figures 1 & 6 for $L(\chi_5(3, .), s)$, in figures 7 & 12 for $L(\chi_5(2, .), s)$, in figures 13 & 18 for $f_1(s)$ and in figures 19 & 24 for $f_2(s)$, that after binning the relative positions of the largest peaks in each piecewise interval by $N \bmod 5$ where $[N^2 \cdot \frac{2\pi}{5}, (N+1)^2 \cdot \frac{2\pi}{5}], N \in \mathbb{Z}$ into the interval $\sqrt{\frac{t \cdot 5}{2\pi}} - \left\lfloor \sqrt{\frac{t \cdot 5}{2\pi}} \right\rfloor$ that there is a higher density of large peaks at particular relative positions $N \bmod 5$ depending on each 5-periodic function. A heuristic approximation (currently only empirically valid) on the critical line for the indefinite integral of each 5-periodic function is presented proposing an explanation for the density behaviour of the extreme peak position within $[N^2 \cdot \frac{2\pi}{5}, (N+1)^2 \cdot \frac{2\pi}{5}]$.

The 5-periodic Davenport-Heilbronn functions and their underlying L function components

In L-function, Dirichlet series and Hurwitz Zeta function form the two 5-periodic Davenport-Heilbronn functions are of the form [2]

$$f_1(s) = \frac{1}{2\cos(\theta_1)} \left[e^{i\theta_1} L(\chi_5(2, .), s) + e^{-i\theta_1} L(\chi_5(3, .), s) \right] \quad (1)$$

$$= 1 + \frac{\tan(\theta_1)}{2^s} - \frac{\tan(\theta_1)}{3^s} - \frac{1}{4^s} + \frac{0}{5^s} + \dots, \Re(s) > 1 \quad (2)$$

$$= 5^{-s} \left(\zeta(s, \frac{1}{5}) + \tan(\theta_1) \cdot \zeta(s, \frac{2}{5}) - \tan(\theta_1) \cdot \zeta(s, \frac{3}{5}) - \zeta(s, \frac{4}{5}) \right) \quad (3)$$

where

$$\tan(\theta_1) = \frac{(\sqrt{10 - 2\sqrt{5}} - 2)}{(\sqrt{5} - 1)} \quad (4)$$

$$= 0.284079043840412296028291832393 \quad (5)$$

and

$$\theta_1 = 0.276787179448522625754266365045 \quad \text{radians} \quad (6)$$

The Davenport-Heilbronn $f_1(s)$ function has the functional equation

$$f_1(s) = 5^{(\frac{1}{2}-s)} 2(2\pi)^{(s-1)} \cos\left(\frac{\pi s}{2}\right) \Gamma(1-s) f_1(1-s) = \chi(f_1(s)) \cdot f_1(1-s) \quad (7)$$

The second linear combination of L-functions 5-periodic Davenport Heilbronn function example $f_2(s)$ [3,4] has the designation $\tau_-(s)$ [4] arising from $f_1(s)$ ($\tau_+(s)$) & $f_2(s)$ being the two coupled solutions of linear combinations of the $\chi_5(2, .)$ and $\chi_5(3, .)$ L-functions. The more recent work [4] as well as providing the functional equation, estimates the highest(lowest) $\Re(s)$ values for non-trivial zeroes of $f_2(s)$ are approximately bounded by $\Re(s)=2.37$ (-1.37).

Expressed in L-function, Dirichlet series and Hurwitz Zeta function form the $f_2(s)$ 5-periodic function is

$$f_2(s) = \frac{1}{2\cos(\theta_2)} \left[e^{i\theta_2} L(\chi_5(2, .), s) + e^{-i\theta_2} L(\chi_5(3, .), s) \right] \quad (8)$$

$$= 1 - \frac{\tan(\theta_2)}{2^s} + \frac{\tan(\theta_2)}{3^s} - \frac{1}{4^s} + \frac{0}{5^s} + \dots \quad , \Re(s) > 1 \quad (9)$$

$$= 5^{-s} \left(\zeta(s, \frac{1}{5}) - \tan(\theta_2) \cdot \zeta(s, \frac{2}{5}) + \tan(\theta_2) \cdot \zeta(s, \frac{3}{5}) - \zeta(s, \frac{4}{5}) \right) \quad (10)$$

where

$$\tan(\theta_2) = \frac{1}{0.284079043840412296028291832393} \quad (11)$$

and

$$\theta_2 = 1.2940091473463739934770553265951171821 \quad \text{radians} \quad (12)$$

The Davenport-Heilbronn $f_2(s)$ function has the functional equation [4]

$$f_2(s) = -5^{(\frac{1}{2}-s)} 2(2\pi)^{(s-1)} \cos\left(\frac{\pi s}{2}\right) \Gamma(1-s) f_2(1-s) = -\chi(f_1(s)) \cdot f_2(1-s) \quad (13)$$

where the multiplicative factor on the RHS of equations (13) and (7) differ by a factor of -1. ¹

The underlying L-functions of $f_1(s)$ and $f_2(s)$ are a dual-pair of L functions with 5-periodic Dirichlet Series form [1]

$$L(\chi_5(2, .), s) = 1 + \frac{I}{2^s} - \frac{I}{3^s} - \frac{1}{4^s} + \frac{0}{5^s} + \dots \quad , \Re(s) > 1 \quad (14)$$

$$L(\chi_5(3, .), s) = 1 - \frac{I}{2^s} + \frac{I}{3^s} - \frac{1}{4^s} + \frac{0}{5^s} + \dots \quad , \Re(s) > 1 \quad (15)$$

and the functional equations [1]

$$L(\chi_5(2, .), s) = \epsilon \cdot \chi(f_1(s)) L(\chi_5(3, .), 1-s) \quad (16)$$

$$L(\chi_5(3, .), s) = \bar{\epsilon} \cdot \chi(f_1(s)) L(\chi_5(2, .), 1-s) \quad (17)$$

where

$$\begin{aligned} \epsilon(L(\chi_5(2, .), s)) = & (0.85065080835203993218154049706301107225... \\ & + i * 0.52573111211913360602566908484787660729...) \end{aligned} \quad (18)$$

is the sign of the functional equation for the L-function $L(\chi_5(2, .), s)$ [1].

¹The earliest papers by Martin examining $f_2(s)$ incorrectly omitted the -1 factor in the RHS definition of $f_2(s)$. In those papers only $\text{abs}(f_2(s))$ was used in the Z function calculations that were performed so the omission does not change the numerical results. Recent papers by Martin examine the full lineshape behaviour of $f_2(s)$ and do use equation (13).

Zeroth order and tapered Riemann Siegel Z function formulae for $L(\chi_5(3,.), s)$, $L(\chi_5(2,.), s)$, $f_1(s)$ and $f_2(s)$ with truncation at the first and second quiescent regions

To efficiently conduct a grid search of 226,345,493 grid points in order to identify the most extreme Riemann Siegel Z function peak in 3001 contiguous intervals $N=\{0,3000\}$ from $0 \leq t \leq 11,317,275$ for each of the four functions $L(\chi_5(3,.), s)$, $L(\chi_5(2,.), s)$, $f_1(s)$ and $f_2(s)$

1. the intrinsic high precision Pari-GP [5] L-function calculations were only employed in the grid search for $0 \leq t \leq 608.3$ since their runtime and need for RAM rapidly increases as t increases,
2. for $608.3 < t < 5147.19$ 128 point tapered Dirichlet Series calculations with truncation at the second quiescent region ($N_2 = \lfloor \frac{t}{\pi} \cdot 5 \rfloor$) were employed delivering several decimal place accuracy sufficient to identify peak height differences and
3. for $t > 5147.19$ a combined approach of (i) 128 point tapered Dirichlet Series calculations adapting the zeroth order Riemann Siegel formula [6-8] for the four 5-periodic functions and (ii) fourier transform filtered finite Euler Product calculations both truncated at the first quiescent region ($N_1 = \lfloor \sqrt{\left(\frac{t}{2\pi} \cdot 5\right)} \rfloor$) [9] delivering 3+ decimal place accuracy sufficient to identify peak height differences (where extreme peaks $|Z| > 15$ for $t > 5147.19$ and growing) were conducted.

The intrinsic high precision Pari-GP [5] L-function calculations were also employed in figures 2-4, 8-10, 14-16, and 20-22 of this paper to calculate the true Riemann Siegel Z function on the critical line for the intervals $t=(40,126)$, $t=(5800,5820)$ and $t=(46,181)$ for the four functions $L(\chi_5(3,.), s)$, $L(\chi_5(2,.), s)$, $f_1(s)$ and $f_2(s)$. These figures then provide information on the accuracy of 128 point tapered Dirichlet Series calculations with truncation at the second quiescent region, 128 point tapered Dirichlet Series calculations with truncation at the first quiescent region and zeroth order Riemann Siegel formula calculations [6-8] but in a roundabout way. The comparison of the true Riemann Siegel Z function with approximations in figures 2-4, 8-10, 14-16, and 20-22 is not directly with the Dirichlet series based approximations described in the current section but the numerical total derivative $\frac{d}{ds}$ of heuristic approximations (described in later sections) of the indefinite integrals of the Dirichlet series described in the current section.

Tables 1-4 for the four functions respectively provide a comparison of the $|Z|$ for $N=\{2995-3000\}$ extreme peaks on the critical line via (i) 128 point tapered Dirichlet Series calculations with truncation at the first quiescent region and (ii) fourier transform filtered finite Euler Product based calculations also truncated at the first quiescent region.

Exact Riemann Siegel Z function analogues: Given the definitions in the previous section the Riemann-Siegel Z function analogues of the four functions $L(\chi_5(3,.), s)$, $L(\chi_5(2,.), s)$, $f_1(s)$ and $f_2(s)$ **on the critical line** $s = 1/2 + I \cdot t$ are

$$Z_{L53}(1/2 + I \cdot t) = \frac{1}{\sqrt{\epsilon}} e^{I \cdot \theta_{f1}(t)} L(\chi_5(3,.), 1/2 + I \cdot t) \equiv \frac{1}{\sqrt{\epsilon}} e^{I \cdot \theta_{f1}(t)} \bar{\epsilon} \chi(f_1(1/2 + I \cdot t)) L(\chi_5(2,.), 1/2 - I \cdot t) \quad (19)$$

$$Z_{L52}(1/2 + I \cdot t) = \frac{1}{\sqrt{\epsilon}} e^{I \cdot \theta_{f1}(t)} L(\chi_5(2,.), 1/2 + I \cdot t) \equiv \frac{1}{\sqrt{\epsilon}} e^{I \cdot \theta_{f1}(t)} \epsilon \chi(f_1(1/2 + I \cdot t)) L(\chi_5(3,.), 1/2 - I \cdot t) \quad (20)$$

$$Z_{f1}(1/2 + I \cdot t) = e^{I \cdot \theta_{f1}(t)} f_1(1/2 + I \cdot t) \equiv e^{I \cdot \theta_{f1}(t)} \chi(f_1(1/2 + I \cdot t)) f_1(1/2 - I \cdot t) \quad (21)$$

$$Z_{f2}(1/2 + I \cdot t) = e^{I \cdot \theta_{f2}(t)} f_2(1/2 + I \cdot t) \equiv e^{I \cdot \theta_{f2}(t)} \chi(f_2(1/2 + I \cdot t)) f_2(1/2 - I \cdot t) \quad (22)$$

where the Riemann-Siegel Theta function $\theta_{f1}(t)$ on the critical line is obtained from the definitions

$$\chi(f_1(1/2 + I \cdot t)) \equiv e^{-I \cdot 2\theta_{f1}(t)} \quad (23)$$

$$\text{real} \left[\log \left(\chi(f_1(1/2 + I \cdot t)) \right) \right] = 0 \quad (24)$$

$$\therefore \theta_{f1}(t) = -\frac{1}{2} \cdot \text{imag} \left[\log \left(\chi(f_1(1/2 + I \cdot t)) \right) \right] \quad (25)$$

and likewise for the Riemann-Siegel Theta function $\theta_{f2}(t)$ on the critical line

$$\chi(f_2(1/2 + I \cdot t)) \equiv e^{-I \cdot 2\theta_{f2}(t)} \quad (26)$$

$$\text{real} \left[\log \left(\chi(f_2(1/2 + I \cdot t)) \right) \right] = 0 \quad (27)$$

$$\therefore \theta_{f2}(t) = -\frac{1}{2} \cdot \text{imag} \left[\log \left(\chi(f_2(1/2 + I \cdot t)) \right) \right] \quad (28)$$

$$\equiv -\frac{1}{2} \cdot \text{imag} \left[\log \left(-\chi(f_1(1/2 + I \cdot t)) \right) \right] \quad (29)$$

Approximation I: Tapered Dirichlet Series approximations of the Riemann Siegel Z function analogues with truncation at the second quiescent region ($N_2 = \lfloor \frac{t}{\pi} \cdot 5 \rfloor$) for 1st degree L-functions with conductor value $N_C = 5$ and linear combinations of such L-functions are therefore given by

$$Z_{L53}(1/2 + I \cdot t)_{\lfloor \frac{t}{\pi} \cdot 5 \rfloor, \text{tapered}} \approx \frac{1}{\sqrt{\epsilon}} \cdot e^{I \cdot \theta_{f1}(t)} \cdot \left[\sum_{n=1}^{\lfloor \frac{t}{\pi} \cdot 5 \rfloor - p} \left(\frac{\chi_{L53}(n)}{n^{(1/2+I \cdot t)}} \right) + \sum_{i=(-p+1)}^p \frac{\frac{1}{2^{2p}} \left(2^{2p} - \sum_{k=1}^{i+p} \binom{2p}{2p-k} \right) \cdot \chi_{L53}(\lfloor \frac{t}{\pi} \cdot 5 \rfloor + i)}{(\lfloor \frac{t}{\pi} \cdot 5 \rfloor + i)^{(1/2+I \cdot t)}} \right], \quad t \rightarrow \infty \quad (30)$$

$$Z_{L52}(1/2 + I \cdot t)_{\lfloor \frac{t}{\pi} \cdot 5 \rfloor, \text{tapered}} \approx \frac{1}{\sqrt{\epsilon}} \cdot e^{I \cdot \theta_{f1}(t)} \cdot \left[\sum_{n=1}^{\lfloor \frac{t}{\pi} \cdot 5 \rfloor - p} \left(\frac{\chi_{L52}(n)}{n^{(1/2+I \cdot t)}} \right) + \sum_{i=(-p+1)}^p \frac{\frac{1}{2^{2p}} \left(2^{2p} - \sum_{k=1}^{i+p} \binom{2p}{2p-k} \right) \cdot \chi_{L52}(\lfloor \frac{t}{\pi} \cdot 5 \rfloor + i)}{(\lfloor \frac{t}{\pi} \cdot 5 \rfloor + i)^{(1/2+I \cdot t)}} \right], \quad t \rightarrow \infty \quad (31)$$

$$Z_{f1}(1/2 + I \cdot t)_{\lfloor \frac{t}{\pi} \cdot 5 \rfloor, \text{tapered}} \approx e^{I \cdot \theta_{f1}(t)} \cdot \left[\sum_{n=1}^{\lfloor \frac{t}{\pi} \cdot 5 \rfloor - p} \left(\frac{\chi_{f1}(n)}{n^{(1/2+I \cdot t)}} \right) + \sum_{i=(-p+1)}^p \frac{\frac{1}{2^{2p}} \left(2^{2p} - \sum_{k=1}^{i+p} \binom{2p}{2p-k} \right) \cdot \chi_{f1}(\lfloor \frac{t}{\pi} \cdot 5 \rfloor + i)}{(\lfloor \frac{t}{\pi} \cdot 5 \rfloor + i)^{(1/2+I \cdot t)}} \right], \quad t \rightarrow \infty \quad (32)$$

$$Z_{f2}(1/2 + I \cdot t)_{\lfloor \frac{t}{\pi} \cdot 5 \rfloor, \text{tapered}} \approx e^{I \cdot \theta_{f2}(t)} \cdot \left[\sum_{n=1}^{\left(\lfloor \frac{t}{\pi} \cdot 5 \rfloor - p\right)} \left(\frac{\chi_{f2}(n)}{n^{(1/2+I \cdot t)}} \right) \right. \\ \left. + \sum_{i=(-p+1)}^p \frac{\frac{1}{2^{2p}} \left(2^{2p} - \sum_{k=1}^{i+p} \binom{2p}{2p-k} \right) \cdot \chi_{f2}(\lfloor \frac{t}{\pi} \cdot 5 \rfloor + i)}{(\lfloor \frac{t}{\pi} \cdot 5 \rfloor + i)^{(1/2+I \cdot t)}} \right] , \quad t \rightarrow \infty \quad (33)$$

where (i) $\chi_{L53}(n)$, $\chi_{L52}(n)$, $\chi_{f1}(n)$ and $\chi_{f2}(n)$ are the 5-periodic dirichlet characters of the Dirichlet Series corresponding to the respective functions given in equations (15) (14), (2) and (9) respectively, (ii) $2p$ is the number of end taper weighted points present in the second term of the equations and (iii) $\binom{2p}{2p-k}$ are the binomial coefficients.

Away from the real axis ($t > 64 \cdot \frac{\pi}{5}$), a 128 point tapered Dirichlet Series sum using the second quiescent region provides an excellent approximation of its 5-periodic function analogue [11].

Alternative expressions to equations (32) and (33) can be obtained via explicit use of the constituent L-functions of $f_1(1/2 + I \cdot t)$ and $f_2(1/2 + I \cdot t)$ using equations (1) and (8) respectively. Such alternative expressions are important when attempting partial Euler product based approximations for $Z_{f1}(1/2 + I \cdot t)$ and $Z_{f2}(1/2 + I \cdot t)$.

Approximation II: Tapered Dirichlet Series approximations of the Riemann Siegel Z function analogues with truncation at the first quiescent region ($N_1 = \left\lfloor \sqrt{\left(\frac{t}{2\pi} \cdot 5\right)} \right\rfloor$) for 1st degree L-functions with conductor value $N_C = 5$ and linear combinations of such L-functions are obtained by co-opting the zeroth order Riemann Siegel formula term [6-8]

$$Z_{L53}(1/2 + I \cdot t)_{\left\lfloor \sqrt{\left(\frac{t}{2\pi} \cdot 5\right)} \right\rfloor, \text{tapered}} \approx \frac{1}{\sqrt{\epsilon}} \cdot e^{I \cdot \theta_{f1}(t)} \cdot \left[\sum_{n=1}^{\left(\left\lfloor \sqrt{\left(\frac{t}{2\pi} \cdot 5\right)} \right\rfloor - p\right)} \left(\frac{\chi_{L53}(n)}{n^{(1/2+I \cdot t)}} \right) \right. \\ \left. + \sum_{i=(-p+1)}^p \frac{\frac{1}{2^{2p}} \left(2^{2p} - \sum_{k=1}^{i+p} \binom{2p}{2p-k} \right) \cdot \chi_{L53}(\left\lfloor \sqrt{\left(\frac{t}{2\pi} \cdot 5\right)} \right\rfloor + i)}{(\left\lfloor \sqrt{\left(\frac{t}{2\pi} \cdot 5\right)} \right\rfloor + i)^{(1/2+I \cdot t)}} \right. \\ \left. + \bar{\epsilon} \cdot \chi(f_1(s)) \left\{ \sum_{n=1}^{\left(\left\lfloor \sqrt{\left(\frac{t}{2\pi} \cdot 5\right)} \right\rfloor - p\right)} \left(\frac{\chi_{L53}(n)}{n^{(1-(1/2+I \cdot t))}} \right) \right. \right. \\ \left. \left. + \sum_{i=(-p+1)}^p \frac{\frac{1}{2^{2p}} \left(2^{2p} - \sum_{k=1}^{i+p} \binom{2p}{2p-k} \right) \cdot \chi_{L53}(\left\lfloor \sqrt{\left(\frac{t}{2\pi} \cdot 5\right)} \right\rfloor + i)}{(\left\lfloor \sqrt{\left(\frac{t}{2\pi} \cdot 5\right)} \right\rfloor + i)^{(1-(1/2+I \cdot t))}} \right\} \right] , \quad t \rightarrow \infty \quad (34)$$

$$\begin{aligned}
Z_{L52}(1/2 + I \cdot t)_{\left[\sqrt{\left(\frac{t}{2\pi} \cdot 5\right)}\right], \text{tapered}} &\approx \frac{1}{\sqrt{\epsilon}} \cdot e^{I \cdot \theta_{f1}(t)} \cdot \left[\sum_{n=1}^{\left(\left[\sqrt{\left(\frac{t}{2\pi} \cdot 5\right)}\right] - p\right)} \left(\frac{\chi_{L52}(n)}{n^{(1/2+I \cdot t)}} \right) \right. \\
&+ \sum_{i=(-p+1)}^p \frac{\frac{1}{2^{2p}} \left(2^{2p} - \sum_{k=1}^{i+p} \binom{2p}{2p-k} \right) \cdot \chi_{L52}(\left[\sqrt{\left(\frac{t}{2\pi} \cdot 5\right)}\right] + i)}{(\left[\sqrt{\left(\frac{t}{2\pi} \cdot 5\right)}\right] + i)^{(1/2+I \cdot t)}} \\
&+ \epsilon \cdot \chi(f_1(s)) \left\{ \sum_{n=1}^{\left(\left[\sqrt{\left(\frac{t}{2\pi} \cdot 5\right)}\right] - p\right)} \left(\frac{\chi_{L52}(n)}{n^{(1-(1/2+I \cdot t))}} \right) \right. \\
&+ \left. \left. \sum_{i=(-p+1)}^p \frac{\frac{1}{2^{2p}} \left(2^{2p} - \sum_{k=1}^{i+p} \binom{2p}{2p-k} \right) \cdot \chi_{L52}(\left[\sqrt{\left(\frac{t}{2\pi} \cdot 5\right)}\right] + i)}{(\left[\sqrt{\left(\frac{t}{2\pi} \cdot 5\right)}\right] + i)^{(1-(1/2+I \cdot t))}} \right\} \right] , \quad t \rightarrow \infty
\end{aligned} \tag{35}$$

$$\begin{aligned}
Z_{f1}(1/2 + I \cdot t)_{\left[\sqrt{\left(\frac{t}{2\pi} \cdot 5\right)}\right], \text{tapered}} &\approx e^{I \cdot \theta_{f1}(t)} \cdot \left[\sum_{n=1}^{\left(\left[\sqrt{\left(\frac{t}{2\pi} \cdot 5\right)}\right] - p\right)} \left(\frac{\chi_{f1}(n)}{n^{(1/2+I \cdot t)}} \right) \right. \\
&+ \sum_{i=(-p+1)}^p \frac{\frac{1}{2^{2p}} \left(2^{2p} - \sum_{k=1}^{i+p} \binom{2p}{2p-k} \right) \cdot \chi_{f1}(\left[\sqrt{\left(\frac{t}{2\pi} \cdot 5\right)}\right] + i)}{(\left[\sqrt{\left(\frac{t}{2\pi} \cdot 5\right)}\right] + i)^{(1/2+I \cdot t)}} \\
&+ \chi(f_1(s)) \left\{ \sum_{n=1}^{\left(\left[\sqrt{\left(\frac{t}{2\pi} \cdot 5\right)}\right] - p\right)} \left(\frac{\chi_{f1}(n)}{n^{(1-(1/2+I \cdot t))}} \right) \right. \\
&+ \left. \left. \sum_{i=(-p+1)}^p \frac{\frac{1}{2^{2p}} \left(2^{2p} - \sum_{k=1}^{i+p} \binom{2p}{2p-k} \right) \cdot \chi_{f1}(\left[\sqrt{\left(\frac{t}{2\pi} \cdot 5\right)}\right] + i)}{(\left[\sqrt{\left(\frac{t}{2\pi} \cdot 5\right)}\right] + i)^{(1-(1/2+I \cdot t))}} \right\} \right] , \quad t \rightarrow \infty
\end{aligned} \tag{36}$$

$$\begin{aligned}
Z_{f2}(1/2 + I \cdot t)_{\left[\sqrt{\left(\frac{t}{2\pi} \cdot 5\right)}\right], \text{tapered}} &\approx e^{I \cdot \theta_{f2}(t)} \cdot \left[\sum_{n=1}^{\left(\left[\sqrt{\left(\frac{t}{2\pi} \cdot 5\right)}\right] - p\right)} \left(\frac{\chi_{f2}(n)}{n^{(1/2+I \cdot t)}} \right) \right. \\
&+ \sum_{i=(-p+1)}^p \frac{\frac{1}{2^{2p}} \left(2^{2p} - \sum_{k=1}^{i+p} \binom{2p}{2p-k} \right) \cdot \chi_{f2}(\left[\sqrt{\left(\frac{t}{2\pi} \cdot 5\right)}\right] + i)}{(\left[\sqrt{\left(\frac{t}{2\pi} \cdot 5\right)}\right] + i)^{(1/2+I \cdot t)}} \\
&+ \chi(f_2(s)) \left\{ \sum_{n=1}^{\left(\left[\sqrt{\left(\frac{t}{2\pi} \cdot 5\right)}\right] - p\right)} \left(\frac{\chi_{f2}(n)}{n^{(1-(1/2+I \cdot t))}} \right) \right. \\
&+ \left. \left. \sum_{i=(-p+1)}^p \frac{\frac{1}{2^{2p}} \left(2^{2p} - \sum_{k=1}^{i+p} \binom{2p}{2p-k} \right) \cdot \chi_{f2}(\left[\sqrt{\left(\frac{t}{2\pi} \cdot 5\right)}\right] + i)}{(\left[\sqrt{\left(\frac{t}{2\pi} \cdot 5\right)}\right] + i)^{(1-(1/2+I \cdot t))}} \right\} \right] , \quad t \rightarrow \infty
\end{aligned} \tag{37}$$

where (i) $\chi_{L53}(n)$, $\chi_{L52}(n)$, $\chi_{f1}(n)$ and $\chi_{f2}(n)$ are the 5-periodic dirichlet characters of the Dirichlet Series corresponding to the respective functions given in equations (15) (14), (2) and (9) respectively, (ii) $2p$ is the number of end taper weighted points present in the second term of the equations and (iii) $\binom{2p}{2p-k}$ are the binomial coefficients.

Further away from the real axis ($t > 64^2 \cdot \frac{2\pi}{5}$), a 128 point tapered Dirichlet Series sum using the first quiescent region provides a good and improving approximation of its 5-periodic function analogue [11].

Alternative expressions to equations (32) and (33) can be obtained via explicit use of the constituent L-functions of $f_1(1/2 + I \cdot t)$ and $f_2(1/2 + I \cdot t)$ using equations (1) and (8) respectively. Such alternative expressions are important when attempting partial Euler product based approximations for $Z_{f1}(1/2 + I \cdot t)$ and $Z_{f2}(1/2 + I \cdot t)$.

Approximation III: Zeroth order Riemann Siegel formula [6-8] approximations of the Riemann Siegel Z function analogues for 1st degree L-functions with conductor value $N_C = 5$ and linear combinations of such L-functions

$$Z_{L53}(1/2 + I \cdot t)_{\text{RSzeroth}} \approx \frac{e^{I \cdot \theta_{f1}(t)}}{\sqrt{\epsilon}} \cdot \left[\sum_{n=1}^{\left(\left\lfloor \sqrt{\left(\frac{t}{2\pi} \cdot 5\right)} \right\rfloor\right)} \left(\frac{\chi_{L53}(n)}{n^{(1/2+I \cdot t)}} \right) + \bar{\epsilon} \cdot \chi(f_1(s)) \cdot \sum_{n=1}^{\left(\left\lfloor \sqrt{\left(\frac{t}{2\pi} \cdot 5\right)} \right\rfloor\right)} \left(\frac{\chi_{L52}(n)}{n^{(1-(1/2+I \cdot t))}} \right) \right], t \rightarrow \infty \quad (38)$$

$$Z_{L52}(1/2 + I \cdot t)_{\text{RSzeroth}} \approx \frac{e^{I \cdot \theta_{f1}(t)}}{\sqrt{\epsilon}} \cdot \left[\sum_{n=1}^{\left(\left\lfloor \sqrt{\left(\frac{t}{2\pi} \cdot 5\right)} \right\rfloor\right)} \left(\frac{\chi_{L52}(n)}{n^{(1/2+I \cdot t)}} \right) + \epsilon \cdot \chi(f_1(s)) \cdot \sum_{n=1}^{\left(\left\lfloor \sqrt{\left(\frac{t}{2\pi} \cdot 5\right)} \right\rfloor\right)} \left(\frac{\chi_{L53}(n)}{n^{(1-(1/2+I \cdot t))}} \right) \right], t \rightarrow \infty \quad (39)$$

$$Z_{f1}(1/2 + I \cdot t)_{\text{RSzeroth}} \approx e^{I \cdot \theta_{f1}(t)} \cdot \left[\sum_{n=1}^{\left(\left\lfloor \sqrt{\left(\frac{t}{2\pi} \cdot 5\right)} \right\rfloor\right)} \left(\frac{\chi_{f1}(n)}{n^{(1/2+I \cdot t)}} \right) + \chi(f_1(s)) \cdot \sum_{n=1}^{\left(\left\lfloor \sqrt{\left(\frac{t}{2\pi} \cdot 5\right)} \right\rfloor\right)} \left(\frac{\chi_{f1}(n)}{n^{(1-(1/2+I \cdot t))}} \right) \right], t \rightarrow \infty \quad (40)$$

$$Z_{f2}(1/2 + I \cdot t)_{\text{RSzeroth}} \approx e^{I \cdot \theta_{f2}(t)} \cdot \left[\sum_{n=1}^{\left(\left\lfloor \sqrt{\left(\frac{t}{2\pi} \cdot 5\right)} \right\rfloor\right)} \left(\frac{\chi_{f2}(n)}{n^{(1/2+I \cdot t)}} \right) + \chi(f_2(s)) \cdot \sum_{n=1}^{\left(\left\lfloor \sqrt{\left(\frac{t}{2\pi} \cdot 5\right)} \right\rfloor\right)} \left(\frac{\chi_{f2}(n)}{n^{(1-(1/2+I \cdot t))}} \right) \right], t \rightarrow \infty \quad (41)$$

Further away from the real axis this sharply truncated Dirichlet Series sum provides an increasingly better approximation of its 5-periodic function analogue but exhibits residual nuisance discontinuities at $\left\lfloor \sqrt{\left(\frac{t}{2\pi} \cdot 5\right)} \right\rfloor \in \mathbb{Z}$.

Approximation IV: Spectrally filtered partial Euler Product based approximations of the Riemann Siegel Z function analogues of the four functions were deployed (in order to best scale up the grid search calculations at the highest t values) with cross-checking confirmation of the final identified extreme peak height within each piecewise interval using equations (34-37) of approximation II for benchmarking as appropriate.

In this method, the partial Euler Product based analogue of the zeroth order Riemann Siegel formula terms is calculated and then subject to spectral filtering, some imputation (see next sub-section and [9]) and the inverse fourier transform is returned. This spectral cleaning of the partial Euler product using truncation at the first quiescent region greatly improves the partial Euler product estimate [9]. On the critical line due to its higher symmetry only one component of the zeroth order Riemann Siegel formula using partial Euler Products needs to be calculated and conjugate phase imputation is then used for the other half of the fourier components.

$$Z_{L53}(1/2 + I \cdot t)_{\text{EPfiltered}} \approx \frac{1}{\sqrt{\epsilon}} \cdot e^{I \cdot \theta_{f1}(1/2+I \cdot t)} \underbrace{\left[\prod_{p=2}^{\left\lfloor \beta \cdot \sqrt{\left(\frac{t}{2\pi}\right) \cdot 5} \right\rfloor} \frac{1}{\left(1 - \frac{\chi_{L53}(p)}{p^{(1/2+I \cdot t)}}\right)} + \bar{\epsilon}\chi(f_1(s)) \prod_{p=2}^{\left\lfloor \beta \cdot \sqrt{\left(\frac{t}{2\pi}\right) \cdot 5} \right\rfloor} \frac{1}{\left(1 - \frac{\chi_{L52}(p)}{p^{(1-(1/2+I \cdot t))}}\right)} \right]}_{\text{Individual terms spectrally filtered, then combined and inverse fourier transform returned.}} \quad (42)$$

$$= \underbrace{EP_{RS1,L53}(1/2 + I \cdot t, \beta) + EP_{RS2,L53}(1/2 + I \cdot t, \beta)}_{\text{Individual terms spectrally filtered, then combined and inverse fourier transform returned.}} \quad (43)$$

$$= \underbrace{EP_{RS1,L53}(1/2 + I \cdot t, \beta)}_{\text{Spectrally filtered, conjugate phase reflection imputation and inverse fourier transform returned.}} \quad \text{a reduction in required calculations} \quad (44)$$

$$Z_{L52}(1/2 + I \cdot t)_{\text{EPfiltered}} \approx \frac{1}{\sqrt{\epsilon}} \cdot e^{I \cdot \theta_{f1}(1/2+I \cdot t)} \underbrace{\left[\prod_{p=2}^{\left\lfloor \beta \cdot \sqrt{\left(\frac{t}{2\pi}\right) \cdot 5} \right\rfloor} \frac{1}{\left(1 - \frac{\chi_{L52}(p)}{p^{(1/2+I \cdot t)}}\right)} + \epsilon\chi(f_1(s)) \prod_{p=2}^{\left\lfloor \beta \cdot \sqrt{\left(\frac{t}{2\pi}\right) \cdot 5} \right\rfloor} \frac{1}{\left(1 - \frac{\chi_{L53}(p)}{p^{(1-(1/2+I \cdot t))}}\right)} \right]}_{\text{Individual terms spectrally filtered, then combined and inverse fourier transform returned.}} \quad (45)$$

$$= \underbrace{EP_{RS1,L52}(1/2 + I \cdot t, \beta) + EP_{RS2,L52}(1/2 + I \cdot t, \beta)}_{\text{Individual terms spectrally filtered, then combined and inverse fourier transform returned.}} \quad (46)$$

$$= \underbrace{EP_{RS1,L52}(1/2 + I \cdot t, \beta)}_{\text{Spectrally filtered, conjugate phase reflection imputation and inverse fourier transform returned.}} \quad \text{a reduction in required calculations} \quad (47)$$

using equation (1)

$$\begin{aligned}
& Z_{f1}(1/2 + I \cdot t)_{\text{EPfiltered}} \\
& \approx e^{I \cdot \theta_{f1}(1/2+I \cdot t)} \cdot \frac{e^{i\theta_1}}{2\cos(\theta_1)} \left[\prod_{p=2}^{\lfloor \beta \cdot \sqrt{\left(\frac{t}{2\pi}\right) \cdot 5} \rfloor} \frac{1}{\left(1 - \frac{\chi_{L52}(p)}{p^{(1/2+I \cdot t)}}\right)} + \epsilon \chi(f_1(s)) \prod_{p=2}^{\lfloor \beta \cdot \sqrt{\left(\frac{t}{2\pi}\right) \cdot 5} \rfloor} \frac{1}{\left(1 - \frac{\chi_{L53}(p)}{p^{(1-(1/2+I \cdot t))}}\right)} \right] \\
& + e^{I \cdot \theta_{f1}(1/2+I \cdot t)} \cdot \frac{e^{-i\theta_1}}{2\cos(\theta_1)} \left[\prod_{p=2}^{\lfloor \beta \cdot \sqrt{\left(\frac{t}{2\pi}\right) \cdot 5} \rfloor} \frac{1}{\left(1 - \frac{\chi_{L53}(p)}{p^{(1/2+I \cdot t)}}\right)} + \bar{\epsilon} \chi(f_1(s)) \prod_{p=2}^{\lfloor \beta \cdot \sqrt{\left(\frac{t}{2\pi}\right) \cdot 5} \rfloor} \frac{1}{\left(1 - \frac{\chi_{L52}(p)}{p^{(1-(1/2+I \cdot t))}}\right)} \right]
\end{aligned}$$

Four individual terms spectrally filtered, then combined and inverse fourier transform returned.

(48)

re-arranging terms into different pairings

$$\begin{aligned}
& \approx e^{I \cdot \theta_{f1}(1/2+I \cdot t)} \cdot \left[\frac{e^{i\theta_1}}{2\cos(\theta_1)} \prod_{p=2}^{\lfloor \beta \cdot \sqrt{\left(\frac{t}{2\pi}\right) \cdot 5} \rfloor} \frac{1}{\left(1 - \frac{\chi_{L52}(p)}{p^{(1/2+I \cdot t)}}\right)} + \frac{e^{-i\theta_1}}{2\cos(\theta_1)} \prod_{p=2}^{\lfloor \beta \cdot \sqrt{\left(\frac{t}{2\pi}\right) \cdot 5} \rfloor} \frac{1}{\left(1 - \frac{\chi_{L53}(p)}{p^{(1/2+I \cdot t)}}\right)} \right] \\
& + e^{I \cdot \theta_{f1}(1/2+I \cdot t)} \cdot \chi(f_1(s)) \cdot \left[\frac{e^{i\theta_1} \cdot \epsilon}{2\cos(\theta_1)} \prod_{p=2}^{\lfloor \beta \cdot \sqrt{\left(\frac{t}{2\pi}\right) \cdot 5} \rfloor} \frac{1}{\left(1 - \frac{\chi_{L53}(p)}{p^{(1-(1/2+I \cdot t))}}\right)} + \frac{e^{-i\theta_1} \cdot \bar{\epsilon}}{2\cos(\theta_1)} \prod_{p=2}^{\lfloor \beta \cdot \sqrt{\left(\frac{t}{2\pi}\right) \cdot 5} \rfloor} \frac{1}{\left(1 - \frac{\chi_{L52}(p)}{p^{(1-(1/2+I \cdot t))}}\right)} \right]
\end{aligned}$$

newly paired terms spectrally filtered, then combined and inverse fourier transform returned.

(49)

$$= \underbrace{EP_{RS1,f1}(1/2 + I \cdot t, \beta) + EP_{RS2,f1}(1/2 + I \cdot t, \beta)}_{\text{Spectrally filtered, then combined and inverse fourier transform returned.}} \quad (50)$$

Spectrally filtered, conjugate phase reflection imputation and inverse fourier transform returned.

$$= \underbrace{EP_{RS1,f1}(1/2 + I \cdot t, \beta)}_{\text{Spectrally filtered, conjugate phase reflection imputation and inverse fourier transform returned.}} \quad \text{a reduction in required calculations}$$

(51)

using equation (8)

$$\begin{aligned}
& Z_{f2}(1/2 + I \cdot t)_{\text{EPfiltered}} \\
& \approx e^{I \cdot \theta_{f2}(1/2+I \cdot t)} \cdot \frac{e^{i\theta_2}}{2\cos(\theta_2)} \left[\prod_{p=2}^{\lfloor \beta \cdot \sqrt{\left(\frac{t}{2\pi}\right) \cdot 5} \rfloor} \frac{1}{\left(1 - \frac{\chi_{L52}(p)}{p^{(1/2+I \cdot t)}}\right)} + \epsilon \chi(f_1(s)) \prod_{p=2}^{\lfloor \beta \cdot \sqrt{\left(\frac{t}{2\pi}\right) \cdot 5} \rfloor} \frac{1}{\left(1 - \frac{\chi_{L53}(p)}{p^{(1-(1/2+I \cdot t))}}\right)} \right] \\
& + e^{I \cdot \theta_{f2}(1/2+I \cdot t)} \cdot \frac{e^{-i\theta_2}}{2\cos(\theta_2)} \left[\prod_{p=2}^{\lfloor \beta \cdot \sqrt{\left(\frac{t}{2\pi}\right) \cdot 5} \rfloor} \frac{1}{\left(1 - \frac{\chi_{L53}(p)}{p^{(1/2+I \cdot t)}}\right)} + \bar{\epsilon} \chi(f_1(s)) \prod_{p=2}^{\lfloor \beta \cdot \sqrt{\left(\frac{t}{2\pi}\right) \cdot 5} \rfloor} \frac{1}{\left(1 - \frac{\chi_{L52}(p)}{p^{(1-(1/2+I \cdot t))}}\right)} \right]
\end{aligned}$$

Four individual terms spectrally filtered, then combined and inverse fourier transform returned.

(52)

re-arranging terms into different pairings

$$\begin{aligned}
& \approx e^{I \cdot \theta_{f2}(1/2+I \cdot t)} \cdot \left[\frac{e^{i\theta_2}}{2\cos(\theta_2)} \prod_{p=2}^{\lfloor \beta \cdot \sqrt{\left(\frac{t}{2\pi}\right) \cdot 5} \rfloor} \frac{1}{\left(1 - \frac{\chi_{L52}(p)}{p^{(1/2+I \cdot t)}}\right)} + \frac{e^{-i\theta_2}}{2\cos(\theta_2)} \prod_{p=2}^{\lfloor \beta \cdot \sqrt{\left(\frac{t}{2\pi}\right) \cdot 5} \rfloor} \frac{1}{\left(1 - \frac{\chi_{L53}(p)}{p^{(1/2+I \cdot t)}}\right)} \right] \\
& + e^{I \cdot \theta_{f2}(1/2+I \cdot t)} \cdot \chi(f_1(s)) \cdot \left[\frac{e^{i\theta_2} \cdot \epsilon}{2\cos(\theta_2)} \prod_{p=2}^{\lfloor \beta \cdot \sqrt{\left(\frac{t}{2\pi}\right) \cdot 5} \rfloor} \frac{1}{\left(1 - \frac{\chi_{L53}(p)}{p^{(1-(1/2+I \cdot t))}}\right)} + \frac{e^{-i\theta_2} \cdot \bar{\epsilon}}{2\cos(\theta_2)} \prod_{p=2}^{\lfloor \beta \cdot \sqrt{\left(\frac{t}{2\pi}\right) \cdot 5} \rfloor} \frac{1}{\left(1 - \frac{\chi_{L52}(p)}{p^{(1-(1/2+I \cdot t))}}\right)} \right]
\end{aligned}$$

newly paired terms spectrally filtered, then combined and inverse fourier transform returned.

(53)

$$= \underbrace{EP_{RS1,f2}(1/2 + I \cdot t, \beta) + EP_{RS2,f2}(1/2 + I \cdot t, \beta)}_{\text{Spectrally filtered, then combined and inverse fourier transform returned.}}$$

(54)

$$= \underbrace{EP_{RS1,f2}(1/2 + I \cdot t, \beta)}_{\text{Spectrally filtered, conjugate phase reflection imputation and inverse fourier transform returned.}}$$

(55)

where

1. $\beta \sim 1.25 > 1$ is a hyperparameter found to improve approximation IV's accuracy [9],
2. for the purposes of this paper, i.e., extreme peak identification, only a single fourier analysis run is needed over a given (sufficiently long) interval and grid point spacing since 3+ decimal place accuracy is sufficient,
3. however, examination of closely spaced zeroes (which is **not** the purpose of this paper) requires 7+ decimal place accuracy and including the further steps of (i) averaging of fourier analyses from different spectral sample lengths and (ii) interpolation between grid points has been found to remove additional spectral leakage allowing further accuracy gains [9].

Some empirical details on an implementation of approximation IV using Pari-GP language

In approximation IV which has the quickest speed as $t \rightarrow \infty$ since only the primes are used, the fourier transform filtered partial Euler Product calculation was also completely calculated using Pari-GP code by using its intrinsic FFT function. An extract of necessary parts of the Pari-GP code to perform FFT analysis and spectral filtering of a vector of 32768 points (spaced by $\Delta t = 0.05$) with respect to $L(\chi_5(3, .), s)$ calculations is shown below.

```
{
\\need to load FFT library
\\FFT analysis example that I adapted was first described in
\\https://pari.math.u-bordeaux.fr/archives/pari-users-1808/msg00023.html

allocatemem(64000000)\\ need enough memory to hold 32k Vector for FFT
install(FFTinit,Lp);
install(FFT,GG);

\\\chi_{53}
L52 = lfuncreate(Mod(2,5)); \\ chi5(2,.) \\high precision Pari-GP L-function
lfunan(L52,15);\\ coefs of series
L53 = lfuncreate(Mod(3,5)); \\ chi5(3,.) \\high precision Pari-GP L-function
lfunan(M53,15);\\ coefs of series
Nc=5;\\Conductor of L53
\\ functional equation multiplier
fun_rat(res,t,Nc)=Nch^((res+I*t)/2)*Pi^(-(res+I*t+1)/2)*gamma((res+I*t+1)/2);
\\sign of the functional equation for L52
extra=(lfun(L52,0.5+I*6.18)/lfun(M53,1-(0.5+I*6.18)))/(fun_rat(1-0.5,0-6.18,Nc)/fun_rat(0.5,6.18,Nc));

\\exponent of the Riemann Siegel theta function for L53
logfun_chi5s_f1(res,t)=log(5)*(-(res+I*t)+1/2)+log(Pi)*((res+I*t)-1/2)+lngamma((2-(res+I*t))/2)-lngamma((1+(res+I*t))/2);
\\vthetaf1 is purely imaginary on the critical line and substitutes directly
\\for the product I\cdot\dot{\theta}(t)
\\where \theta(t) is the Riemann Siegel Theta function on the critical line
vthetaf1(z)=-1/2*logfun_chi5s_f1(real(z),imag(z))

\\5-periodic Dirichlet series characters for L53
coef53=[1,-I,I,-1,0];
fun_coeff53(p)=if(p%5==0,0,coef53[p%5]);

funcEP7chi53(z,N)={
nlim=floor(1.25*sqrt(abs(imag(z))/2/Pi*5));
ntot=nlim+N;
prodeuler(p=2,ntot,1/(1-fun_coeff53(p)/p^z));
};

\\line breaks inserted below in this printed version of double forloop
\\line breaks need to be removed to successfully run in a Pari-GP session
forstep(n=65,3000,1,[adj53=1/sqrt(conj(extra));nold=n-1;peak=0;
t0=^2*Pi/5-8192*0.1;t1=(n+1)^2*2*Pi/5;
intervals=ceil((2*n+1)*2*Pi/5/32768/.05);
for(j=1,intervals,[t0=t0+(+16384)*.1;if(t0+16384*.05>=t1,t0=-.0001+(t1-(16384*.05)));
y1=listcreate(10);forstep(i=t0-819.15,t0+819.2,.05,
[est=(funcEP7chi53((0.5+I*i),0))*adj53*exp((vthetaf1(0.5+I*i))),listput(y1,est)]);
length(y1);k=15;N=2^k;w=FFTinit(k);vhat=FFT(Vec(y1),w);
fh=(concat(real(vhat[1]),concat(concat(vecrev(vecrev(vhat,"16386..32768"))),
concat(real(vhat[16385]),vecrev(vhat,"16386..32768"))));
w=FFTinit(k);vinvhat=conj(FFT(conj(Vec(fh)),w))/N;Z_max=vecmax(abs(vinvhat),&v);elem_max=v;
max_t=(t0+(v-16384)*.05);Q1_max=sqrt(max_t/2/Pi*5);nval=floor(Q1_max);
seg_est=real(dirichRS_L53sum128(0.5+I*max_t)*adj53*exp((vthetaf1(0.5+I*max_t))));
print(max_t,",",sqrt(max_t/2/Pi*5),"Z_max,",seg_est);
if(Z_max>peak && nval==n,[peak=Z_max,peak_pos=max_t,peak_Q1=Q1_max,peak_nval=nval,Q1_est=seg_est]);
print(j,",",peak_pos,",",peak_Q1,",",peak_Q1-peak_nval,",",peak)];
print("grid search in one interval completed");
write("filtered_L53EP_est.csv",peak_pos,",",peak_Q1,",",peak_Q1-peak_nval,",",peak,",",Q1_est)]);
}
```

The displayed forstep function has extra line breaks inserted for easier reading but such line breaks need to be removed in order for the forstep function to execute. In practice the forstep function used larger steps (e.g. 14) as parallel calculations were conducted across two laptops (MSI GT72 and MacBook Pro) where each laptop had multiple Pari-GP sessions operating simultaneously. In contrast to [9] where the objective was to identify positions of zeroes of the function of interest, in this paper the height (and position) of extreme

peaks is of interest. An observed property so far of L-function and Davenport Heilbronn function extreme peaks is that the extreme peaks exhibit wide FWHM compared to small peaks and closely spaced zeroes. This observed property helps justify the use of $\Delta t = 0.05$ for the grid search and compared to [9] averaging of FFT analysis from different spectral sample lengths is not necessary for the purpose of estimating extreme peak height, i.e. only a single FFT run suffices per FFT spectrum sample. However, as a check to ensure the extreme peak height calculated by the fourier transform filtered partial Euler Product was sufficiently accurate a 128 point tapered Dirichlet Series calculation i.e, approximation II, using the zeroth order Riemann Siegel formula [6-8] was also produced for the extreme peak as a cross-check. Since the FFT analysis was of fixed length interval $t=(t_0-819.2, t_0+819.2)$ with 32768 data points (i) as t_0 increases the number of FFTs conducted per $[N, N+1]$ interval gradually increases and (ii) for the final FFT spectrum sample within an interval $[N, N+1]$ $t = ((N+1)^2 \cdot \frac{2\pi}{5} - 1638.4 - 0.0001, (N+1)^2 \cdot \frac{2\pi}{5} - .0001)$ so some t value regions were present in both the second last and final FFT analysis of an interval which is okay (but a slight inefficiency) given the purpose is to find the most extreme peak within an interval.

Of critical interest compared to the r language [10] fourier transform calculations in [9] the informative fourier component results under Pari-GP calculation of equations (42-44) were found to be elements 1 and $(M/2+1, \dots M)$ i.e, the $(-, 0]$ frequency components of the Riemann Siegel Z function using the partial Euler Product analogue of the zeroth order Riemann Siegel formula. In contrast, using the r language for fourier analysis in [9] it was identified that the $[0, +)$ frequency components elements $1, \dots, M/2$ should be retained and used for conjugate phase reflection.

On the critical line this conjugate phase reflection step allows a calculation efficiency gain and hence the raw unfiltered input estimate in the code above “`funcEP7chi53((0.5+Ii),0))adj53exp((vthetaf1(0.5+Ii)))`” arises **only** from the first term in (the zeroth order Riemann Siegel formula analogue using partial Euler Products) equation (42)

$$EP_{RS1,L53}(1/2 + I \cdot t, \beta) = \frac{1}{\sqrt{\epsilon}} \cdot e^{I \cdot \theta_{f1}(1/2 + I \cdot t)} \prod_{p=2}^{\left\lfloor \beta \cdot \sqrt{\left(\frac{t}{2\pi}\right)^d \cdot 5} \right\rfloor} \frac{1}{\left(1 - \frac{\chi_{L53}(p)}{p^{(1/2 + I \cdot t)}}\right)} \quad (56)$$

That is more generically, given the following critical line approximation of a partial Euler product based approximation for the Riemann Siegel Z function for the case of a dirichlet character L-function with critical line $s = 1/2 + I \cdot t$

$$\begin{aligned} & \frac{1}{\sqrt{\epsilon}} \cdot e^{I \cdot \theta_L(1/2 + I \cdot t)} \cdot L(\chi, s) \\ & \approx \frac{1}{\sqrt{\epsilon}} \cdot e^{I \cdot \theta_L(1/2 + I \cdot t)} \left[\prod_{p=2}^{\left\lfloor \beta \cdot \sqrt{\left(\frac{t}{2\pi}\right)^d \cdot N_C} \right\rfloor} \frac{1}{\left(1 - \frac{\chi(p)}{p^{(1/2 + I \cdot t)}}\right)} + \epsilon \chi(L(\chi, s)) \prod_{p=2}^{\left\lfloor \beta \cdot \sqrt{\left(\frac{t}{2\pi}\right)^d \cdot N_C} \right\rfloor} \frac{1}{\left(1 - \frac{\chi(p)}{p^{(1-(1/2 + I \cdot t))}}\right)} \right] \end{aligned} \quad (57)$$

$$= EP_{RS1,L}(1/2 + I \cdot t, \beta) + EP_{RS2,L}(1/2 + I \cdot t, \beta) \quad (58)$$

where for the given L-function ϵ is the sign of the functional equation, $\chi(L(\chi, s))$ is the functional equation multiplier, $\theta_L(1/2 + I \cdot t)$ is the Riemann Siegel Theta function on the critical line, d is the degreee, N_C is the conductor value, $\chi(p)$ are the dirichlet characters of the underlying Dirichlet Series and $\beta \gtrsim 1$ is a hyperparameter (to improve the estimate when fourier analysis filtering is also conducted).

Importantly this Riemann Siegel Z function approximation is greatly improved by spectral filtering using fourier analysis whereby on the critical line through conjugate phase reflection of fourier components only

one component $EP_{RS1,L}(1/2 + I \cdot t, \beta)$ or $EP_{RS2,L}(1/2 + I \cdot t, \beta)$ is necessary to obtain good estimates as $t \rightarrow \infty$ (see in particular figures 11, 13, 15, 17, 19 and 21 of [9]).

For example, only the first term need be calculated (on the critical line)

$$EP_{RS1,L}(1/2 + I \cdot t, \beta) = \frac{1}{\sqrt{\epsilon}} \cdot e^{I \cdot \theta_L(1/2+I \cdot t)} \prod_{p=2}^{\left\lfloor \beta \cdot \sqrt{\left(\frac{t}{2\pi}\right)^d \cdot N_C} \right\rfloor} \frac{1}{\left(1 - \frac{\chi(p)}{p^{(1/2+I \cdot t)}}\right)} \quad (59)$$

which is therefore a shortcut speed improvement since only one component of the Riemann Siegel formula analogue (using euler products) needs to be calculated (on the critical line) [9].

To quality assure the partial Euler Product based approximation the extreme peak height was also calculated via approximation II. In the provided code snippet

“seg_est=real(dirichRS_L53sum128(0.5+Imax_t)adj53exp((vthetaf1(0.5+Imax_t))))” implements equation (34) for 128 point end tapering of $L(\chi_5(3, .), s)$. In practice, there is good agreement between approximation II and approximation IV estimates of the extreme peak height (of the order of 3 decimal places, see Table 1 below) with the hyperparameters of spectrum length 32768 and grid spacing $\Delta t = 0.05$ and indeed this comparison was the evidence driving the decision to use $\Delta t = 0.05$ for the t intervals investigated.

In algorithm form to accompany the above code snippet, spectrally filtered partial Euler Product based approximations of the Riemann Siegel Z function analogues can be constructed adequate for identification of peak height to >2 decimal places using Pari-GP fast fourier transform calculations as follows

1. Obtain a maximum discrete spectrum sample $\Delta t = (t_0 - 819.2, t_0 + 819.2)$, spacing 0.05, $n = 32,768$ of $EP_{RS1,L}(k + I \cdot t, \beta = 1.25)$. Using truncation at βN_1 rather than N_1 to reduce spectral leakage from unwanted higher frequency components [9].
2. use spectral filtering to retain only the discrete fourier transform components of $EP_{RS1,L}(k + I \cdot t, \beta)$ arising from primes 2, ..., $\lfloor N_1 \rfloor$ i.e., the $(-, 0]$ angular frequencies ("concat(real(vhat[16385]), vecextract(vhat, "16386..32768"))" in the above code). This is particular to the Pari-GP FFT output this author is obtaining and a different specification (retaining the $[0, +)$ frequencies) was found to be needed with r language fourier analysis calculations [9].
3. using phase conjugate reflection (about the DC fourier component) of the $(-, 0]$ angular frequencies to impute the $[0, +)$ discrete fourier components of the fourier transform of the Riemann-Siegel formula ("concat(real(vhat[1]), concat(conj(Vecrev(vecextract(vhat, "16386..32768"))))" in the above code) greatly improving the discrete fourier transform approximation with respect to the actual Riemann-Siegel Z function's discrete fourier transform). This is particular to the Pari-GP FFT output this author is obtaining and a different specification (using phase conjugation of the $[0, +)$ frequencies) was found to be needed with r language fourier analysis calculations [9].
4. setting the imaginary(DC fourier component) = 0 ("real(vhat[1])" in the above code) and imaginary(fft[$\lceil \frac{n}{2} \rceil + 1]) = 0 ("real(vhat[16385]" in the above code) to enhance the symmetry/continuity of the approximate fourier transform to improve approximation accuracy since the true (Riemann Siegel Z function) spectra on the critical line is purely real$
5. execute and average fourier analyses of differing lengths from the original stored spectrum ... as the fourier transform component errors in this partial Euler Product Riemann-Siegel Z function approximation appears to vary in random manner across the different length transforms. **Not conducted in this paper** since it is not necessary for L-function extreme peak height investigations since 2-3 decimal place accuracy on extreme peak height is sufficient.
6. use interpolation of the final fitted results (spacing 0.05) onto a finer interpolation grid to estimate extreme peak or non-trivial zero positions. **Not conducted in this paper** since it is not necessary

for L-function extreme peak height investigations since $\Delta t = 0.05$ accuracy on extreme peak location is sufficient for study of the $\left(\sqrt{\frac{t}{2\pi} \cdot 5} - \left\lfloor \sqrt{\frac{t}{2\pi} \cdot 5} \right\rfloor\right)$ distribution given the large FWHM of extreme peaks.

RESULTS

The results for the observed $N \bmod 5$ behaviour on the critical line $s = 0.5 + I \cdot t$ of the distribution of relative positions of extreme peaks of $L(\chi_5(3, .), s)$, $L(\chi_5(2, .), s)$, $f_1(s)$ and $f_2(s)$ within each piecewise interval $[N^2 \cdot \frac{2\pi}{5}, (N+1)^2 \cdot \frac{2\pi}{5})$ for $N=\{0,3000\}$ covering the interval $t=[0-11,317,275]$ using the transformation $\left(\sqrt{\frac{t \cdot 5}{2\pi}} - \left\lfloor \sqrt{\frac{t \cdot 5}{2\pi}} \right\rfloor\right)$ via a range of high precision and approximate Riemann Siegel Z function calculations will be presented sequentially for each function

1. Extreme peak $\left(\sqrt{\frac{t \cdot 5}{2\pi}} - \left\lfloor \sqrt{\frac{t \cdot 5}{2\pi}} \right\rfloor\right)$ behaviour for each $N \bmod 5$ subgroup:

- Evidence displayed in figures 1, (7, 13 and 19) illustrating (i) the $N \bmod 5$ behaviour of the relative position $\left(\sqrt{\frac{t \cdot 5}{2\pi}} - \left\lfloor \sqrt{\frac{t \cdot 5}{2\pi}} \right\rfloor\right)$ of the extreme peaks within the $[N, N+1)$ interval and (ii) the growth rate versus $\log(t)$ of the extreme peak heights. In particular there are regions of higher density in the relative position $\left(\sqrt{\frac{t \cdot 5}{2\pi}} - \left\lfloor \sqrt{\frac{t \cdot 5}{2\pi}} \right\rfloor\right)$ of extreme peaks depending on $N \bmod 5$ and the four 5-periodic functions.

2. Accuracy performance of Riemann Siegel Z function approximations I, II and III:

- A comparison in Tables 1, (2, 3 and 4) of the $|Z|$ for $N=\{2995-3000\}$ extreme peaks on the critical line displaying evidence of 3+ decimal place accuracy between (i) 128 point tapered Dirichlet Series calculations with truncation about the first quiescent region and (ii) Fourier transform filtered finite Euler Product based calculations also truncated at the first quiescent region.
- In figures 2 (8, 14 and 20) for $t=(41,126)$ (i) an overlay graph and (ii) an error graph of approximation I and approximation III compared to the true Riemann Siegel Z function providing evidence of the difference in relative accuracy of the Riemann Siegel Z function approximations at low t .
- In figures 3 (9, 15 and 21) for $t=(5800,5820)$ (i) an overlay graph and (ii) an error graph of approximation I, approximation II and approximation III compared to the true Riemann Siegel function providing evidence of the difference in relative accuracy of the Riemann Siegel Z function approximations at higher t .

3. Indefinite Integral of Riemann Siegel Z function approximations $s = 1/2 + I \cdot t$ only:

- A description of a proposed heuristic approximation for the indefinite integrals of approximation I, approximation II and approximation III on the critical line which are then investigated to uncover a possible explanation of the regions of higher density in the relative position $\left(\sqrt{\frac{t \cdot 5}{2\pi}} - \left\lfloor \sqrt{\frac{t \cdot 5}{2\pi}} \right\rfloor\right)$ of extreme peaks depending on $N \bmod 5$ and the four 5-periodic functions.

4. Indefinite Integral approximation I behaviour and its total derivative performance:

- In figures 4 (10, 16 and 22) for $t=(46,181)$ an overlay graph using (i) the regular t scale and (ii) $[N, N+1)$ scale comparing the real and imaginary parts of approximation I indefinite integral, its numerical total derivative $\frac{d}{ds}$ and the true Riemann Siegel Z function providing evidence of the proposed heuristic approximation behaviour and relevance with respect to the true Riemann Siegel Z function.

5. Universal scaling behaviour of Indefinite Integrals approximations I, II and III as $t \rightarrow \infty$:

- Using a universal vertical scaling $(\frac{t}{2\pi} \cdot 5)^{0.25}$ for these four 1st degree 5-periodic functions in figures 5 (11, 17 and 23) for various intervals $t = (46, 181)$ top row, $t = (5148, 6158)$ second row, $t = (50266, 53327)$ third row, $t = (1256637, 1271762)$ fourth row and $t = (125663706, 125814548)$ the real and imaginary parts of the heuristic approximation based indefinite integrals of approximation I, approximation II and approximation III are compared (i) indicating common, contrasting and sharpening mesoscale features as $t \rightarrow \infty$ of the indefinite integrals and (ii) a $(\frac{t}{2\pi} \cdot 5)^{0.25}$ growth rate in the indefinite integral magnitude.

6. Indefinite Integral approximation II $N \bmod 10$ behaviour and extreme peak Riemann Siegel Z function $N \bmod 5$ behaviour comparison:

- Finally, in figures 6 (12, 18 and 24) the $N \bmod 5$ behaviour of the relative position $\left(\sqrt{\frac{t \cdot 5}{2\pi}} - \left\lfloor \sqrt{\frac{t \cdot 5}{2\pi}} \right\rfloor\right)$ of the extreme peaks within the $[N, N+1]$ interval of the four functions is compared to the $N \bmod 10$ of the imaginary component of the indefinite integral for approximation II at high t for $N=\{3000-3009\}$ and $N=\{10000-10009\}$. In particular there is evidence presented that the regions of higher density in the relative position $\left(\sqrt{\frac{t \cdot 5}{2\pi}} - \left\lfloor \sqrt{\frac{t \cdot 5}{2\pi}} \right\rfloor\right)$ of extreme peaks depending on $N \bmod 5$ and the four 5-periodic functions has some relationship to regions of distinctive curvature in mesoscale features of the imaginary component of approximations for the indefinite integral for the Riemann Siegel Z function.

The paper was prepared as a rmarkdown file and used the RStudio IDE [12].

Relative position of $L(\chi_5(3, .), 1/2 + I \cdot t)$ extreme peaks under $\left(\sqrt{\frac{t \cdot 5}{2\pi}} - \left\lfloor \sqrt{\frac{t \cdot 5}{2\pi}} \right\rfloor\right)$ transformation

The lefthand column in figure 1 presents the $N \bmod 5$ $\left(\sqrt{\frac{t \cdot 5}{2\pi}} - \left\lfloor \sqrt{\frac{t \cdot 5}{2\pi}} \right\rfloor\right)$ behaviour of the distribution of the relative position of extreme Riemann Siegel peaks from every piecewise interval $[N^2 \cdot \frac{2\pi}{5}, (N+1)^2 \cdot \frac{2\pi}{5}]$ obtained for $N=\{0, 3000\}$ for $L(\chi_5(3, .), s)$, on the critical line. The estimates were obtained using equations (19), (30), (34) and (44).

Rows 1-5 presents the extreme peaks data for 3001 piecewise interval segmented by $N \bmod 5 = \{0, 1, 2, 3, 4\}$ respectively.

The righthand column in figure 1 presents the growth in the absolute magnitude of the extreme Riemann Siegel Z function peak height on the critical line as a function of $\log(t)$ for $N \bmod 5 = \{0, 1, 2, 3, 4\}$ (shown in black, red, green, blue, cyan) overlayed on the total dataset (shown in gray).

In the lefthand column it can be seen that there is some evidence of a higher density of extreme peaks at particular relative positions depending on $N \bmod 5$ for $L(\chi_5(3, .), s)$.

In the righthand column there is weaker evidence that $N \bmod 5 = 2$ peaks (middle row in green) for $L(\chi_5(3, .), s)$ may tend to have slightly higher extreme peaks than the other $N \bmod 5$ values.

Table 1 gives a snapshot of the numerical comparison between the absolute magnitude of peak heights obtained at the highest t investigated via (i) spectrally filtered finite Euler Product estimates truncated at the first quiescent region equation (44) and (ii) tapered Dirichlet Series estimates with truncation at the first quiescent region equation (34). Also included is the grid point of the peak, the value of grid point in the interval $[N, N+1]$ and the relative position of the peak in the interval $[0, 1]$. The grid point spacing was $\Delta t = 0.05$ starting from $t = N^2 \cdot \frac{2\pi}{5}$ for each successive piecewise interval $N=\{0, 3000\}$.

Table 1: Grid search results $L(\chi_5(3, .), s)$ for $N=2996-3000$. A comparison of fourier transform filtered Euler Product estimate and 128 point tapered Dirchlet Series estimate based peak heights both using truncation at the first quiescent region $N_1 = \left\lfloor \sqrt{\frac{t}{2\pi} \cdot 5} \right\rfloor$

t value of peak	$\sqrt{\frac{t}{2\pi} \cdot 5}$	$\sqrt{\frac{t}{2\pi} \cdot 5} - \left\lfloor \sqrt{\frac{t}{2\pi} \cdot 5} \right\rfloor$	filtered Euler Product estimate	tapered Dirichlet series estimate
11285347.619641 2996.764		0.7639698	51.22794	51.22955
11287577.845550 2997.060		0.0600675	49.60661	49.60663
11296751.584734 2998.278		0.2777186	49.90783	49.90598
11307801.287191 2999.744		0.7437144	53.68286	53.67738
11314962.252923 3000.693		0.6933977	44.64440	44.64571

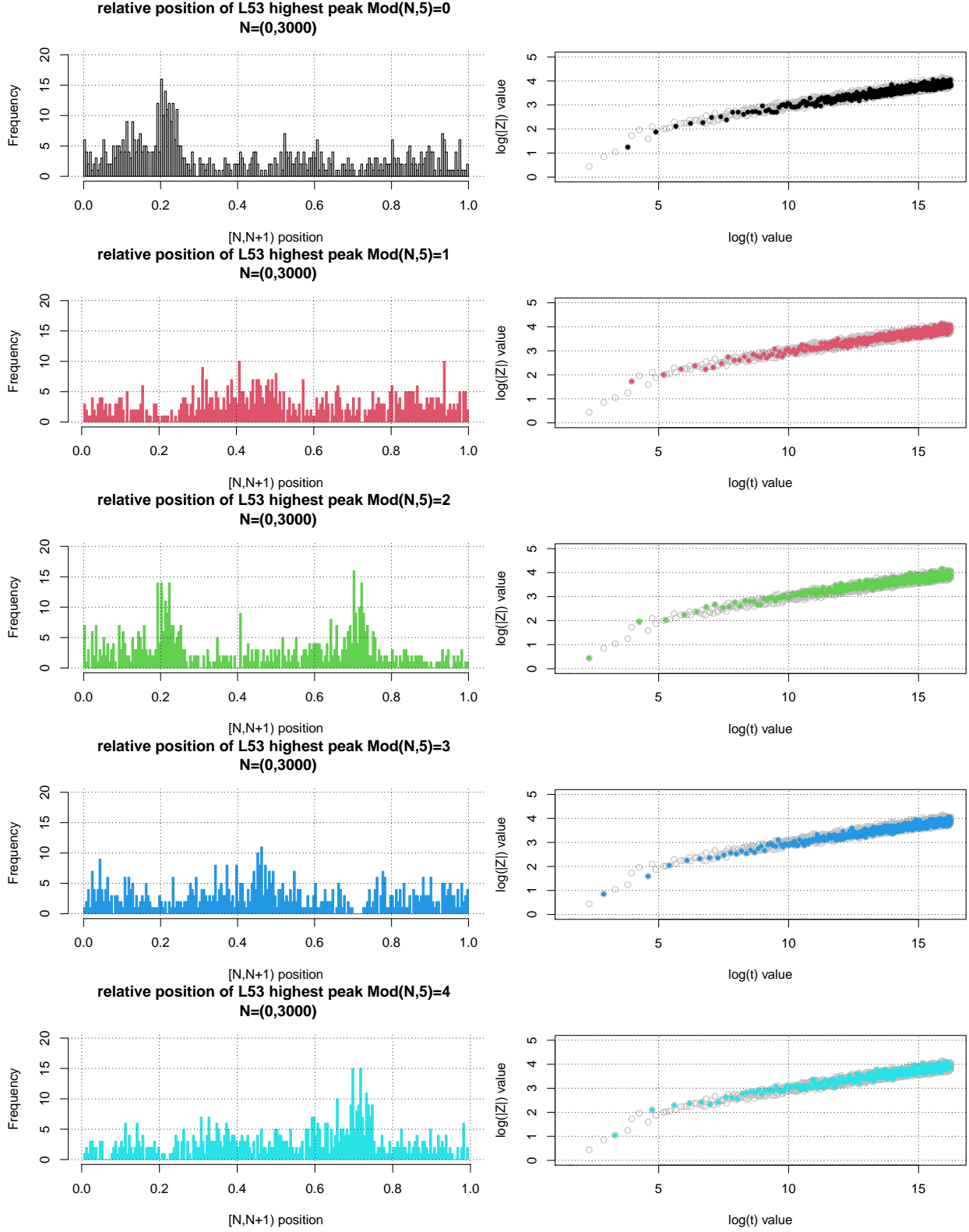


Figure 1: **Lefthand column** - Distribution of the highest peaks of the Riemann Siegel Z function analogue of L53 within each $[N^2 \cdot 2 \cdot \pi/5, (N + 1)^2 \cdot 2 \cdot \pi/5]$ piecewise interval segmented according to $N \bmod 5 = \{0, 1, 2, 3, 4\}$ (top row to bottom row) for $N=\{0-3000\}$ using their normalised positions $\sqrt{\frac{t-5}{2\pi}} - \lfloor \sqrt{\frac{t-5}{2\pi}} \rfloor$. **Righthand column** - Overlay of growth of largest Riemann Siegel Z function peaks from each given $\text{Mod}(N,5)$ intervals compared to all $[N^2 \cdot 2 \cdot \pi/5, (N + 1)^2 \cdot 2 \cdot \pi/5]$ intervals.

Accuracy performance of dirichlet series based approximations I, II and III for the Riemann Siegel Z function analogue of $L(\chi_5(3,.), s)$

Figures 2 and 3 provide an accuracy assessment of equations (30,34,38) in approximating the Riemann Siegel Z function for $L(\chi_5(3,.), s)$ on the critical line, for the two intervals $t=(46,126)$ and $t=(5800,5820)$ respectively.

The left column of Figure 2 shows an overlay of the real (green) and imaginary (black) parts of equations (30) (top row) and (38) (bottom row) respectively with the real (red) and imaginary (blue) parts of the true Riemann Siegel Z function for $L(\chi_5(3,.), s)$. The right column of Figure 2 shows the real and imaginary parts (shown in red and green respectively) of the differences with the true Riemann Siegel Z function – top row numerical($\frac{d}{ds}$ (equation (30)) $- \frac{e^{I\theta f_1(t)}}{\sqrt{\epsilon}} L(\chi_5(3,.), 1/2 + I \cdot t)$), – bottom row numerical ($\frac{d}{ds}$ (equation (38)) $- \frac{e^{I\theta f_1(t)}}{\sqrt{\epsilon}} L(\chi_5(3,.), 1/2 + I \cdot t)$).

The left column of Figure 3 shows an overlay of the real (green) and imaginary (black) parts of equations (30) (top row), (34) (middle row) and (38) (bottom row) respectively with the real (red) and imaginary (blue) parts of the true Riemann Siegel Z function for $L(\chi_5(3,.), s)$. The right column of Figure 3 shows the real and imaginary parts (shown in red and green respectively) of the differences with the true Riemann Siegel Z function – top row numerical($\frac{d}{ds}$ (equation (30)) $- \frac{e^{I\theta f_1(t)}}{\sqrt{\epsilon}} L(\chi_5(3,.), 1/2 + I \cdot t)$), – middle row numerical ($\frac{d}{ds}$ (equation (34)) $- \frac{e^{I\theta f_1(t)}}{\sqrt{\epsilon}} L(\chi_5(3,.), 1/2 + I \cdot t)$), – bottom row numerical ($\frac{d}{ds}$ (equation (38)) $- \frac{e^{I\theta f_1(t)}}{\sqrt{\epsilon}} L(\chi_5(3,.), 1/2 + I \cdot t)$). At $t=(5800,5820)$, the high precision $L(\chi_5(3,.), s)$ Pari-GP functions the required runtime exceeded 10 hours to complete 1000 data points on a single thread.

From the two figures,

- equation (30) has excellent multi decimal place agreement with $\frac{e^{I\theta f_1(t)}}{\sqrt{\epsilon}} \cdot L(\chi_5(3,.), 1/2 + I \cdot t)$ with an oscillating residual error contribution monotonically decreasing with t except for nuisance higher error spikes at $\sqrt{(\frac{t}{2\pi} \cdot 5)} = \left\lfloor \sqrt{(\frac{t}{2\pi} \cdot 5)} \right\rfloor$
- equation (38) has small visible systematic deviations from $\frac{e^{I\theta f_1(t)}}{\sqrt{\epsilon}} \cdot L(\chi_5(3,.), 1/2 + I \cdot t)$. The visible systematic difference, in principle, will be analogous to the first order Riemann Siegel formula (catenary shaped) correction for $\zeta(s)$ however figure 2 indicates that such a first order Riemann Siegel formula correction for $L(\chi_5(3,.), s)$ has an $N \bmod 5$ behaviour with jump discontinuities at $\sqrt{(\frac{t}{2\pi} \cdot 5)} = \left\lfloor \sqrt{(\frac{t}{2\pi} \cdot 5)} \right\rfloor$ and varying correction lineshape dependence where $N = \left\lfloor \sqrt{(\frac{t}{2\pi} \cdot 5)} \right\rfloor$.
- equation (34) has smaller but still systematic deviations than equation (38) because equation (34) includes tapering which should introduce higher order corrections to equation (38).

Thus equations (30,34,38) on the critical line provide good performance in approximating $\frac{e^{I\theta f_1(t)}}{\sqrt{\epsilon}} \cdot L(\chi_5(3,.), 1/2 + I \cdot t)$ the Riemann Siegel Z function for $L(\chi_5(3,.), s)$ on the critical line.

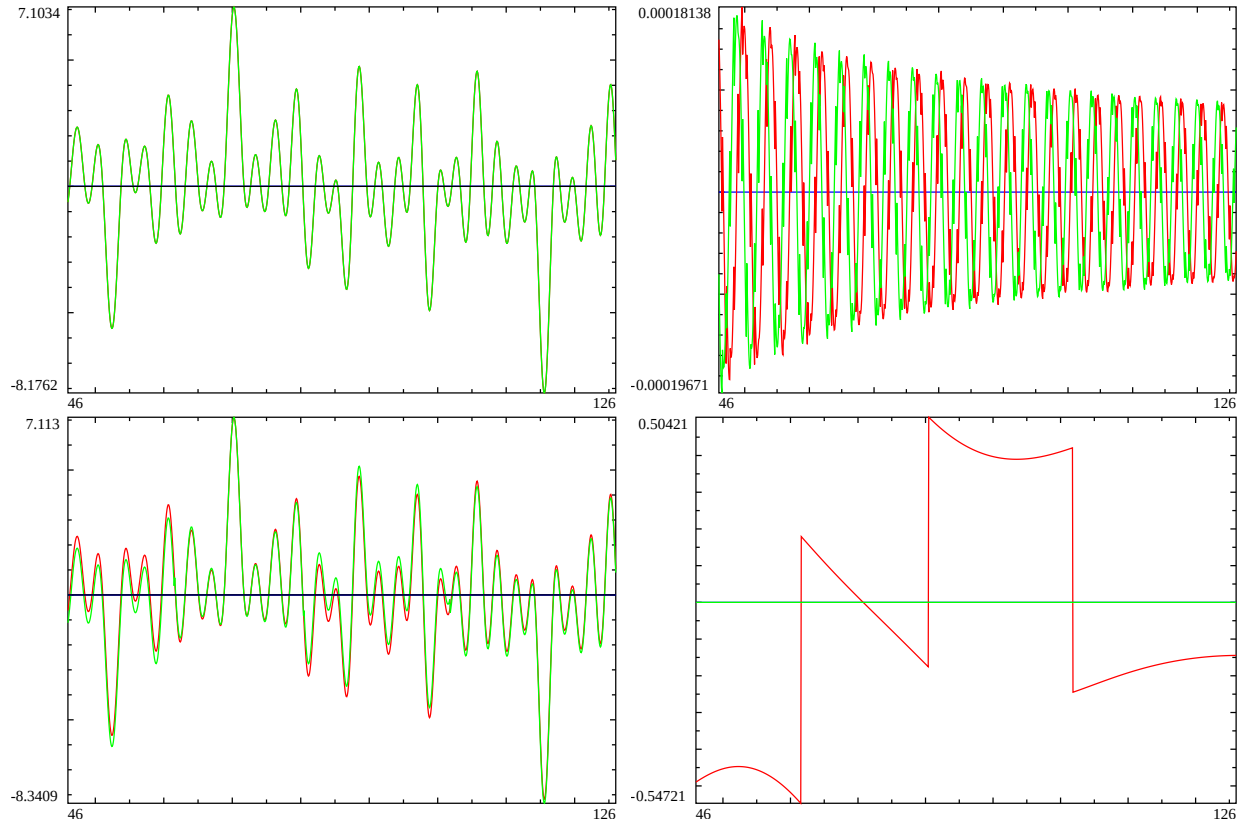


Figure 2: On the critical line, for the interval $t=(46,126)$. Left column - A overlay of real and imaginary components of Riemann Siegel Z function of L53 (red and blue) and equations (30), (38) (green and black) in top (bottom row). Right column - the difference in the real (red) and imaginary (green) components of approximations I and III and the true Riemann Siegel Z function for L53.

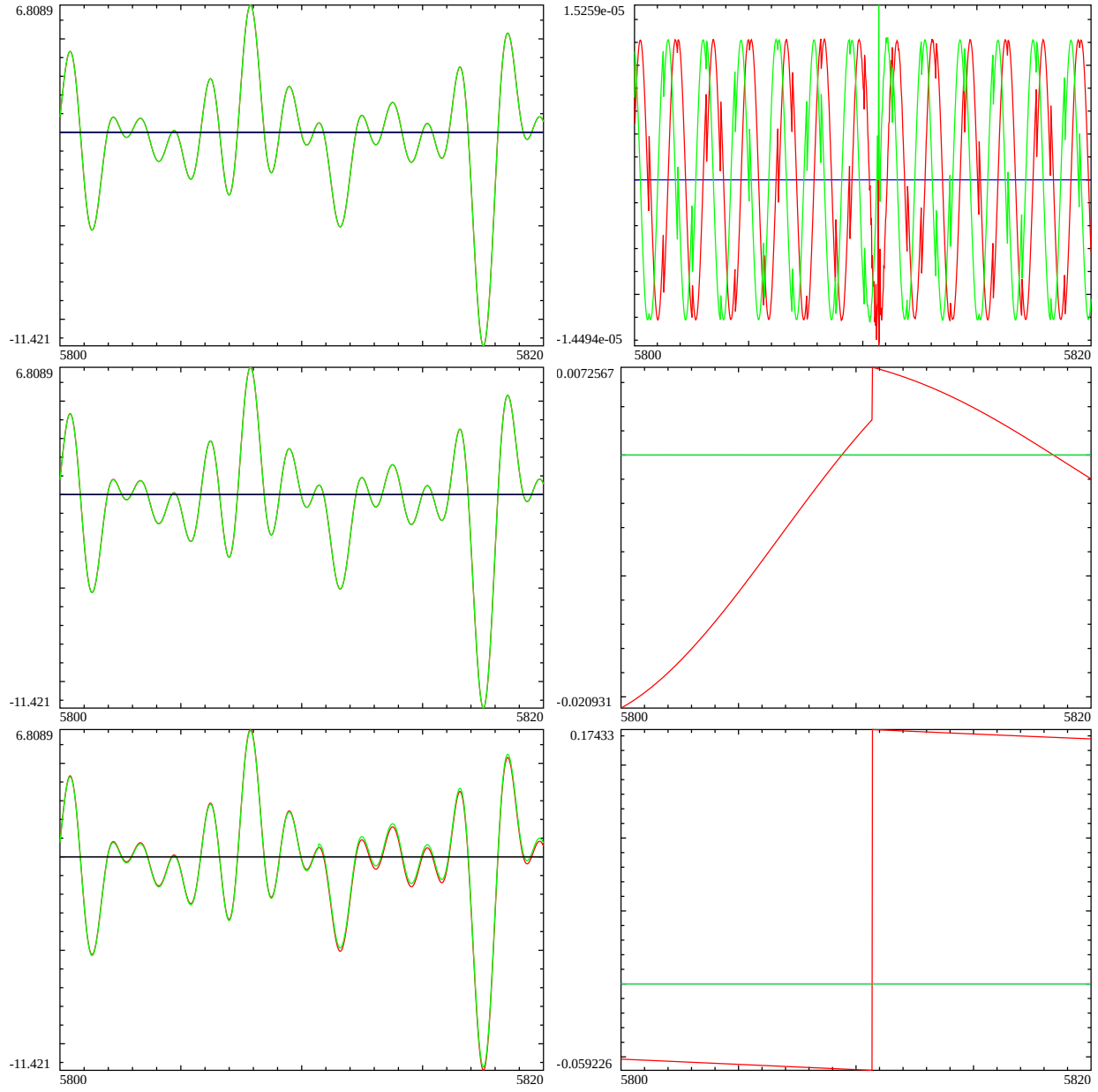


Figure 3: On the critical line, for the interval $t=(5800,5820)$. Left column - A overlay of real and imaginary components of Riemann Siegel Z function of L53 (red and blue) and equations (30), (34) and (38) (green and black) in top, middle and bottom row. Right column - the difference in the real (red) and imaginary (green) components of approximations I, II, III and the true Riemann Siegel Z function for L53.

A heuristic approximation for the indefinite integrals of the Riemann Siegel Z function analogue of tapered and untapered finite $L(\chi_5(3, .), s)$ function Dirichlet Series truncated at the second and first quiescent regions

Following [13] a possible approach to investigating insights into the $\sqrt{\frac{t}{2\pi}} - \left\lfloor \sqrt{\frac{t}{2\pi}} \right\rfloor$ behaviour of Riemann Siegel Z function peak height of $L(\chi_5(3, .), s)$ would be to investigate approximations for the first principles calculation of the indefinite integral of the Riemann Siegel Z function.

Therefore in this paper, co-opting [13] the following three critical line heuristic approximations of the indefinite integral of the Riemann Siegel Z function of $L(\chi_5(3, .), s)$ are attempted

- (i) tapered truncation at the second quiescent region for $L(\chi_5(3, .), s)$ Dirichlet Series $\left\lfloor \frac{t}{\pi} \cdot 5 \right\rfloor$

$$\begin{aligned} & \left(\int \frac{e^{-\frac{1}{2} \log \chi(f_1(s))}}{\sqrt{\epsilon}} L(\chi_5(3, .), s) ds \right)_{s=1/2+I \cdot t, \left\lfloor \frac{t}{\pi} \cdot 5 \right\rfloor, \text{tapered}} \\ & \approx \frac{e^{I \cdot \theta_{f_1}(t)}}{\sqrt{\epsilon}} \cdot \left[\sum_{n=1}^{\left(\left\lfloor \frac{t}{\pi} \cdot 5 \right\rfloor - p \right)} \left(\frac{\chi_{L53}(n)}{\left[\Re \left(\frac{d}{ds} \left[-\frac{1}{2} \log \{\chi(f_1(s))\} \right]_{s=(1/2+I \cdot t)} \right) - \log(n) \right] \cdot n^{(1/2+I \cdot t)}} \right) \right. \\ & + \left. \sum_{i=(-p+1)}^p \frac{\frac{1}{2^{2p}} \left(2^{2p} - \sum_{k=1}^{i+p} \binom{2p}{2p-k} \right) \cdot \chi_{L53}(\left\lfloor \frac{t}{\pi} \cdot 5 \right\rfloor + i)}{\left(\left[\Re \left(\frac{d}{ds} \left[-\frac{1}{2} \log \{\chi(f_1(s))\} \right]_{s=(1/2+I \cdot t)} \right) - \log(\left\lfloor \frac{t}{\pi} \cdot 5 \right\rfloor + i) \right] \cdot (\left\lfloor \frac{t}{\pi} \cdot 5 \right\rfloor + i)^{(1/2+I \cdot t)}} \right], t \rightarrow \infty \end{aligned} \quad (60)$$

- (ii) tapered truncation at the first quiescent region $N_2 = \left\lfloor \sqrt{\frac{t}{2\pi} \cdot 5} \right\rfloor$ for $L(\chi_5(3, .), s)$ Dirichlet Series

$$\begin{aligned} & \left(\int \frac{e^{-\frac{1}{2} \log \chi(f_1(s))}}{\sqrt{\epsilon}} L(\chi_5(3, .), s) ds \right)_{s=1/2+I \cdot t, \left\lfloor \sqrt{\frac{t}{2\pi} \cdot 5} \right\rfloor, \text{tapered}} \\ & \approx \frac{e^{I \cdot \theta_{f_1}(t)}}{\sqrt{\epsilon}} \cdot \left[\sum_{n=1}^{\left(\left\lfloor \sqrt{\frac{t}{2\pi} \cdot 5} \right\rfloor - p \right)} \left(\frac{\chi_{L53}(n)}{\left[\Re \left(\frac{d}{ds} \left[-\frac{1}{2} \log \{\chi(f_1(s))\} \right]_{s=(1/2+I \cdot t)} \right) - \log(n) \right] \cdot n^{(1/2+I \cdot t)}} \right) \right. \\ & + \left. \sum_{i=(-p+1)}^p \frac{\frac{1}{2^{2p}} \left(2^{2p} - \sum_{k=1}^{i+p} \binom{2p}{2p-k} \right) \cdot \chi_{L53}(\left\lfloor \sqrt{\frac{t}{2\pi} \cdot 5} \right\rfloor + i)}{\left(\left[\Re \left(\frac{d}{ds} \left[-\frac{1}{2} \log \{\chi(f_1(s))\} \right]_{s=(1/2+I \cdot t)} \right) - \log(\left\lfloor \sqrt{\frac{t}{2\pi} \cdot 5} \right\rfloor + i) \right] \cdot (\left\lfloor \sqrt{\frac{t}{2\pi} \cdot 5} \right\rfloor + i)^{(1/2+I \cdot t)}} \right. \\ & + \bar{\epsilon} \chi_{f_1}(1/2 + I \cdot t) \cdot \left(\sum_{n=1}^{\left(\left\lfloor \sqrt{\frac{t}{2\pi} \cdot 5} \right\rfloor - p \right)} \left(\frac{\chi_{L53}(n)}{\left[-\Re \left(\frac{d}{ds} \left[-\frac{1}{2} \log \{\chi(f_1(s))\} \right]_{s=(1/2+I \cdot t)} \right) + \log(n) \right] \cdot n^{(1-(1/2+I \cdot t))}} \right) \right. \\ & + \left. \left. \sum_{i=(-p+1)}^p \frac{\frac{1}{2^{2p}} \left(2^{2p} - \sum_{k=1}^{i+p} \binom{2p}{2p-k} \right) \cdot \chi_{L53}(\left\lfloor \sqrt{\frac{t}{2\pi} \cdot 5} \right\rfloor + i)}{\left(\left[-\Re \left(\frac{d}{ds} \left[-\frac{1}{2} \log \{\chi(f_1(s))\} \right]_{s=(1/2+I \cdot t)} \right) + \log(\left\lfloor \sqrt{\frac{t}{2\pi} \cdot 5} \right\rfloor + i) \right] \cdot (\left\lfloor \sqrt{\frac{t}{2\pi} \cdot 5} \right\rfloor + i)^{(1-(1/2+I \cdot t))}} \right) \right], t \rightarrow \infty \end{aligned} \quad (61)$$

- (ii) truncation at the first quiescent region $N_1 = \left\lfloor \sqrt{\frac{t}{2\pi} \cdot 5} \right\rfloor$ for $L(\chi_5(3, .), s)$ Dirichlet Series

$$\begin{aligned}
& \left(\int \frac{e^{-\frac{1}{2} \log \chi(f_1(s))}}{\sqrt{\epsilon}} L(\chi_5(3, .), s) ds \right)_{s=1/2+I \cdot t, \lfloor \sqrt{\frac{t}{2\pi} \cdot 5} \rfloor, \text{tapered}} \\
& \approx \frac{e^{I \cdot \theta_{f_1}(t)}}{\sqrt{\epsilon}} \cdot \left[\sum_{n=1}^{\lfloor \sqrt{\frac{t}{2\pi} \cdot 5} \rfloor} \left(\frac{\chi_{L53}(n)}{\left[\Re \left(\frac{d}{ds} \left[-\frac{1}{2} \log \{\chi(f_1(s))\} \right]_{s=(1/2+I \cdot t)} \right] - \log(n) \right] \cdot n^{(1/2+I \cdot t)}} \right) \right. \\
& \quad \left. + \bar{\epsilon} \chi_{f_1}(1/2 + I \cdot t) \cdot \left(\sum_{n=1}^{\lfloor \sqrt{\frac{t}{2\pi} \cdot 5} \rfloor} \left(\frac{\chi_{L53}(n)}{\left[-\Re \left(\frac{d}{ds} \left[-\frac{1}{2} \log \{\chi(f_1(s))\} \right]_{s=(1/2+I \cdot t)} \right] + \log(n) \right] \cdot n^{(1-(1/2+I \cdot t))}} \right) \right), t \rightarrow \infty \right] \tag{62}
\end{aligned}$$

where

1. $\Re \left(\frac{d}{ds} \left[-\frac{1}{2} \log \{\chi(f_1(s))\} \right]_{s=(1/2+I \cdot t)} \right) \equiv \frac{\partial}{\partial t} [\theta_{f_1}(t)]$ on the critical line and
2. the nomenclature $e^{-\frac{1}{2} \log \chi(f_1(s))}$ is used to avoid confusion with the real valued Riemann Siegel Theta function ($\theta_{f_1}(t) = -\frac{1}{2} \cdot \text{imag} \left[\log \left(\chi(f_1(1/2 + I \cdot t)) \right) \right]$) see equation (25) which applies only to the critical line.
3. $-\frac{1}{2} \log \{\chi(f_1(s))\}$ appears as "vthetaf1(z)" in the code snippet presented earlier in the paper.

As shown in figure 5, the magnitude across the horizontal axis for the real part of equation (60) has symmetry and the real parts of equations (61) & (62) on the critical line are zero. Therefore the integration constant(s) explicitly required for the indefinite integral approximations given by equations (60,61,62) have all been set to zero.

As discussed below, a crucial part of the approximation prescription is explicitly using only $\Re \left(\frac{d}{ds} \left[-\frac{1}{2} \log \{\chi(f_1(s))\} \right] \right)$ and its role in terms of delivering a total derivative estimation that is equivalent to the approximations I (II and III) for the Riemann Siegel Z function of the $L(\chi_5(3, .), s)$ is examined.

Total derivative behaviour of individual terms of equations (60,61,62) on the critical line

To be useful heuristic approximations of the indefinite integral of the Riemann Siegel Z function for the 1st degree 5-periodic function $L(\chi_5(3, .), s)$ the total derivatives $\frac{d}{ds}$ (equations(60, 61, 62)) must result in useful approximations of the $L(\chi_5(3, .), s)$ Riemann Siegel Z function and ideally be equivalent to equations (30), (34) and (38).

In the following discussion, it is demonstrated that there is a term by term agreement **on the critical line** between $\frac{d}{ds}$ (equations(60, 61, 62)) and approximations I,II,III.

Firstly a single term of the dirichlet terms of equation (60) and half the terms of equations (61) and (62) can be presented in the generic form

$$\frac{e^{I \cdot \theta_{f_1}(t)}}{\sqrt{\epsilon}} \cdot \left(\frac{\chi_{L53}(n)}{\left[\Re \left(\frac{d}{ds} \left[-\frac{1}{2} \log \{\chi(f_1(s))\} \right]_{s=(1/2+I \cdot t)} \right] - \log(n) \right] \cdot n^{(1/2+I \cdot t)}} \right) \cdot w(n) \tag{63}$$

and the other half of the terms of equations (61) and (62) can be presented in the second generic form

$$e^{-I \cdot \theta_{f_1}(t)} \cdot \sqrt{\bar{\epsilon}} \cdot \left(\frac{\chi_{L53}(n)}{\left[-\Re \left(\frac{d}{ds} \left[-\frac{1}{2} \log\{\chi(f_1(s))\} \right]_{s=(1/2+I \cdot t)} \right) + \log(n) \right] \cdot n^{(1-(1/2+I \cdot t))}} \right) \cdot w(n) \quad (64)$$

where $w(n)$ describes that each term provides a weighted contribution $w(n) \leq 1$, in particular the $w(n)=1$ below where tapering of the endpoints occurs and $w(n)=0$ above the tapered endpoints and (ii) the second generic form arises from equations (17) and (23)

$$\frac{e^{I \cdot \theta_{f_1}(t)}}{\sqrt{\bar{\epsilon}}} \cdot \bar{\epsilon} \cdot \chi(f_1(1/2 + I \cdot t)) = e^{I \cdot \theta_{f_1}(t)} \cdot e^{-I \cdot 2 \cdot \theta_{f_1}(t)} \cdot \sqrt{\bar{\epsilon}} = e^{-I \cdot \theta_{f_1}(t)} \sqrt{\bar{\epsilon}} \iff s = 1/2 + I \cdot t \quad (65)$$

In practice, while the overall length of non-zero weighted terms of the truncated Dirichlet series in equations (60,61,62) is dependent on t being piecewise functions, the individual n , $w(n)$ and $\chi_{L53}(n)$ values are constants with respect to **infinitesimal changes** in t . $\bar{\epsilon}$ is also a constant.

Hence, each single term of the dirichlet terms of equations (60,61,62) can be re-written as a triple product

$$\left\{ \frac{1}{\left[\Re \left(\frac{d}{ds} \left[-\frac{1}{2} \log\{\chi(f_1(s))\} \right] \right) - \log(n) \right]} \right\} \cdot \left\{ \frac{e^{I \cdot \theta_{f_1}(t)}}{n^{(1/2+I \cdot t)}} \right\} \cdot \left\{ \frac{w(n) \cdot \chi_{L53}(n)}{\sqrt{\bar{\epsilon}}} \right\} \equiv A(s) \cdot B(s) \cdot C(n) \quad (66)$$

$$\left\{ \frac{1}{\left[-\Re \left(\frac{d}{ds} \left[-\frac{1}{2} \log\{\chi(f_1(s))\} \right] \right) + \log(n) \right]} \right\} \cdot \left\{ \frac{e^{-I \cdot \theta_{f_1}(t)}}{n^{(1-(1/2+I \cdot t))}} \right\} \cdot \left\{ w(n) \cdot \chi_{L53}(n) \cdot \sqrt{\bar{\epsilon}} \right\} \equiv -A(s) \cdot D(s) \cdot C(n) \cdot \bar{\epsilon} \quad (67)$$

Using the chain rule, one obtains the generic form of the total derivative $\frac{d}{ds}$ for each dirichlet term of equations (60,61,62)

$$\frac{d}{ds} [A(s) \cdot B(s) \cdot C(n)] = \left\{ \frac{dA(s)}{ds} \cdot B(s) + A(s) \cdot \frac{dB(s)}{ds} \right\} \cdot C(n) \quad (68)$$

or

$$\frac{d}{ds} [-A(s) \cdot D(s) \cdot C(n) \cdot \bar{\epsilon}] = - \left\{ \frac{dA(s)}{ds} \cdot D(s) + A(s) \cdot \frac{dB(s)}{ds} \right\} \cdot C(n) \cdot \bar{\epsilon} \quad (69)$$

Examining $\frac{dA(s)}{ds}$ explicitly

$$\frac{dA(s)}{ds} = \frac{d}{ds} \left\{ \frac{1}{\left[\Re \left(\frac{d}{ds} \left[-\frac{1}{2} \log\{\chi(f_1(s))\} \right] \right) - \log(n) \right]} \right\} \quad (70)$$

$$= \frac{1}{\left[\Re \left(\frac{d}{ds} \left[-\frac{1}{2} \log\{\chi(f_1(s))\} \right] \right) - \log(n) \right]^2} \cdot \frac{d}{ds} \Re \left(\frac{d}{ds} \left[-\frac{1}{2} \log\{\chi(f_1(s))\} \right] \right) \quad (71)$$

Secondly, to make further progress it is simpler to (i) inspect the second total derivative of $\left[-\frac{1}{2} \log\{\chi(f_1(s))\}\right]$ rather than $\Re\left(\frac{d}{ds}\left[-\frac{1}{2} \log\{\chi(f_1(s))\}\right]\right)$ i.e. ignore the $\Re()$ operation for the moment in equation (71),

$$\frac{d}{ds} \left(\frac{d}{ds} \left[-\frac{1}{2} \log\{\chi(f_1(s))\} \right] \right) \quad (72)$$

(ii) and instead of equation (17) use the following alternative functional equation multiplicative factor representation (see [1])

$$L(\chi_5(3, .), s) = \bar{\epsilon} \cdot 5^{(\frac{1}{2}-s)} \pi^{(s-\frac{1}{2})} \cdot \frac{\Gamma(\frac{2-s}{2})}{\Gamma(\frac{1+s}{2})} \cdot L(\chi_5(2, .), 1-s) \quad (73)$$

$$= \bar{\epsilon} \cdot \chi(f_1(s)) \cdot L(\chi_5(2, .), 1-s) \quad (74)$$

$$\therefore \chi(f_1(s)) \equiv 5^{(\frac{1}{2}-s)} \pi^{(s-\frac{1}{2})} \cdot \frac{\Gamma\left[\frac{(2-s)}{2}\right]}{\Gamma\left[\frac{(1+s)}{2}\right]} \quad (75)$$

and (iii) use the $\log(\Gamma(s))$ identity [14,15] obtained from the Weierstrass product form of the $\Gamma(s)$ function

$$\log(\Gamma(s)) = -\gamma \cdot s - \log(s) + \sum_{k=1}^{\infty} \left[\frac{s}{k} - \log\left(1 + \frac{s}{k}\right) \right] \quad (76)$$

to obtain the following $-\frac{1}{2} \cdot \log(\chi(f_1(s)))$ expansion

$$\begin{aligned} -\frac{1}{2} \cdot \log(\chi(f_1(s))) &= -\frac{1}{2} \left\{ \left(\frac{1}{2} - s \right) \cdot \log(5) + \left(s - \frac{1}{2} \right) \cdot \log(\pi) \right. \\ &\quad - \gamma \cdot \left[\frac{(2-s)}{2} \right] - \log\left[\frac{(2-s)}{2} \right] + \sum_{k=1}^{\infty} \left[\frac{\left[\frac{(2-s)}{2} \right]}{k} - \log\left(1 + \frac{\left[\frac{(2-s)}{2} \right]}{k}\right) \right] \\ &\quad \left. - \left(-\gamma \cdot \left[\frac{(1+s)}{2} \right] - \log\left[\frac{(1+s)}{2} \right] + \sum_{k=1}^{\infty} \left[\frac{\left[\frac{(1+s)}{2} \right]}{k} - \log\left(1 + \frac{\left[\frac{(1+s)}{2} \right]}{k}\right) \right] \right) \right\} \end{aligned} \quad (77)$$

from which the following first total derivative is obtained

$$\begin{aligned} \frac{d}{ds} \left[-\frac{1}{2} \log\{\chi(f_1(s))\} \right] &= -\frac{1}{2} \left\{ -\log(5) + \log(\pi) + \frac{\gamma}{2} + \frac{1}{(2-s)} + \sum_{k=1}^{\infty} \left[-\frac{1}{2k} + \frac{1}{(2k+2-s)} \right] \right. \\ &\quad \left. - \left(-\frac{\gamma}{2} - \frac{1}{(1+s)} + \sum_{k=1}^{\infty} \left[\frac{1}{2k} - \frac{1}{(2k+1+s)} \right] \right) \right\} \end{aligned} \quad (78)$$

$$= -\frac{1}{2} \left\{ -\log(5) + \log(\pi) + \gamma + \frac{1}{(2-s)} + \frac{1}{(1+s)} - \sum_{k=1}^{\infty} \left[\frac{1}{k} - \frac{1}{(2k+2-s)} - \frac{1}{(2k+1+s)} \right] \right\} \quad (79)$$

and the second total derivative is then iteratively obtained from $\frac{d}{ds}$ [equation(79)]

$$\frac{d^2}{ds^2} \left[-\frac{1}{2} \log\{\chi(f_1(s))\} \right] = -\frac{1}{2} \left\{ \frac{1}{(2-s)^2} - \frac{1}{(1+s)^2} - \sum_{k=1}^{\infty} \left[-\frac{1}{(2k+2-s)^2} + \frac{1}{(2k+1+s)^2} \right] \right\} \quad (80)$$

Looking at the values of the first and second total derivative of $-\frac{1}{2} \log\{\chi(f_1(s))\}$ on the critical line $s = 1/2 + I \cdot t$

$$\begin{aligned} \frac{d}{ds} \left[-\frac{1}{2} \log\{\chi(f_1(s))\} \right]_{s=1/2+I \cdot t} &= -\frac{1}{2} \left\{ -\log(5) + \log(\pi) + \gamma + \frac{1}{(3/2 - I \cdot t)} + \frac{1}{(3/2 + I \cdot t)} \right. \\ &\quad \left. - \sum_{k=1}^{\infty} \left[\frac{1}{k} - \frac{1}{(2k+3/2-I \cdot t)} - \frac{1}{(2k+3/2+I \cdot t)} \right] \right\} \end{aligned} \quad (81)$$

$$\begin{aligned} &= -\frac{1}{2} \left\{ -\log(5) + \log(\pi) + \gamma + \frac{3/2 + I \cdot t + (3/2 - I \cdot t)}{(3/2 - I \cdot t)(3/2 + I \cdot t)} \right. \\ &\quad \left. - \sum_{k=1}^{\infty} \left[\frac{1}{k} - \frac{(2k+3/2+I \cdot t) + (2k+3/2-I \cdot t)}{(2k+3/2-I \cdot t)(2k+3/2+I \cdot t)} \right] \right\} \end{aligned} \quad (82)$$

$$= -\frac{1}{2} \left\{ -\log(5) + \log(\pi) + \gamma + \frac{3}{(9/4 + t^2)} - \sum_{k=1}^{\infty} \left[\frac{1}{k} - \frac{(4k+3)}{[(2k+3/2)^2 + t^2]} \right] \right\} \quad (83)$$

$$\therefore \frac{d}{ds} \left[-\frac{1}{2} \log\{\chi(f_1(s))\} \right]_{s=1/2+I \cdot t} \in \mathbb{R} \quad (84)$$

$$\begin{aligned} \frac{d^2}{ds^2} \left[-\frac{1}{2} \log\{\chi(f_1(s))\} \right]_{s=1/2+I \cdot t} &= -\frac{1}{2} \left\{ \frac{1}{(3/2 - I \cdot t)^2} - \frac{1}{(3/2 + I \cdot t)^2} \right. \\ &\quad \left. - \sum_{k=1}^{\infty} \left[-\frac{1}{(2k+3/2-I \cdot t)^2} + \frac{1}{(2k+3/2+I \cdot t)^2} \right] \right\} \end{aligned} \quad (85)$$

$$\begin{aligned} &= -\frac{1}{2} \left\{ \frac{(9/4 + I \cdot 3 \cdot t + t^2) - (9/4 - I \cdot 3 \cdot t + t^2)^2}{(3/2 - I \cdot t)^2 \cdot (3/2 + I \cdot t)^2} \right. \\ &\quad \left. - \sum_{k=1}^{\infty} \left[-\frac{(2k+3/2+I \cdot t)^2 - (2k+3/2-I \cdot t)^2}{(2k+3/2-I \cdot t)^2 \cdot (2k+3/2+I \cdot t)^2} \right] \right\} \end{aligned} \quad (86)$$

$$= -\frac{1}{2} \left\{ \frac{I \cdot 6 \cdot t}{(9/4 + t^2)^2} - \sum_{k=1}^{\infty} \left[-\frac{I \cdot (4k+3) \cdot t}{[(2k+3/2)^2 + t^2]^2} \right] \right\} \quad (87)$$

$$\therefore \frac{d^2}{ds^2} \left[-\frac{1}{2} \log\{\chi(f_1(s))\} \right]_{s=1/2+I \cdot t} \in \mathbb{C} - \mathbb{R} \quad \text{i.e., purely imaginary} \quad (88)$$

The relationship $* \left[-\frac{1}{2} \log\{\chi(f_1(s))\} \right]_{s=1/2+I \cdot t} \in \text{pure imaginary}$, $* \frac{d}{ds} \left[-\frac{1}{2} \log\{\chi(f_1(s))\} \right]_{s=1/2+I \cdot t} \in \mathbb{R}$, $* \frac{d^2}{ds^2} \left[-\frac{1}{2} \log\{\chi(f_1(s))\} \right]_{s=1/2+I \cdot t} \in \text{pure imaginary}$ is a demonstration of a analytic complex function $(\left[-\frac{1}{2} \log\{\chi(f_1(s))\} \right]_{s=1/2+I \cdot t})$ following the Cauchy Riemann conditions.

Since differentiation of a **real valued** function (e.g. $\frac{d}{ds} \left[\Re \left(\frac{d}{ds} \left[-\frac{1}{2} \log\{\chi(f_1(s))\} \right] \right) \right]_{s=1/2+I \cdot t}$) must result in a **real valued** result but $\frac{d^2}{ds^2} \left[-\frac{1}{2} \log\{\chi(f_1(s))\} \right]_{s=1/2+I \cdot t} \in \text{pure imaginary}$

$$\therefore \frac{d}{ds} \Re \left(\frac{d}{ds} \left[-\frac{1}{2} \log\{\chi(f_1(s))\} \right] \right)_{s=1/2+I \cdot t} = 0 \quad \forall \quad t \quad (89)$$

Which implies going back to equations (66-69) that the generic form of the total derivative $\frac{d}{ds}$ for each dirichlet term of equations (60,61,62) when calculated for $s = 1/2 + I \cdot t$ reduces to

$$\frac{d}{ds} [A(s) \cdot B(s) \cdot C(n)]_{s=1/2+I \cdot t} \Rightarrow \left\{ \underbrace{\frac{dA(s)}{ds}}_{=0, s=1/2+I \cdot t} \cdot B(s) + A(s) \cdot \frac{dB(s)}{ds} \right\} \cdot C(n) \quad (90)$$

$$= A(s) \cdot \frac{dB(s)}{ds} \cdot C(n)_{s=1/2+I \cdot t} \quad (91)$$

(92)

$$\frac{d}{ds} [-A(s) \cdot D(s) \cdot C(n) \cdot \bar{\epsilon}]_{s=1/2+I \cdot t} \Rightarrow - \left\{ \underbrace{\frac{dA(s)}{ds}}_{=0, s=1/2+I \cdot t} \cdot D(s) + A(s) \cdot \frac{dD(s)}{ds} \right\} \cdot C(n) \cdot \bar{\epsilon} \quad (93)$$

$$= -A(s) \cdot \frac{dD(s)}{ds} \cdot C(n) \cdot \bar{\epsilon}_{s=1/2+I \cdot t} \quad (94)$$

(95)

However

$$A(s) \cdot \frac{dB(s)}{ds} \Big|_{s=1/2+I \cdot t} = \left[\frac{1}{\left[\Re \left(\frac{d}{ds} \left[-\frac{1}{2} \log\{\chi(f_1(s))\} \right] \right) - \log(n) \right]} \cdot \frac{d}{ds} \left\{ \frac{e^{I \cdot \theta_{f1}(t)}}{n^{(1/2+I \cdot t)}} \right\} \right]_{s=1/2+I \cdot t} \quad (96)$$

$$= \left[\frac{1}{\left[\Re \left(\frac{d}{ds} \left[-\frac{1}{2} \log\{\chi(f_1(s))\} \right] \right) - \log(n) \right]} \cdot \frac{d}{ds} \left\{ e^{-\frac{1}{2} \log\{\chi(f_1(s))\}} \cdot e^{-s \cdot \log(n)} \right\} \right]_{s=1/2+I \cdot t} \quad (97)$$

$$= \left[\frac{\frac{d}{ds} \left[-\frac{1}{2} \log\{\chi(f_1(s))\} \right] - \log(n)}{\left[\Re \left(\frac{d}{ds} \left[-\frac{1}{2} \log\{\chi(f_1(s))\} \right] \right) - \log(n) \right]} \cdot \left(e^{-\frac{1}{2} \log\{\chi(f_1(s))\}} \cdot e^{-s \cdot \log(n)} \right) \right]_{s=1/2+I \cdot t} \quad (98)$$

$$= \frac{e^{I \cdot \theta_{f1}(t)}}{n^{(1/2+I \cdot t)}} \Big|_{s=1/2+I \cdot t} \quad (99)$$

$$\begin{aligned}
-A(s) \cdot \frac{dD(s)}{ds} \Big|_{s=1/2+I \cdot t} &= - \left[\frac{1}{\left[\Re \left(\frac{d}{ds} \left[-\frac{1}{2} \log \{\chi(f_1(s))\} \right] \right) - \log(n) \right]} \cdot \frac{d}{ds} \left\{ \frac{e^{-I \cdot \theta_{f_1}(t)}}{n^{(1-(1/2+I \cdot t))}} \right\} \right]_{s=1/2+I \cdot t} \\
&= - \left[\frac{1}{\left[\Re \left(\frac{d}{ds} \left[-\frac{1}{2} \log \{\chi(f_1(s))\} \right] \right) - \log(n) \right]} \cdot \frac{d}{ds} \left\{ e^{\frac{1}{2} \log \{\chi(f_1(s))\}} \cdot e^{s \cdot \log(n)} \right\} \right]_{s=1/2+I \cdot t} \\
&= - \left[\underbrace{\frac{\frac{d}{ds} \left[\frac{1}{2} \log \{\chi(f_1(s))\} \right] + \log(n)}{\left[\Re \left(\frac{d}{ds} \left[-\frac{1}{2} \log \{\chi(f_1(s))\} \right] \right) - \log(n) \right]} \cdot \left(e^{\frac{1}{2} \log \{\chi(f_1(s))\}} \cdot e^{s \cdot \log(n)} \right)}_{=-1, s=1/2+I \cdot t} \right]_{s=1/2+I \cdot t} \\
&= \frac{e^{-I \cdot \theta_{f_1}(t)}}{n^{(1-(1/2+I \cdot t))}} \Big|_{s=1/2+I \cdot t} \tag{103}
\end{aligned}$$

Therefore

$$\frac{d}{ds} \left[\left\{ \frac{1}{\left[\Re \left(\frac{d}{ds} \left[-\frac{1}{2} \log \{\chi(f_1(s))\} \right] \right) - \log(n) \right]} \right\} \cdot \left\{ \frac{e^{I \cdot \theta_{f_1}(t)}}{n^{(1/2+I \cdot t)}} \right\} \cdot \left\{ \frac{w(n) \cdot \chi_{L53}(n)}{\sqrt{\epsilon}} \right\} \right]_{s=1/2+I \cdot t} \tag{104}$$

$$\equiv \left[\frac{e^{I \cdot \theta_{f_1}(t)}}{\sqrt{\epsilon}} \cdot \frac{\chi_{L53}(n)}{n^{(1/2+I \cdot t)}} \cdot w(n) \right]_{s=1/2+I \cdot t} \tag{105}$$

$$\frac{d}{ds} \left[\left\{ \frac{1}{\left[-\Re \left(\frac{d}{ds} \left[-\frac{1}{2} \log \{\chi(f_1(s))\} \right] \right) + \log(n) \right]} \right\} \cdot \left\{ \frac{e^{-I \cdot \theta_{f_1}(t)}}{n^{(1-(1/2+I \cdot t))}} \right\} \cdot \left\{ w(n) \cdot \chi_{L53}(n) \cdot \sqrt{\epsilon} \right\} \right]_{s=1/2+I \cdot t} \tag{106}$$

$$\equiv \left[e^{-I \cdot \theta_{f_1}(t)} \cdot \sqrt{\epsilon} \cdot \frac{\chi_{L53}(n)}{n^{(1-(1/2+I \cdot t))}} \cdot w(n) \right]_{s=1/2+I \cdot t} \tag{107}$$

which together covers all the dirichlet terms of equations (30,34,38) when $s = 1/2 + I \cdot t$.

That is, **on the critical line**, the total derivative of equations (60-62) produces a term by term agreement with approximations I, II and III (equations (30,34,38)) respectively for $L(\chi_5(3, \cdot), s)$.

A similar derivation has now been performed for the indefinite integral of the Riemann Siegel Z function of the Riemann Zeta function using tapered Dirichlet Series (see appendix) and explains the surprisingly good behaviour of the numerical total behaviour on the critical line reported in [13].

It can be observed numerically that $\frac{dA(s)}{ds} \neq 0$ when $s \neq 1/2 + \cdot t$ and so equations (60-62) are not sufficiently accurate away from the critical line.

The $N \bmod 5$ piecewise nature of the indefinite integral approximation equation (60)

In order to show the piecewise nature of the heuristic approximation equation (60) and its total derivative on the same graph with enough resolution of its approximation of the $L(\chi_5(3, .), s)$ non-trivial zero positions, the lowest t interval for 128 point tapering Dirichlet Series truncation at the second quiescent region approximations of the $L(\chi_5(3, .), s)$ function its Riemann Siegel Z function. Figure 4 displays along $s = 0.5 + I * t$ in the lowest possible interval $t = (46, 181)$ for 128 point tapering at the second quiescent region, the behaviour of (i) the **numerical total derivative** of equation (60) –imaginary part in violetred, real part in black–, (ii) the approximate indefinite integral equation (60) itself –imaginary part in red, real part in blue– and (iii) the high precision Pari-GP calculation of $\frac{e^{I\theta f_1(t)}}{\sqrt{\epsilon}} L(\chi_5(3, .), 1/2 + I \cdot t)$ the true Riemann Siegel Z function –imaginary part in gray, real part in green–. In practice, at the resolution of the graph, the **numerical total derivative** of equation (60) results (black and violetred) are completely overlayed by the true Riemann Siegel Z function (green and gray) since the difference between the two functions is very small.

The top row of figure 4 displays the approximate indefinite integral function, its numerical total derivative and the true Riemann Siegel Z function using the regular t scale, while the bottom row displays the functions using a $\sqrt{(\frac{t}{2\pi} \cdot 5)}$ transformed scale. Thus quasi-discontinuities in the indefinite integral at $\sqrt{(\frac{t}{2\pi} \cdot 5)} = \{6, 7, 8, 9, 10, 11, 12\}$ can be observed there are clearly mesoscale features, on the critical line, that are common (but not exactly the same) across the piecewise segments.

The real(indefinite integral equation (60)) shown in blue is smooth, hyperbolic in nature and changes character for each piecewise segment sequentially. Furthermore while the real(indefinite integral) shown in blue has curvature with respect to t , its total derivative (not the partial derivative with respect to t) numerically computed along the critical line and coinciding with the $\text{imag}(\text{Riemann Siegel Z function approximation})$ shown in violetred hidden behind the gray line of the true imaginary part of the Riemann Siegel Z function (on the critical line) is zero! This behaviour for the imaginary part of the **total derivative** of the indefinite integral implies that the $\text{imag}(\text{total derivative of the approximate indefinite integral equation (60)})$ has a $(\sigma - 1/2)$ multiplicative factor on the critical line. A similar behaviour (a $(\sigma - 1/2)$ multiplicative factor) was also interpreted for the numerical total derivative of the approximate indefinite integral of the $\zeta(1/2 + I \cdot t)$ Riemann Siegel Z function in [13].

The $\text{imag}(\text{indefinite integral equation (60)})$ shown in red has mesoscale features eg. the hyperbolic component changes behaviour each piecewise segment and contains fine scale features which dominate the contribution to its total derivative being (an approximation) of the $L(\chi_5(3, .), s)$ Riemann Siegel Z function.

To aid in highlighting the $\sqrt{\frac{t}{2\pi} \cdot 5} - \lfloor \sqrt{\frac{t}{2\pi} \cdot 5} \rfloor$ behaviour of the indefinite integral and the potential for a varying density of the relative position of the highest Riemann Siegel Z function peaks the bottom row of the figure 4 uses $\sqrt{\frac{t}{2\pi} \cdot 5} - \lfloor \sqrt{\frac{t}{2\pi} \cdot 5} \rfloor$ scaling of the t coordinate axis. This results in two widths of piecewise intervals of the approximate indefinite integral equation (60). Numerically, the height of the function at $(N)^2 \cdot \frac{2\pi}{5}$ while large does not appear to be infinity so the piecewise intervals are described as having quasi-discontinuities driven by the contribution of the Dirichlet Series term with $k \approx \sqrt{(\frac{t}{2\pi} \cdot 5)}$. On the bottom row it can be seen that the piecewise intervals for $N=[6,7],[7,8],[8,9],[11,12]$ have width $\Delta N = 1$ while the piecewise interval for $N[9,11]$ has width $\Delta N = 2$. On remembering that the dirichlet characters for $N \bmod 5 = 0$ are zero immediately suggests that the mesoscale quasi-discontinuities features are reflecting whether the dirichlet characters are zero or non-zero.

Following [13], with respect to interpreting the relative position of higher density of extreme peaks in figure 1, it is of interest whether at increasing t the mesoscale features of $\text{imag}(\text{indefinite integral equation (60)})$ settle down to particular relative positions.

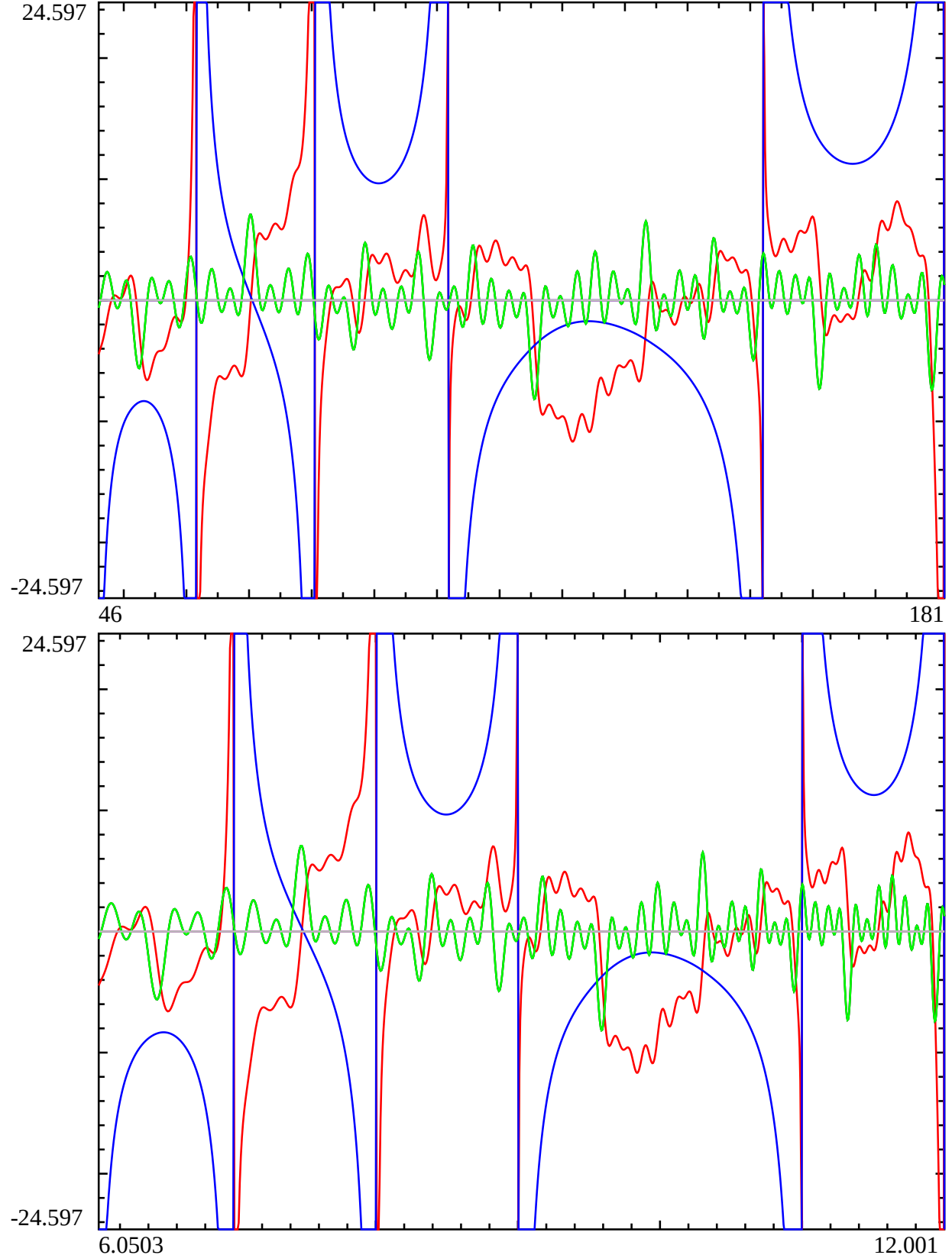


Figure 4: The behaviour of a heuristic approximation of the indefinite integral of the Riemann Siegel Z function for L53 **imag part in red, real part in blue**, its numerical derivative (approximating the Riemann Siegel Z function itself) real (imag) part shown in black (violet-red) based on **128 point end tapered** finite L53 Dirichlet Series sum (truncated at the second quiescent region). The critical line $s = 0.5 + I * t$ in the interval $t = (46, 181)$. The black, and violet-red lines of the real (imag) parts of the numerical total derivative of equation (4) are overlayed by the green, gray lines respectively of the true L53 L-function. From $t > 40.212$ ($64 \cdot \frac{t}{2\pi}$), **128 point end tapered** finite L53 Dirichlet Series sums provide an excellent approximation of the L53 function to many decimal places. First row displays the functions using regular t scale, while the second row displays the functions using $\sqrt{\left(\frac{t-5}{2\pi}\right)}$ scale. Thus quasi discontinuities in the indefinite integral at $\sqrt{\left(\frac{t-5}{2\pi}\right)} = \{6, 7, 8, 9, 11\}$ can be observed and the mesoscale structure across each piecewise domain has a 5-periodic behaviour. There is no discontinuity at $\sqrt{\left(\frac{t-5}{2\pi}\right)} = \{10, 15, 20, \dots\}$ which is a mesoscale reflection of the **zero** Dirichlet character value for $\text{Mod}(N, 5)=0$ for L53. The **real(Riemann Siegel Z function approximation for L53)** zeroes are turning points at the co-ordinates of $\text{imag}(\text{indefinite integral})$. While the **real(indefinite integral)** has curvature with respect to t , the **real(total derivative** $\frac{d}{ds}$) (**not** $\frac{\partial}{\partial t}$) numerically computed along the critical line and coinciding with the **imag(Riemann Siegel Z function approximation for L53)** is zero!

Differences in the piecewise nature of the indefinite integral approximations equations (60), (61) and (62) for the $L(\chi_5(3,.), s)$ Riemann Siegel Z function on the critical line.

Similar to [13], Figure 5 presents the normalised magnitude of the heuristic approximations equations (60,61,62) of the indefinite integral of the Riemann Siegel Z function of $L(\chi_5(3,.), s)$ **imag part in red, real part in blue** based on the finite Riemann Zeta Dirichlet Series sum truncated at the tapered second (lefthand column equation (60)), tapered first (middle column equation (61)) and first (righthand column equation (62)) quiescent regions along the critical line $s = 0.5 + I * t$ in various intervals $t = (46, 181)$, $t = (5148, 6158)$, $t = (50266, 53327)$, $t = (1256637, 1271762)$ and $t = (125663706, 125814548)$. The x axis is standardised by the transformation $\sqrt{\frac{t}{2\pi}} \cdot 5$. Importantly, very similar to [13] the figure shows that the y axis can be normalised to compare the heuristic approximation calculated values of the indefinite integral Riemann Siegel Z function for vastly different t values using a scaling factor of $(\frac{t}{2\pi} \cdot 5)^{0.25}$.

With respect to the piecewise nature of the indefinite integral approximations equations (60), (61) and (62) for the $L(\chi_5(3,.), s)$ Riemann Siegel Z function on the critical line, the normalised y scale shows that

1. there is little evolution of the real(equation(60)) shown in blue (lefthand column) with the smooth hyperbolic lineshapes becoming more symmetric with each $[N, N+1]$ interval while the real(equations(61,62)) remain zero (on the critical line) as t increases.
2. the evolution of the imag(equations(60,61,62)) shown in red can clearly be seen with the sharpening of mesoscale features that vary across the $[N, N+1]$ piecewise intervals. The imag(equation(61)) (middle column) behaviour is close to the imag(equation(60)) (lefthand column) behaviour but imag(equation(62)) (righthand column) clearly displays large differences at the righthand end of the $[N, N+1]$ piecewise intervals. (On careful examination there are also differences at the lefthand end of the $[N, N+1]$ piecewise intervals of the imag(equation(62)) (righthand column) behaviour compared to the other two indefinite integral approximations.)

In [13] the mesoscale features of the approximate indefinite integrals of the Riemann Siegel Z function of the ζ function on the critical line changed sign every piecewise interval $[N, N+1]$. For $L(\chi_5(3,.), s)$ the rate of sign change is observed to occur every tenth piecewise interval.

Figure 6 attempts to juxtapose (i) the mesoscale features of imag(equation(61)) for $N=\{10000-10004\}$ top row, (ii) the mesoscale features of imag(equation(61)) for $N=\{3000-3004\}$ second row, (iii) the $N \bmod 5$ behaviour of the extreme peaks for $N=\{0-3000\}$ under $\sqrt{\frac{t}{2\pi}} \cdot 5 - \left\lfloor \sqrt{\frac{t}{2\pi}} \cdot 5 \right\rfloor$ transformation middle row, (ii) the mesoscale features of imag(equation(61)) for $N=\{3005-3009\}$ second row and (ii) the mesoscale features of imag(equation(61)) for $N=\{10005-10009\}$ bottom row. Such a vertical juxtaposition helps clearly display the $N \bmod 10$ change in sign of the mesoscale features of the approximate indefinite integral of $L(\chi_5(3,.), s)$ Riemann Siegel Z function on the critical line. The vertical juxtaposition also indicates that the higher density in the relative position of the extreme peaks in the $L(\chi_5(3,.), s)$ Riemann Siegel Z function on the critical line (middle row) align well with regions of higher curvature in the approximate indefinite integral of $L(\chi_5(3,.), s)$ Riemann Siegel Z function on the critical line that occur with $N \bmod 5$ periodicity.

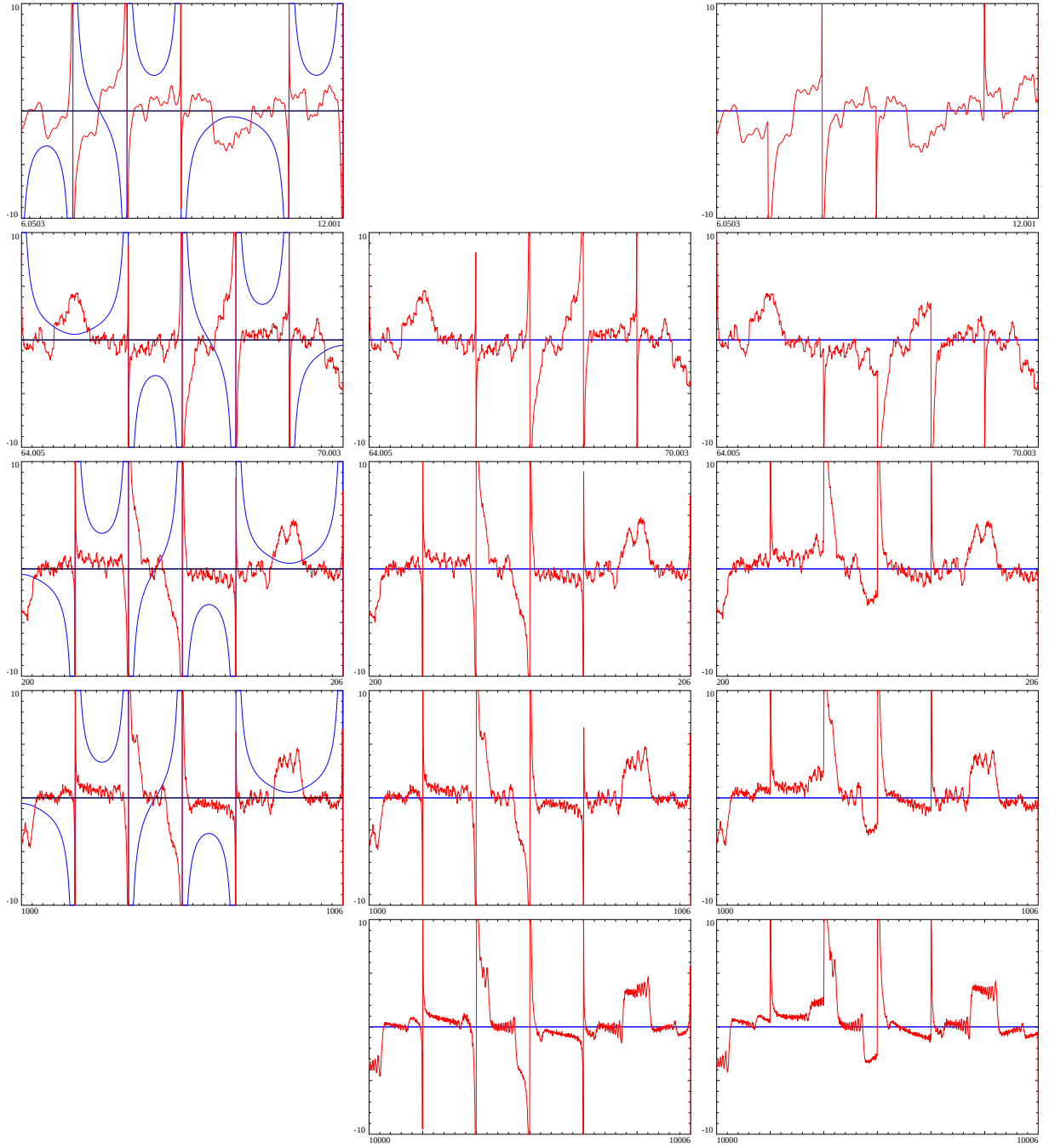


Figure 5: The normalised magnitude of the heuristic approximations equations (60,61,62) (using $\left(\frac{t-5}{2\pi}\right)^{0.25}$ scaling) of the indefinite integral of the Riemann Siegel Z function of L53 **imag part in red**, **real part in blue** based on the finite L53 Dirichlet Series sum truncated at the tapered second (lefthand column), tapered first (middle column) and first (righthand) quiescent region along the critical line $s = 0.5 + I * t$ in various intervals $t = (46, 181)$ top row, $t = (5148, 6158)$ second row, $t = (50266, 53327)$ third row, $t = (1256637, 1271762)$ fourth row and $t = (125663706, 125814548)$ bottom row where the horizontal axis uses a $\sqrt{\left(\frac{t-5}{2\pi}\right)}$ transformed scale. Mesoscale features are observed to evolve as t increases for the three approximations. The real component of equation (4) shown in blue (i) has a minimum absolute magnitude that depends on $\text{Mod}(N,5)$ and (ii) $\text{Mod}(N,10)$ behaviour for the sign of the mesoscale features but (iii) the magnitude scales as $\left(\frac{t-5}{2\pi}\right)^{0.25}$. The gaps in the grid of graphs occur where an approximation is infeasible (below the tapering limit) or calculationally much slower to obtain.

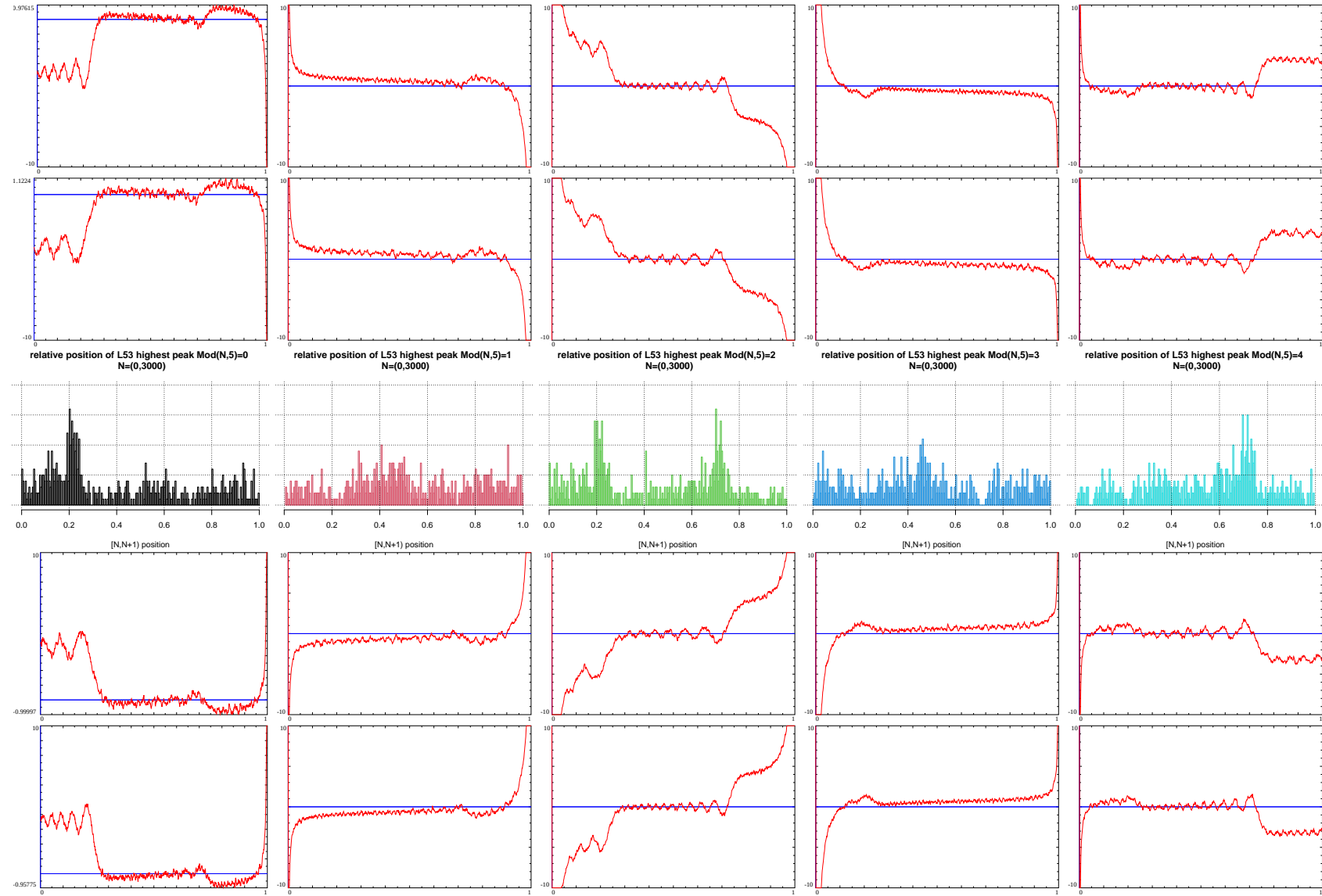


Figure 6: A vertical comparison of the distribution of the highest peaks (absolute magnitude) in $[N, N + 1]$ intervals on the critical line $s = 1/2 + I \cdot t$ where $N = \{0, \dots, 3000\}$ for L53 and $t = N^2 \cdot \frac{2\pi}{5}$ segmented by $N \bmod 5 = \{0, 1, 2, 3, 4\}$ (middle row) with the mesoscale structure features clearly visible at higher t in a heuristic approximation of the imaginary component of the indefinite integral of the Riemann Siegel Z function of L53 along the critical line arranged in order by the intervals $[N, N + 1] \bmod 10$ where $N =$ (i) top row - $\{10000, 10001, 10002, 10003, 10004\}$, (ii) second row - $\{3000, 3001, 3002, 3003, 3004\}$, (iii) fourth row - $\{3005, 3006, 3007, 3008, 3009\}$ and (iv) bottom row - $\{10005, 10006, 10007, 10008, 10009\}$

Relative position of $L(\chi_5(2, .), 1/2 + It)$ extreme peaks under $(\sqrt{\frac{t \cdot 5}{2\pi}} - \lfloor \sqrt{\frac{t \cdot 5}{2\pi}} \rfloor)$ transformation

The lefthand column in Figure 7 presents the $N \bmod 5 (\sqrt{\frac{t \cdot 5}{2\pi}} - \lfloor \sqrt{\frac{t \cdot 5}{2\pi}} \rfloor)$ behaviour of the distribution of the relative position of extreme Riemann Siegel peaks from every piecewise interval $[N^2 \cdot \frac{2\pi}{5}, (N+1)^2 \cdot \frac{2\pi}{5}]$ obtained for $N=\{0,3000\}$ for $L(\chi_5(2, .), s)$, on the critical line. The estimates were obtained using equations (20), (31), (35) and (47).

Rows 1-5 presents the extreme peaks data for 3001 piecewise interval segmented by $N \bmod 5 = \{0, 1, 2, 3, 4\}$ respectively.

The righthand column in Figure 7 presents the growth in the absolute magnitude of the extreme Riemann Siegel Z function peak height on the critical line as a function of $\log(t)$ for $N \bmod 5 = \{0, 1, 2, 3, 4\}$ (shown in black, red, green, blue, cyan) overlayed on the total dataset (shown in gray).

In the lefthand column it can be seen that there is some evidence of a higher density of extreme peaks at particular relative positions depending on $N \bmod 5$ for $L(\chi_5(2, .), s)$.

In the righthand column there is weaker evidence that $N \bmod 5 = 2$ peaks (second and fourth rows in red and blue respectively) for $L(\chi_5(2, .), s)$ may tend to have slightly higher extreme peaks than the other $N \bmod 5$ values.

Table 2 gives a snapshot of the numerical comparison between the absolute magnitude of peak heights obtained at the highest t investigated via (i) spectrally filtered finite Euler Product estimates truncated at the first quiescent region equation (47) and (ii) tapered Dirichlet Series estimates with truncation at the first quiescent region equation (35). Also included is the grid point of the peak, the value of grid point in the interval $[N, N+1]$ and the relative position of the peak in the interval $[0, 1]$. The grid point spacing was $\Delta t = 0.05$ starting from $t = N^2 \cdot \frac{2\pi}{5}$ for each successive piecewise interval $N=\{0,3000\}$.

Table 2: Grid search results $L(\chi_5(2, .), s)$ for $N=2995-3000$. A comparison of fourier transform filtered Euler Product estimate and 128 point tapered Dirchlet Series estimate based peak heights both using truncation at the first quiescent region $N_1 = \left\lfloor \sqrt{\frac{t}{2\pi} \cdot 5} \right\rfloor$

t value of peak	$\sqrt{\frac{t}{2\pi} \cdot 5}$	$\sqrt{\frac{t}{2\pi} \cdot 5} - \left\lfloor \sqrt{\frac{t}{2\pi} \cdot 5} \right\rfloor$	filtered Euler Product estimate	tapered Dirichlet series estimate
11274683.657006 2995.348		0.3477559	42.30170	42.30103
11284509.469641 2996.653		0.6526846	47.56495	46.06157
11290863.745550 2997.496		0.4962693	53.62401	53.62433
11296365.934734 2998.227		0.2265404	52.71470	52.71666
11305693.787191 2999.464		0.4641616	46.84863	46.85024
11314341.152923 3000.611		0.6110397	46.66631	46.66689

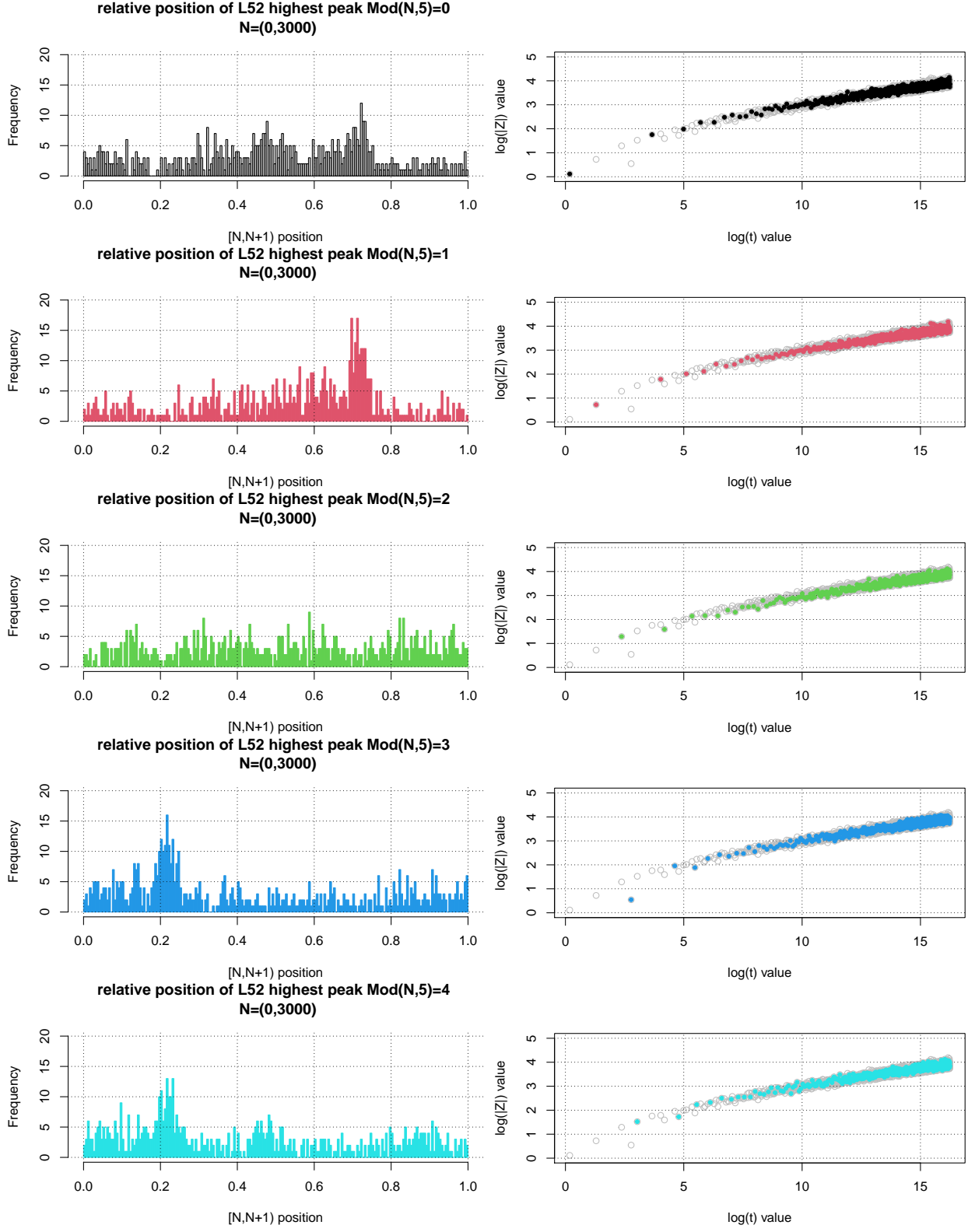


Figure 7: **Lefthand column** - Distribution of highest peaks of the Riemann Siegel Z function analogue of L52 and its approximations within each $[N^2 \cdot 2 \cdot \pi/5, (N+1)^2 \cdot 2 \cdot \pi/5]$ piecewise interval segmented according to $N \bmod 5 = \{0, 1, 2, 3, 4\}$ (top row to bottom row) for $N=\{0-3000\}$ using their normalised positions $\sqrt{\frac{t-5}{2\pi}} - \lfloor \sqrt{\frac{t-5}{2\pi}} \rfloor$. **Righthand column** - Overlay of growth of largest Riemann Siegel Z function peaks from each given $\text{Mod}(N,5)$ intervals compared to all $[N^2 \cdot 2 \cdot \pi/5, (N+1)^2 \cdot 2 \cdot \pi/5]$ intervals.

Accuracy performance of dirichlet series based approximations I, II and III for the Riemann Siegel Z function analogue of $L(\chi_5(2,.), s)$

Figures 8 and 9 provide an accuracy assessment of equations (31,35,39) in approximating the Riemann Siegel Z function for $L(\chi_5(2,.), s)$ on the critical line, for the two intervals $t=(46,126)$ and $t=(5800,5820)$ respectively.

The left column of Figure 8 shows an overlay of the real (green) and imaginary (black) parts of equations (30) (top row) and (38) (bottom row) respectively with the real (red) and imaginary (blue) parts of the true Riemann Siegel Z function for $L(\chi_5(2,.), s)$. The right column of Figure 8 shows the real and imaginary parts (shown in red and green respectively) of the differences with the true Riemann Siegel Z function – top row numerical($\frac{d}{ds}$ (equation (31)) $- \frac{e^{I\theta f_1(t)}}{\sqrt{\epsilon}} \cdot L(\chi_5(2,.), 1/2 + I \cdot t)$), – bottom row numerical($\frac{d}{ds}$ (equation (39)) $- \frac{e^{I\theta f_1(t)}}{\sqrt{\epsilon}} \cdot L(\chi_5(2,.), 1/2 + I \cdot t)$).

The left column of Figure 9 shows an overlay of the real (green) and imaginary (black) parts of equations (31) (top row), (35) (middle row) and (39) (bottom row) respectively with the real (red) and imaginary (blue) parts of the true Riemann Siegel Z function for $L(\chi_5(2,.), s)$. The right column of Figure 9 shows the real and imaginary parts (shown in red and green respectively) of the differences with the true Riemann Siegel Z function – top row numerical($\frac{d}{ds}$ (equation (31)) $- \frac{e^{I\theta f_1(t)}}{\sqrt{\epsilon}} \cdot L(\chi_5(2,.), 1/2 + I \cdot t)$), – middle row numerical($\frac{d}{ds}$ (equation (35)) $- \frac{e^{I\theta f_1(t)}}{\sqrt{\epsilon}} \cdot L(\chi_5(2,.), 1/2 + I \cdot t)$), – bottom row numerical($\frac{d}{ds}$ (equation (39)) $- \frac{e^{I\theta f_1(t)}}{\sqrt{\epsilon}} \cdot L(\chi_5(2,.), 1/2 + I \cdot t)$). At $t=(5800,5820)$, the high precision $L(\chi_5(2,.), s)$ Pari-GP functions the required runtime exceeded 10 hours to complete 1000 data points on a single thread.

From the two figures,

- equation (31) has excellent multi decimal place agreement with $\frac{e^{I\theta f_1(t)}}{\sqrt{\epsilon}} \cdot L(\chi_5(2,.), 1/2 + I \cdot t)$ with an oscillating residual error contribution monotonically decreasing with t except for nuisance higher error spikes at $\sqrt{(\frac{t}{2\pi} \cdot 5)} = \left\lfloor \sqrt{(\frac{t}{2\pi} \cdot 5)} \right\rfloor$
- equation (39) has small visible systematic deviations from $\frac{e^{I\theta f_1(t)}}{\sqrt{\epsilon}} \cdot L(\chi_5(2,.), 1/2 + I \cdot t)$. The visible systematic difference, in principle, will be analogous to the first order Riemann Siegel formula (catenary shaped) correction for $\zeta(s)$ however figure 2 indicates that such a first order Riemann Siegel formula correction for $L(\chi_5(2,.), s)$ has an $N \bmod 5$ behaviour with jump discontinuities at $\sqrt{(\frac{t}{2\pi} \cdot 5)} = \left\lfloor \sqrt{(\frac{t}{2\pi} \cdot 5)} \right\rfloor$ and varying correction lineshape dependence where $N = \left\lfloor \sqrt{(\frac{t}{2\pi} \cdot 5)} \right\rfloor$.
- equation (35) has smaller but still systematic deviations than equation (39) because equation (35) includes tapering which should introduce higher order corrections to equation (39).

Thus equations (31,35,39) on the critical line provide good performance in approximating $\frac{e^{I\theta f_1(t)}}{\sqrt{\epsilon}} \cdot L(\chi_5(2,.), 1/2 + I \cdot t)$ the Riemann Siegel Z function for $L(\chi_5(2,.), s)$ on the critical line.

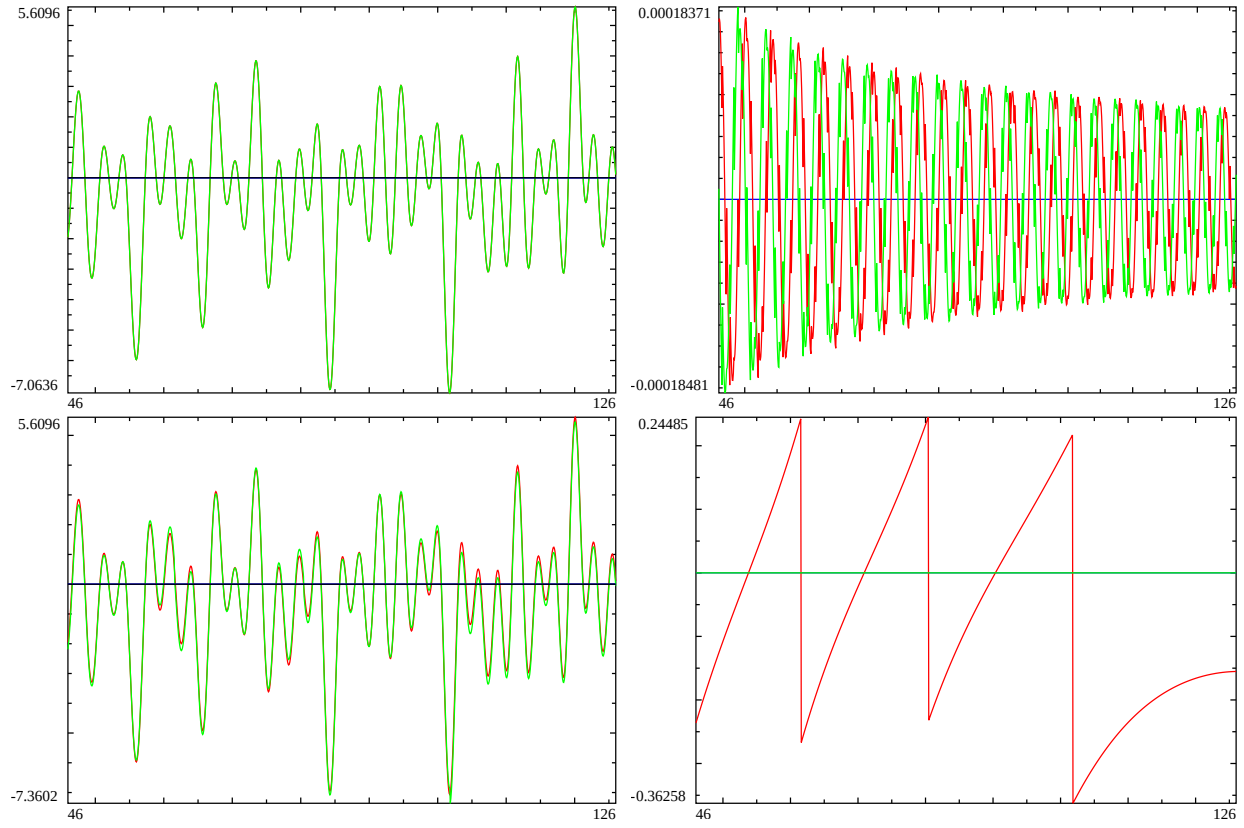


Figure 8: On the critical line, for the interval $t=(46,126)$. Left column - A overlay of real and imaginary components of Riemann Siegel Z function of L52 (red and blue) and and equations (31), (39) (green and black) in top (bottom row). Right column - the difference in the real (red) and imaginary (green) components of approximations I and III and the true Riemann Siegel Z function for L52.

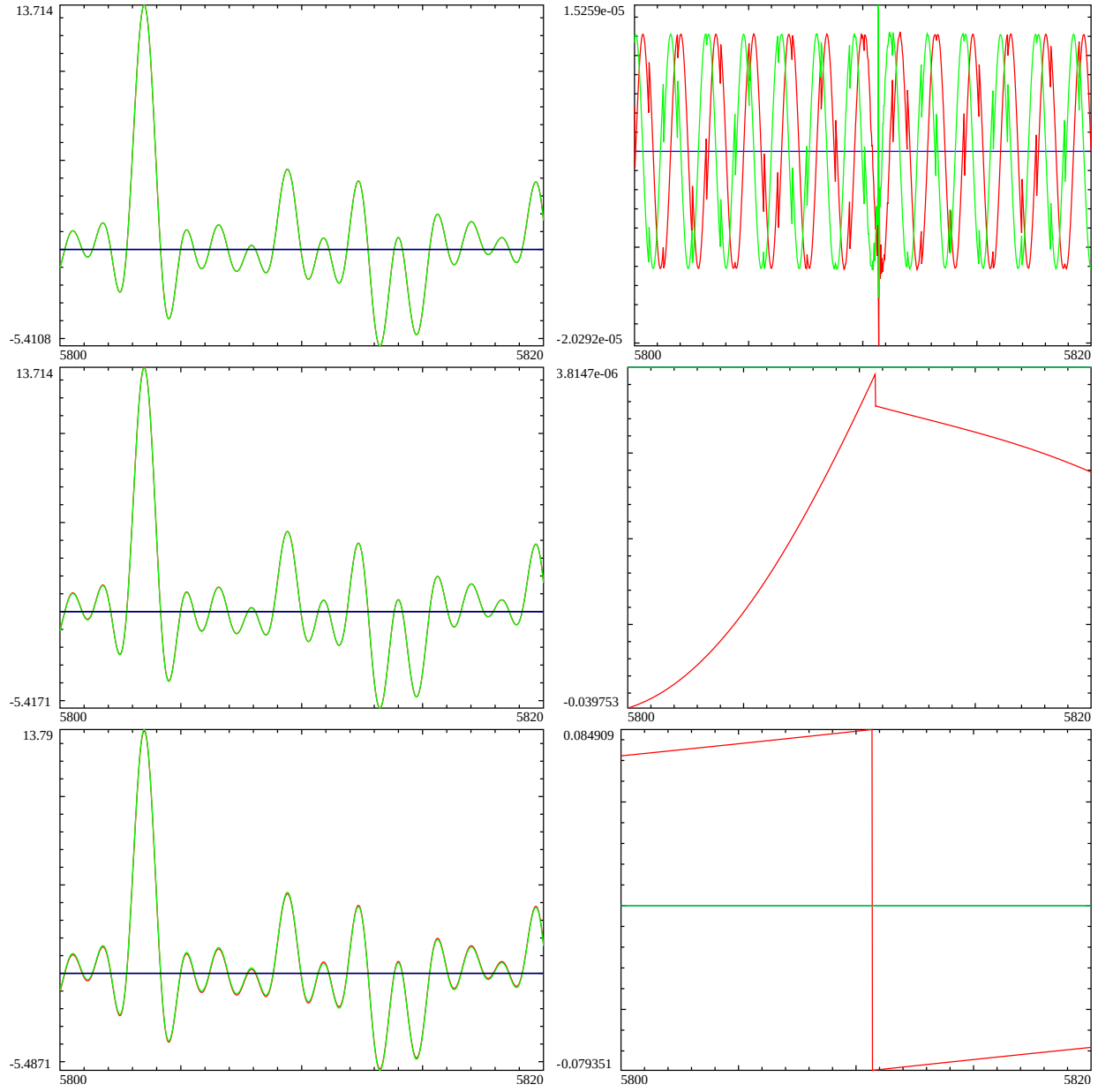


Figure 9: On the critical line, for the interval $t=(5800,5820)$. Left column - A overlay of real and imaginary components of Riemann Siegel Z function of L52 (red and blue) and equations (31), (35) and (39) (green and black) in top, middle and bottom row. Right column - the difference in the real (red) and imaginary (green) components of approximations I, II, III and the true Riemann Siegel Z function for L52.

A heuristic approximation for the indefinite integrals of the Riemann Siegel Z function analogue of tapered and untapered finite $L(\chi_5(2, .), s)$ function Dirichlet Series truncated at the second and first quiescent regions

Following [13] a possible approach to investigating insights into the $\sqrt{\frac{t}{2\pi}} - \left\lfloor \sqrt{\frac{t}{2\pi}} \right\rfloor$ behaviour of Riemann Siegel Z function peak height of $L(\chi_5(2, .), s)$ would be to investigate approximations for the first principles calculation of the indefinite integral of the Riemann Siegel Z function.

Therefore in this paper, co-opting [13] the following three critical line heuristic approximations of the indefinite integral of the Riemann Siegel Z function of $L(\chi_5(2, .), s)$ are attempted

- (i) tapered truncation at the second quiescent region for $L(\chi_5(2, .), s)$ Dirichlet Series $\left\lfloor \frac{t}{\pi} \cdot 5 \right\rfloor$

$$\begin{aligned} & \left(\int \frac{e^{-\frac{1}{2} \log \chi(f_1(s))}}{\sqrt{\epsilon}} L(\chi_5(2, .), s) ds \right)_{s=1/2+I \cdot t, \left\lfloor \frac{t}{\pi} \cdot 5 \right\rfloor, \text{tapered}} \\ & \approx \frac{e^{I \cdot \theta_{f_1}(t)}}{\sqrt{\epsilon}} \cdot \left[\sum_{n=1}^{\left(\left\lfloor \frac{t}{\pi} \cdot 5 \right\rfloor - p \right)} \left(\frac{\chi_{L52}(n)}{\left[\Re \left(\frac{d}{ds} \left[-\frac{1}{2} \log \{\chi(f_1(s))\} \right]_{s=(1/2+I \cdot t)} \right) - \log(n) \right] \cdot n^{(1/2+I \cdot t)}} \right) \right. \\ & \quad \left. + \sum_{i=(-p+1)}^p \frac{\frac{1}{2^{2p}} \left(2^{2p} - \sum_{k=1}^{i+p} \binom{2p}{2p-k} \right) \cdot \chi_{L52}(\left\lfloor \frac{t}{\pi} \cdot 5 \right\rfloor + i)}{\left(\left[\Re \left(\frac{d}{ds} \left[-\frac{1}{2} \log \{\chi(f_1(s))\} \right]_{s=(1/2+I \cdot t)} \right) - \log(\left\lfloor \frac{t}{\pi} \cdot 5 \right\rfloor + i) \right] \cdot (\left\lfloor \frac{t}{\pi} \cdot 5 \right\rfloor + i)^{(1/2+I \cdot t)}} \right], t \rightarrow \infty \end{aligned} \quad (108)$$

- (ii) tapered truncation at the first quiescent region $N_2 = \left\lfloor \sqrt{\frac{t}{2\pi} \cdot 5} \right\rfloor$ for $L(\chi_5(2, .), s)$ Dirichlet Series

$$\begin{aligned} & \left(\int \frac{e^{-\frac{1}{2} \log \chi(f_1(s))}}{\sqrt{\epsilon}} L(\chi_5(2, .), s) ds \right)_{s=1/2+I \cdot t, \left\lfloor \sqrt{\frac{t}{2\pi} \cdot 5} \right\rfloor, \text{tapered}} \\ & \approx \frac{e^{I \cdot \theta_{f_1}(t)}}{\sqrt{\epsilon}} \cdot \left[\sum_{n=1}^{\left(\left\lfloor \sqrt{\frac{t}{2\pi} \cdot 5} \right\rfloor - p \right)} \left(\frac{\chi_{L52}(n)}{\left[\Re \left(\frac{d}{ds} \left[-\frac{1}{2} \log \{\chi(f_1(s))\} \right]_{s=(1/2+I \cdot t)} \right) - \log(n) \right] \cdot n^{(1/2+I \cdot t)}} \right) \right. \\ & \quad \left. + \sum_{i=(-p+1)}^p \frac{\frac{1}{2^{2p}} \left(2^{2p} - \sum_{k=1}^{i+p} \binom{2p}{2p-k} \right) \cdot \chi_{L52}(\left\lfloor \sqrt{\frac{t}{2\pi} \cdot 5} \right\rfloor + i)}{\left(\left[\Re \left(\frac{d}{ds} \left[-\frac{1}{2} \log \{\chi(f_1(s))\} \right]_{s=(1/2+I \cdot t)} \right) - \log(\left\lfloor \sqrt{\frac{t}{2\pi} \cdot 5} \right\rfloor + i) \right] \cdot (\left\lfloor \sqrt{\frac{t}{2\pi} \cdot 5} \right\rfloor + i)^{(1/2+I \cdot t)}} \right. \\ & \quad \left. + \epsilon \chi_{f_1}(1/2 + I \cdot t) \cdot \left(\sum_{n=1}^{\left(\left\lfloor \sqrt{\frac{t}{2\pi} \cdot 5} \right\rfloor - p \right)} \left(\frac{\chi_{L52}(n)}{\left[-\Re \left(\frac{d}{ds} \left[-\frac{1}{2} \log \{\chi(f_1(s))\} \right]_{s=(1/2+I \cdot t)} \right) + \log(n) \right] \cdot n^{(1-(1/2+I \cdot t))}} \right) \right. \\ & \quad \left. + \sum_{i=(-p+1)}^p \frac{\frac{1}{2^{2p}} \left(2^{2p} - \sum_{k=1}^{i+p} \binom{2p}{2p-k} \right) \cdot \chi_{L52}(\left\lfloor \sqrt{\frac{t}{2\pi} \cdot 5} \right\rfloor + i)}{\left(\left[-\Re \left(\frac{d}{ds} \left[-\frac{1}{2} \log \{\chi(f_1(s))\} \right]_{s=(1/2+I \cdot t)} \right) + \log(\left\lfloor \sqrt{\frac{t}{2\pi} \cdot 5} \right\rfloor + i) \right] \cdot (\left\lfloor \sqrt{\frac{t}{2\pi} \cdot 5} \right\rfloor + i)^{(1-(1/2+I \cdot t))}} \right) \right], t \rightarrow \infty \end{aligned} \quad (109)$$

- (ii) truncation at the first quiescent region $N_1 = \left\lfloor \sqrt{\frac{t}{2\pi} \cdot 5} \right\rfloor$ for $L(\chi_5(2, .), s)$ Dirichlet Series

$$\begin{aligned}
& \left(\int \frac{e^{-\frac{1}{2} \log \chi(f_1(s))}}{\sqrt{\epsilon}} L(\chi_5(2, .), s) ds \right)_{s=1/2+I \cdot t, \left[\sqrt{\frac{t}{2\pi} \cdot 5} \right], \text{tapered}} \\
& \approx \frac{e^{I \cdot \theta_{f_1}(t)}}{\sqrt{\epsilon}} \cdot \left[\sum_{n=1}^{\left(\lfloor \sqrt{\frac{t}{2\pi} \cdot 5} \rfloor \right)} \left(\frac{\chi_{L52}(n)}{\left[\Re \left(\frac{d}{ds} \left[-\frac{1}{2} \log \{ \chi(f_1(s)) \} \right]_{s=(1/2+I \cdot t)} \right] - \log(n) \right] \cdot n^{(1/2+I \cdot t)}} \right) \right. \\
& \quad \left. + \epsilon \chi_{f_1}(1/2 + I \cdot t) \cdot \left(\sum_{n=1}^{\left(\lfloor \sqrt{\frac{t}{2\pi} \cdot 5} \rfloor \right)} \left(\frac{\chi_{L52}(n)}{\left[-\Re \left(\frac{d}{ds} \left[-\frac{1}{2} \log \{ \chi(f_1(s)) \} \right]_{s=(1/2+I \cdot t)} \right] + \log(n) \right] \cdot n^{(1-(1/2+I \cdot t))}} \right) \right), t \rightarrow \infty \right. \\
& \quad \left. (110) \right]
\end{aligned}$$

where

1. $\Re \left(\frac{d}{ds} \left[-\frac{1}{2} \log \{ \chi(f_1(s)) \} \right]_{s=(1/2+I \cdot t)} \right) \equiv \frac{\partial}{\partial t} [\theta_{f_1}(t)]$ on the critical line and
2. the nomenclature $e^{-\frac{1}{2} \log \chi(f_1(s))}$ is used to avoid confusion with the real valued Riemann Siegel Theta function ($\theta_{f_1}(t) = -\frac{1}{2} \cdot \text{imag} \left[\log \left(\chi(f_1(1/2 + I \cdot t)) \right) \right]$) see equation (25) which applies only to the critical line.
3. $-\frac{1}{2} \log \{ \chi(f_1(s)) \}$ appears as "vthetaf1(z)" in the code snippet presented earlier in the paper.

As shown in figures 10 and 11, the magnitude across the horizontal axis for the real part of equation (108) has symmetry and the real parts of equations (109) & (110) on the critical line are zero. Therefore the integration constant(s) explicitly required for the indefinite integral approximations given by equations (108,109,110) have all been set to zero.

As discussed below, a crucial part of the approximation prescription is explicitly using only $\Re \left(\frac{d}{ds} \left[-\frac{1}{2} \log \{ \chi(f_1(s)) \} \right] \right)$ and its role in terms of delivering a total derivative estimation that is equivalent to the approximations I (II and III) for the Riemann Siegel Z function of the $L(\chi_5(2, .), s)$ is examined.

Total derivative behaviour of individual terms of equations (108,109,110) on the critical line

To be useful heuristic approximations of the indefinite integral of the Riemann Siegel Z function for the 1st degree 5-periodic function $L(\chi_5(2, .), s)$ the total derivatives $\frac{d}{ds}$ (equations(108, 109, 110)) must result in useful approximations of the $L(\chi_5(2, .), s)$ Riemann Siegel Z function and ideally be equivalent to equations (31), (35) and (39).

In the following discussion, it is demonstrated that there is a term by term agreement **on the critical line** between $\frac{d}{ds}$ (equations(108, 109, 110)) and approximations I,II,III.

Firstly a single term of the dirichlet terms of equation (108) and half the terms of equations (109) and (110) can be presented in the generic form

$$\frac{e^{I \cdot \theta_{f_1}(t)}}{\sqrt{\epsilon}} \cdot \left(\frac{\chi_{L52}(n)}{\left[\Re \left(\frac{d}{ds} \left[-\frac{1}{2} \log \{ \chi(f_1(s)) \} \right]_{s=(1/2+I \cdot t)} \right] - \log(n) \right] \cdot n^{(1/2+I \cdot t)}} \right) \cdot w(n) \quad (111)$$

and the other half of the terms of equations (109) and (110) can be presented in the second generic form

$$e^{-I \cdot \theta_{f_1}(t)} \cdot \sqrt{\epsilon} \cdot \left(\frac{\chi_{L52}(n)}{\left[-\Re \left(\frac{d}{ds} \left[-\frac{1}{2} \log\{\chi(f_1(s))\} \right]_{s=(1/2+I \cdot t)} \right] + \log(n) \right] \cdot n^{(1-(1/2+I \cdot t))}} \right) \cdot w(n) \quad (112)$$

where $w(n)$ describes that each term provides a weighted contribution $w(n) \leq 1$, in particular the $w(n)=1$ below where tapering of the endpoints occurs and $w(n)=0$ above the tapered endpoints and (ii) the second generic form arises from equations (16) and (23)

$$\frac{e^{I \cdot \theta_{f_1}(t)}}{\sqrt{\epsilon}} \cdot \epsilon \cdot \chi(f_1(1/2 + I \cdot t)) = e^{I \cdot \theta_{f_1}(t)} \cdot e^{-I \cdot 2 \cdot \theta_{f_1}(t)} \cdot \sqrt{\epsilon} = e^{-I \cdot \theta_{f_1}(t)} \sqrt{\epsilon} \iff s = 1/2 + I \cdot t \quad (113)$$

In practice, while the overall length of non-zero weighted terms of the truncated Dirichlet series in equations (108,109,110) is dependent on t being piecewise functions, the individual n , $w(n)$ and $\chi_{L52}(n)$ values are constants with respect to **infinitesimal changes** in t . ϵ is also a constant.

Hence, each single term of the dirichlet terms of equations (108,109,110) can be re-written as a triple product

$$\left\{ \frac{1}{\left[\Re \left(\frac{d}{ds} \left[-\frac{1}{2} \log\{\chi(f_1(s))\} \right] \right) - \log(n) \right]} \right\} \cdot \left\{ \frac{e^{I \cdot \theta_{f_1}(t)}}{n^{(1/2+I \cdot t)}} \right\} \cdot \left\{ \frac{w(n) \cdot \chi_{L52}(n)}{\sqrt{\epsilon}} \right\} \equiv A(s) \cdot B(s) \cdot C_{L52}(n) \quad (114)$$

$$\left\{ \frac{1}{\left[-\Re \left(\frac{d}{ds} \left[-\frac{1}{2} \log\{\chi(f_1(s))\} \right] \right) + \log(n) \right]} \right\} \cdot \left\{ \frac{e^{-I \cdot \theta_{f_1}(t)}}{n^{(1-(1/2+I \cdot t))}} \right\} \cdot \{w(n) \cdot \chi_{L52}(n) \cdot \sqrt{\epsilon}\} \equiv -A(s) \cdot D(s) \cdot C_{L52}(n) \cdot \epsilon \quad (115)$$

Using the chain rule, one obtains the generic form of the total derivative $\frac{d}{ds}$ for each dirichlet term of equations (108,109,110)

$$\frac{d}{ds} [A(s) \cdot B(s) \cdot C_{L52}(n)] = \left\{ \frac{dA(s)}{ds} \cdot B(s) + A(s) \cdot \frac{dB(s)}{ds} \right\} \cdot C_{L52}(n) \quad (116)$$

or

$$\frac{d}{ds} [-A(s) \cdot D(s) \cdot C_{L52}(n) \cdot \epsilon] = - \left\{ \frac{dA(s)}{ds} \cdot D(s) + A(s) \cdot \frac{dB(s)}{ds} \right\} \cdot C_{L52}(n) \cdot \epsilon \quad (117)$$

Since $A(s)$ in equations (116) and (117) for $L(\chi_5(2, .), s)$ is the same $A(s)$ in equations (68) and (69) for $L(\chi_5(3, .), s)$ therefore, $L(\chi_5(2, .), s)$ shares the same $\frac{dA(s)}{ds}$ behaviour on the critical line as $L(\chi_5(3, .), s)$. Equation (89) therefore applies to $L(\chi_5(2, .), s)$

$$\therefore \frac{d}{ds} \Re \left(\frac{d}{ds} \left[-\frac{1}{2} \log\{\chi(f_1(s))\} \right] \right)_{s=1/2+I \cdot t} = 0 \quad \forall \quad t \quad (118)$$

and hence

Which implies for equations (114-117) that the generic form of the total derivative $\frac{d}{ds}$ for each dirichlet term of equations (108,109,110) when calculated for $s = 1/2 + I \cdot t$ reduces to either

$$\frac{d}{ds} [A(s) \cdot B(s) \cdot C_{L52}(n)]_{s=1/2+I \cdot t} \Rightarrow \left\{ \underbrace{\frac{dA(s)}{ds}}_{=0, s=1/2+I \cdot t} \cdot B(s) + A(s) \cdot \frac{dB(s)}{ds} \right\} \cdot C_{L52}(n) \quad (119)$$

$$= A(s) \cdot \frac{dB(s)}{ds} \cdot C_{L52}(n)_{s=1/2+I \cdot t} \quad (120)$$

$$(121)$$

or

$$\frac{d}{ds} [-A(s) \cdot D(s) \cdot C_{L52}(n) \cdot \epsilon]_{s=1/2+I \cdot t} \Rightarrow - \left\{ \underbrace{\frac{dA(s)}{ds}}_{=0, s=1/2+I \cdot t} \cdot D(s) + A(s) \cdot \frac{dD(s)}{ds} \right\} \cdot C_{L52}(n) \cdot \epsilon \quad (122)$$

$$= -A(s) \cdot \frac{dD(s)}{ds} \cdot C_{L52}(n) \cdot \epsilon_{s=1/2+I \cdot t} \quad (123)$$

$$(124)$$

and given that $B(s)$ and $D(s)$ in equations (116) and (117) for $L(\chi_5(2, .), s)$ is the same $B(s)$ in equations (68) and (69) for $L(\chi_5(3, .), s)$

$$A(s) \cdot \frac{dB(s)}{ds}_{s=1/2+I \cdot t} = \left[\frac{1}{\left[\Re \left(\frac{d}{ds} \left[-\frac{1}{2} \log\{\chi(f_1(s))\} \right] \right) - \log(n) \right]} \cdot \frac{d}{ds} \left\{ \frac{e^{I \cdot \theta_{f1}(t)}}{n^{(1/2+I \cdot t)}} \right\} \right]_{s=1/2+I \cdot t} \quad (125)$$

$$= \left[\frac{1}{\left[\Re \left(\frac{d}{ds} \left[-\frac{1}{2} \log\{\chi(f_1(s))\} \right] \right) - \log(n) \right]} \cdot \frac{d}{ds} \left\{ e^{-\frac{1}{2} \log\{\chi(f_1(s))\}} \cdot e^{-s \cdot \log(n)} \right\} \right]_{s=1/2+I \cdot t} \quad (126)$$

$$= \left[\underbrace{\frac{d}{ds} \left[-\frac{1}{2} \log\{\chi(f_1(s))\} \right]}_{=1, s=1/2+I \cdot t} - \log(n) \cdot \left(e^{-\frac{1}{2} \log\{\chi(f_1(s))\}} \cdot e^{-s \cdot \log(n)} \right) \right]_{s=1/2+I \cdot t} \quad (127)$$

$$= \frac{e^{I \cdot \theta_{f1}(t)}}{n^{(1/2+I \cdot t)}}_{s=1/2+I \cdot t} \quad (128)$$

$$-A(s) \cdot \frac{dD(s)}{ds} \Big|_{s=1/2+I \cdot t} = - \left[\frac{1}{\left[\Re \left(\frac{d}{ds} \left[-\frac{1}{2} \log \{\chi(f_1(s))\} \right] \right) - \log(n) \right]} \cdot \frac{d}{ds} \left\{ \frac{e^{-I \cdot \theta_{f_1}(t)}}{n^{(1-(1/2+I \cdot t))}} \right\} \right]_{s=1/2+I \cdot t} \quad (129)$$

$$= - \left[\frac{1}{\left[\Re \left(\frac{d}{ds} \left[-\frac{1}{2} \log \{\chi(f_1(s))\} \right] \right) - \log(n) \right]} \cdot \frac{d}{ds} \left\{ e^{\frac{1}{2} \log \{\chi(f_1(s))\}} \cdot e^{s \cdot \log(n)} \right\} \right]_{s=1/2+I \cdot t} \quad (130)$$

$$= - \left[\underbrace{\frac{\frac{d}{ds} \left[\frac{1}{2} \log \{\chi(f_1(s))\} \right] + \log(n)}{\left[\Re \left(\frac{d}{ds} \left[-\frac{1}{2} \log \{\chi(f_1(s))\} \right] \right) - \log(n) \right]} \cdot \left(e^{\frac{1}{2} \log \{\chi(f_1(s))\}} \cdot e^{s \cdot \log(n)} \right)}_{=-1, s=1/2+I \cdot t} \right]_{s=1/2+I \cdot t} \quad (131)$$

$$= \frac{e^{-I \cdot \theta_{f_1}(t)}}{n^{(1-(1/2+I \cdot t))}} \Big|_{s=1/2+I \cdot t} \quad (132)$$

Therefore

$$\frac{d}{ds} \left[\left\{ \frac{1}{\left[\Re \left(\frac{d}{ds} \left[-\frac{1}{2} \log \{\chi(f_1(s))\} \right] \right) - \log(n) \right]} \right\} \cdot \left\{ \frac{e^{I \cdot \theta_{f_1}(t)}}{n^{(1/2+I \cdot t)}} \right\} \cdot \left\{ \frac{w(n) \cdot \chi_{L52}(n)}{\sqrt{\epsilon}} \right\} \right]_{s=1/2+I \cdot t} \quad (133)$$

$$\equiv \left[\frac{e^{I \cdot \theta_{f_1}(t)}}{\sqrt{\epsilon}} \cdot \frac{\chi_{L52}(n)}{n^{(1/2+I \cdot t)}} \cdot w(n) \right]_{s=1/2+I \cdot t} \quad (134)$$

$$\frac{d}{ds} \left[\left\{ \frac{1}{\left[-\Re \left(\frac{d}{ds} \left[-\frac{1}{2} \log \{\chi(f_1(s))\} \right] \right) + \log(n) \right]} \right\} \cdot \left\{ \frac{e^{-I \cdot \theta_{f_1}(t)}}{n^{(1-(1/2+I \cdot t))}} \right\} \cdot \{w(n) \cdot \chi_{L52}(n) \cdot \sqrt{\epsilon}\} \right]_{s=1/2+I \cdot t} \quad (135)$$

$$\equiv \left[e^{-I \cdot \theta_{f_1}(t)} \cdot \sqrt{\epsilon} \cdot \frac{\chi_{L52}(n)}{n^{(1-(1/2+I \cdot t))}} \cdot w(n) \right]_{s=1/2+I \cdot t} \quad (136)$$

which together covers all the dirichlet terms of equations (31,35,39) when $s = 1/2 + I \cdot t$.

That is, **on the critical line**, the total derivative of equations (108-110) produces a term by term agreement with approximations I, II and III (equations (31,35,39)) respectively for $L(\chi_5(2, \cdot), s)$.

It can be observed numerically that $\frac{dA(s)}{ds} \neq 0$ when $s \neq 1/2 + I \cdot t$ and so equations (108-110) are not sufficiently accurate away from the critical line.

The $N \bmod 5$ piecewise nature of the indefinite integral approximation equation (108)

In order to show the piecewise nature of the heuristic approximation equation (108) and its total derivative on the same graph with enough resolution of its approximation of the $L(\chi_5(2, .), s)$ non-trivial zero positions, the lowest t interval for 128 point tapering Dirichlet Series truncation at the second quiescent region approximations of the $L(\chi_5(2, .), s)$ function its Riemann Siegel Z function. Figure 10 displays along $s = 0.5 + I * t$ in the lowest possible interval $t = (46, 181)$ for 128 point tapering at the second quiescent region, the behaviour of (i) the **numerical total derivative** of equation (108) –imaginary part in violetred, real part in black–, (ii) the approximate indefinite integral equation (108) itself –imaginary part in red, real part in blue– and (iii) the high precision Pari-GP calculation of $\frac{e^{I\theta f_1(t)}}{\sqrt{\epsilon}} L(\chi_5(2, .), 1/2 + I \cdot t)$ the true Riemann Siegel Z function –imaginary part in gray, real part in green–. In practice, at the resolution of the graph, the **numerical total derivative** of equation (108) results (black and violetred) are completely overlayed by the true Riemann Siegel Z function (green and gray) since the difference between the two functions is very small.

The top row of figure 10 displays the approximate indefinite integral function, its numerical total derivative and the true Riemann Siegel Z function using the regular t scale, while the bottom row displays the functions using a $\sqrt{(\frac{t}{2\pi} \cdot 5)}$ transformed scale. Thus quasi-discontinuities in the indefinite integral at $\sqrt{(\frac{t}{2\pi} \cdot 5)} = \{6, 7, 8, 9, 10, 11, 12\}$ can be observed there are clearly mesoscale features, on the critical line, that are common (but not exactly the same) across the piecewise segments.

The real(indefinite integral equation (108)) shown in blue is smooth, hyperbolic in nature and changes character for each piecewise segment sequentially. Furthermore while the real(indefinite integral) shown in blue has curvature with respect to t , its total derivative (not the partial derivative with respect to t) numerically computed along the critical line and coinciding with the imag(Riemann Siegel Z function approximation) shown in violetred hidden behind the gray line of the true imaginary part of the Riemann Siegel Z function (on the critical line) is zero! This behaviour for the imaginary part of the **total derivative** of the indefinite integral implies that the imag(total derivative of the approximate indefinite integral equation (108)) has a $(\sigma - 1/2)$ multiplicative factor on the critical line. A similar behaviour (a $(\sigma - 1/2)$ multiplicative factor) was also interpreted for the numerical total derivative of the approximate indefinite integral of the $\zeta(1/2 + I \cdot t)$ Riemann Siegel Z function in [13].

The imag(indefinite integral equation (108)) shown in red has mesoscale features eg. the hyperbolic component changes behaviour each piecewise segment and contains fine scale features which dominate the contribution to its total derivative being (an approximation) of the $L(\chi_5(2, .), s)$ Riemann Siegel Z function.

To aid in highlighting the $\sqrt{\frac{t}{2\pi} \cdot 5} - \lfloor \sqrt{\frac{t}{2\pi} \cdot 5} \rfloor$ behaviour of the indefinite integral and the potential for a varying density of the relative position of the highest Riemann Siegel Z function peaks the bottom row of the figure 10 uses $\sqrt{\frac{t}{2\pi} \cdot 5} - \lfloor \sqrt{\frac{t}{2\pi} \cdot 5} \rfloor$ scaling of the t coordinate axis. This results in two widths of piecewise intervals of the approximate indefinite integral equation (108). Numerically, the height of the function at $(N)^2 \cdot \frac{2\pi}{5}$ while large does not appear to be infinity so the piecewise intervals are described as having quasi-discontinuities driven by the contribution of the Dirichlet Series term with $k \approx \sqrt{(\frac{t}{2\pi} \cdot 5)}$. On the bottom row it can be seen that the piecewise intervals for $N=[6,7],[7,8],[8,9],[11,12]$ have width $\Delta N = 1$ while the piecewise interval for $N[9,11]$ has width $\Delta N = 2$. On remembering that the dirichlet characters for $N \bmod 5 = 0$ are zero immediately suggests that the mesoscale quasi-discontinuities features are reflecting whether the dirichlet characters are zero or non-zero.

Following [13], with respect to interpreting the relative position of higher density of extreme peaks in figure 7, it is of interest whether at increasing t the mesoscale features of imag(indefinite integral equation (108)) settle down to particular relative positions.

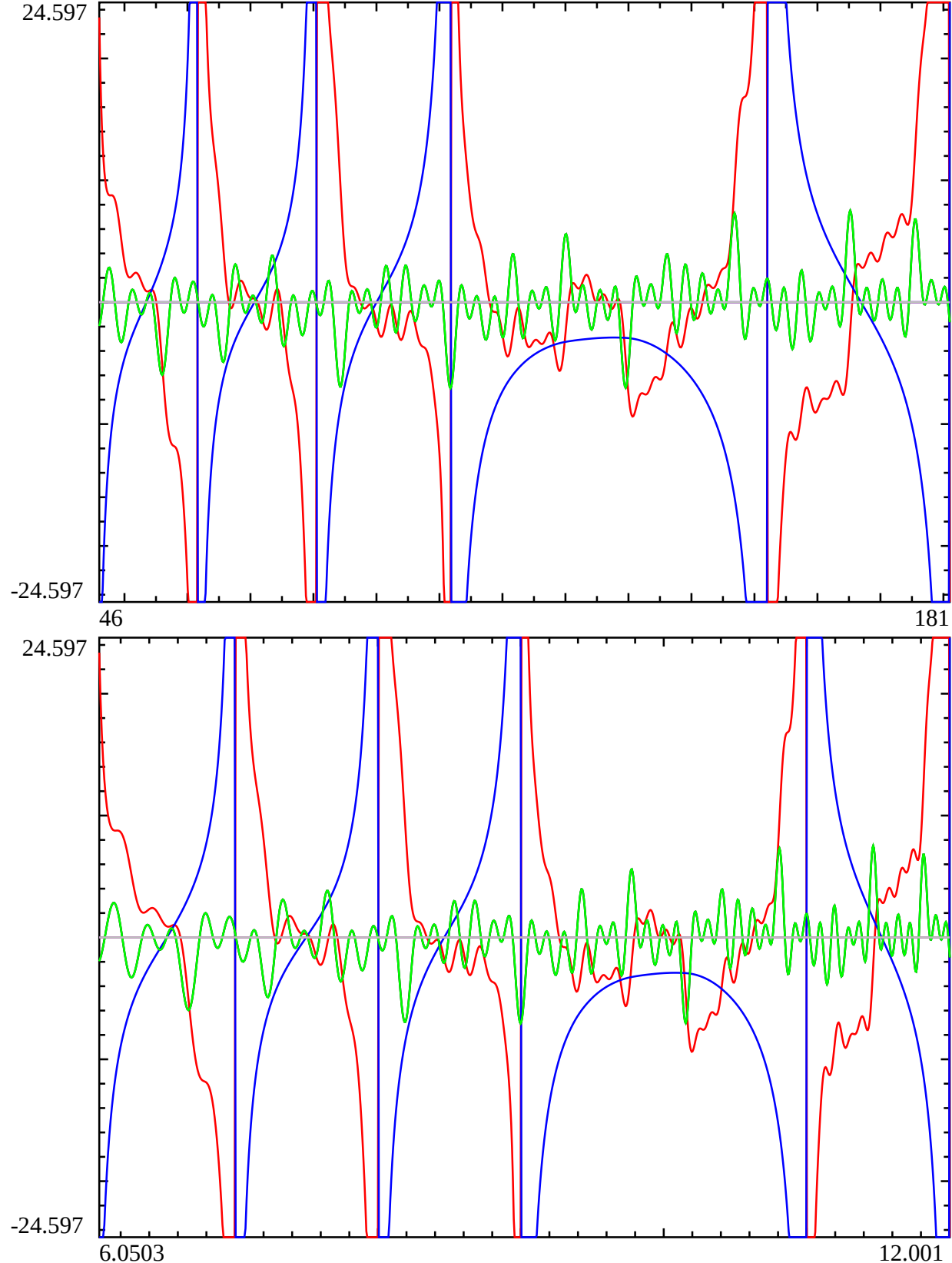


Figure 10: The behaviour of a heuristic approximation of the indefinite integral of the Riemann Siegel Z function for L52 **imag part in red, real part in blue**, its numerical derivative (approximating the Riemann Siegel Z function itself) real (imag) part shown in black (violet-red) based on **128 point end tapered** finite L52 Dirichlet Series sum (truncated at the second quiescent region) and the true L52 function (real (imag) part shown in green (gray)) along the critical line $s = 0.5 + I * t$ in the interval $t = (46, 181)$. The black, and violet-red lines of the real (imag) parts of the numerical total derivative of equation (4) are overlayed by the green, gray lines respectively of the true L52 L-function. From $t > 40.212$ ($64 \cdot \frac{t}{2\pi}$), **128 point end tapered** finite L52 Dirichlet Series sums provide an excellent approximation of the L52 function to many decimal places. First row displays the functions using regular t scale, while the second row displays the functions using $\sqrt{\frac{t-5}{2\pi}}$ scale. Thus qual44 discontinuities in the indefinite integral at $\sqrt{\frac{t-5}{2\pi}} = \{6, 7, 8, 9, 11\}$ can be observed and the mesoscale structure across each piecewise domain has a 5-periodic behaviour. There is no discontinuity at $\sqrt{\frac{t-5}{2\pi}} = \{10, 15, 20, \dots\}$ which is a mesoscale reflection of the **zero** Dirichlet character value for $\text{Mod}(N, 5) = 0$ for L52. The **real(Riemann Siegel Z function approximation for L52)** zeroes are turning points at the co-ordinates of $\text{imag}(\text{indefinite integral})$. While the **real(indefinite integral)** has curvature with respect to t , the **real(total derivative $\frac{d}{ds}$) (not $\frac{\partial}{\partial t}$)** numerically computed along the critical line and coinciding with the **imag(Riemann Siegel Z function approximation for L52)** is zero!

Differences in the piecewise nature of the indefinite integral approximations equations (108), (109) and (110) for the $L(\chi_5(2,.), s)$ Riemann Siegel Z function on the critical line.

Similar to [13], Figure 11 presents the normalised magnitude of the heuristic approximations equations (108,109,110) of the indefinite integral of the Riemann Siegel Z function of $L(\chi_5(2,.), s)$ **imag part in red, real part in blue** based on the finite Riemann Zeta Dirichlet Series sum truncated at the tapered second (lefthand column equation (108)), tapered first (middle column equation (109)) and first (righthand column equation (110)) quiescent regions along the critical line $s = 0.5 + I * t$ in various intervals $t = (46, 181)$, $t = (5148, 10958)$, $t = (50266, 53327)$, $t = (1256637, 12717110)$ and $t = (125663706, 125814548)$. The x axis is standardised by the transformation $\sqrt{\frac{t}{2\pi} \cdot 5}$. Importantly, very similar to [13] figure 11 shows that the y axis can be normalised to compare the heuristic approximation calculated values of the indefinite integral Riemann Siegel Z function for vastly different t values using a scaling factor of $(\frac{t}{2\pi} \cdot 5)^{0.25}$.

With respect to the piecewise nature of the indefinite integral approximations equations (108), (109) and (110) for the $L(\chi_5(2,.), s)$ Riemann Siegel Z function on the critical line, the normalised y scale shows that

1. there is little evolution of the real(equation(108)) shown in blue (lefthand column) with the smooth hyperbolic lineshapes becoming more symmetric with each $[N, N+1]$ interval while the real(equations(109,110)) remain zero (on the critical line) as t increases.
2. the evolution of the imag(equations(108,109,110)) shown in red can clearly be seen with the sharpening of mesoscale features that vary across the $[N, N+1]$ piecewise intervals. The imag(equation(109)) (middle column) behaviour is close to the imag(equation(108)) (lefthand column) behaviour but imag(equation(110)) (righthand column) clearly displays large differences at the righthand end of the $[N, N+1]$ piecewise intervals. (On careful examination there are also differences at the lefthand end of the $[N, N+1]$ piecewise intervals of the imag(equation(110)) (righthand column) behaviour compared to the other two indefinite integral approximations.)

In [13] the mesoscale features of the approximate indefinite integrals of the Riemann Siegel Z function of the ζ function on the critical line changed sign every piecewise interval $[N, N+1]$. For $L(\chi_5(2,.), s)$ the rate of sign change is observed to occur every tenth piecewise interval.

Figure 12 attempts to juxtapose (i) the mesoscale features of imag(equation(109)) for $N=\{10000-10004\}$ top row, (ii) the mesoscale features of imag(equation(109)) for $N=\{3000-3004\}$ second row, (iii) the $N \bmod 5$ behaviour of the extreme peaks for $N=\{0-3000\}$ under $\sqrt{\frac{t}{2\pi} \cdot 5} - \left\lfloor \sqrt{\frac{t}{2\pi} \cdot 5} \right\rfloor$ transformation middle row, (ii) the mesoscale features of imag(equation(109)) for $N=\{3005-3009\}$ second row and (ii) the mesoscale features of imag(equation(109)) for $N=\{10005-10009\}$ bottom row. Such a vertical juxtaposition helps clearly display the $N \bmod 10$ change in sign of the mesoscale features of the approximate indefinite integral of $L(\chi_5(2,.), s)$ Riemann Siegel Z function on the critical line. The vertical juxtaposition also indicates that the higher density in the relative position of the extreme peaks in the $L(\chi_5(2,.), s)$ Riemann Siegel Z function on the critical line (middle row) align well with regions of higher curvature in the approximate indefinite integral of $L(\chi_5(2,.), s)$ Riemann Siegel Z function on the critical line that occur with $N \bmod 5$ periodicity.

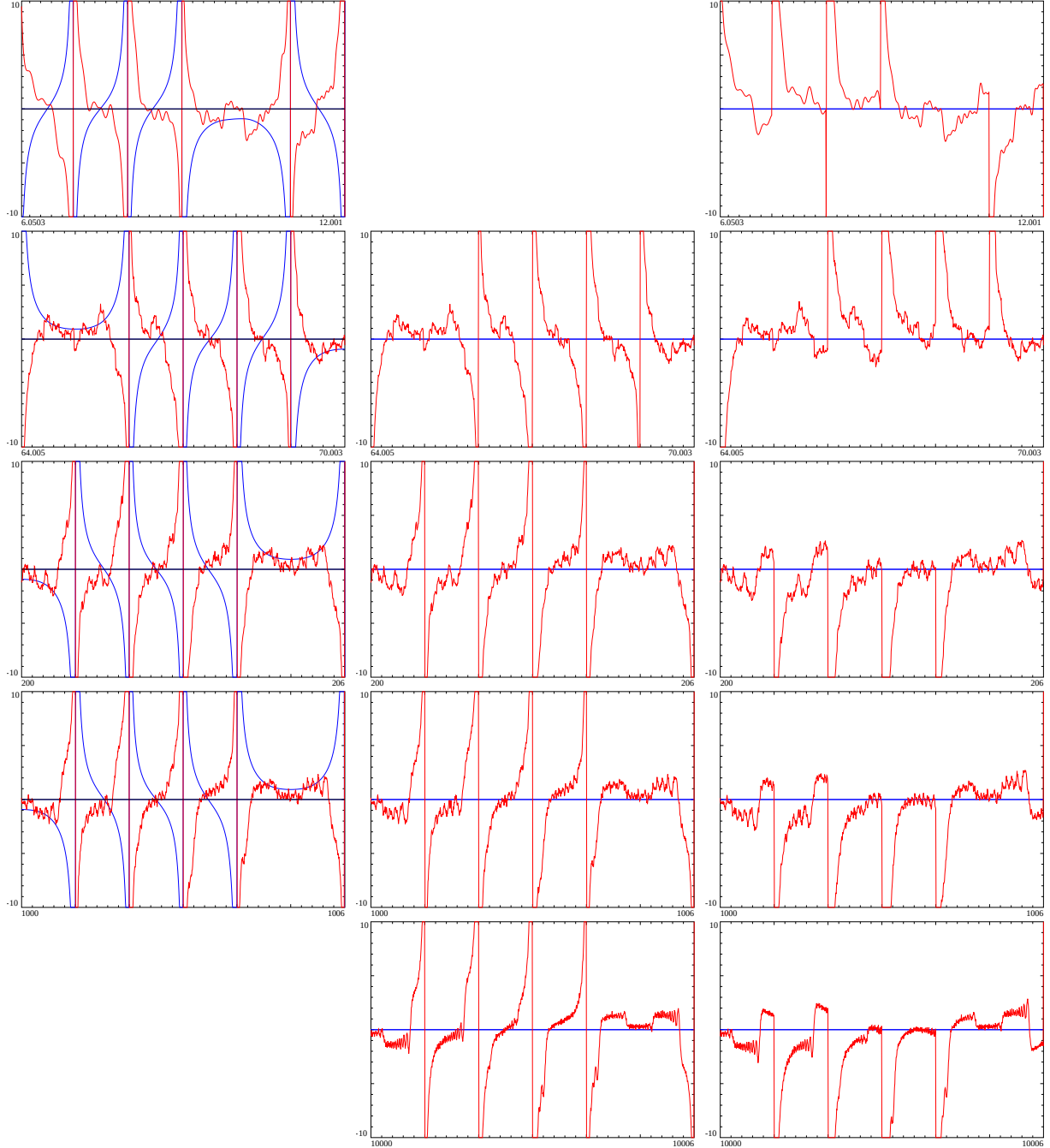


Figure 11: The normalised magnitude of the heuristic approximations equations (108,109,110) (using $\left(\frac{t \cdot 5}{2\pi}\right)^{0.25}$ scaling) of the indefinite integral of the Riemann Siegel Z function of L52 **imag part in red, real part in blue** based on the finite L52 Dirichlet Series sum truncated at the tapered second (lefthand column), tapered first (middle column) and first (righthand) quiescent region along the critical line $s = 0.5 + I * t$ in various intervals $t = (46, 181)$ top row, $t = (5148, 10958)$ second row, $t = (50266, 53327)$ third row, $t = (1256637, 12717110)$ fourth row and $t = (125663706, 125814548)$ bottom row where the horizontal axis uses a $\sqrt{\left(\frac{t \cdot 5}{2\pi}\right)}$ transformed scale. Mesoscale features are observed to evolve as t increases for the three approximations. The real component of equation (4) shown in blue (i) has a minimum absolute magnitude that depends on $\text{Mod}(N,5)$ and (ii) $\text{Mod}(N,10)$ behaviour for the sign of the mesoscale features but (iii) the magnitude scales as $\left(\frac{t \cdot 5}{2\pi}\right)^{0.25}$. The gaps in the grid of graphs occur where an approximation is infeasible (below the tapering limit) or calculationally much slower to obtain.

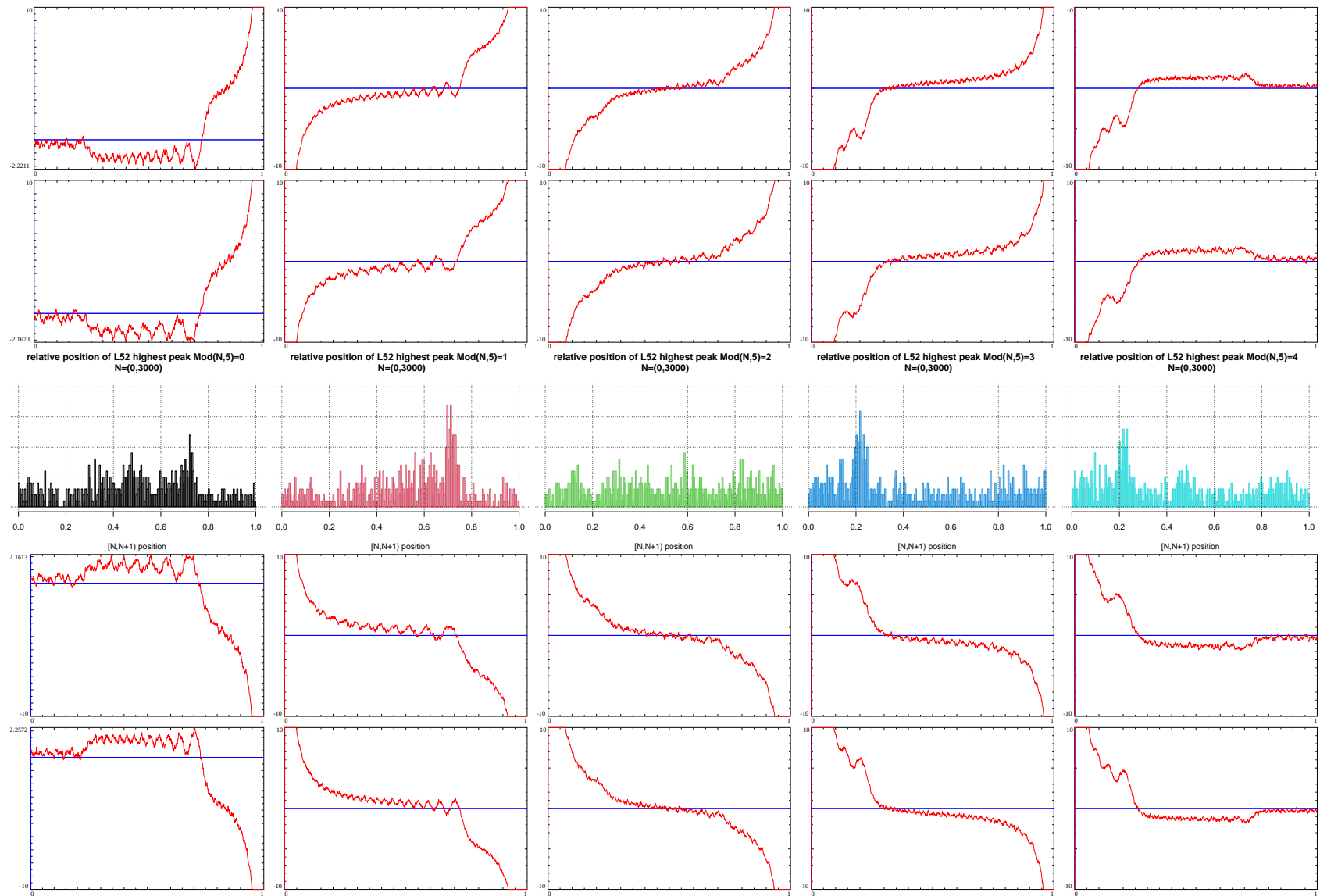


Figure 12: A vertical comparison of the distribution of the highest peaks (absolute magnitude) in $[N, N + 1]$ intervals on the critical line $s = 1/2 + I \cdot t$ where $N = \{0,..,3000\}$ for L52 and $t = N^2 \cdot \frac{2\pi}{5}$ segmented by $N \bmod 5 = \{0,1,2,3,4\}$ (middle row) with the mesoscale structure features clearly visible at higher t in a heuristic approximation of the imaginary component of the indefinite integral of the Riemann Siegel Z function of L52 along the critical line arranged in order by the intervals $[N, N + 1] \bmod 10$ where $N =$ (i) top row - $\{10000, 10001, 10002, 10003, 10004\}$, (ii) second row - $\{3000, 3001, 3002, 3003, 3004\}$, (iii) fourth row - $\{3005, 3006, 3007, 3008, 3009\}$ and (iv) bottom row - $\{10005, 10006, 10007, 10008, 10009\}$

Relative position of $f_1(1/2 + I \cdot t)$ extreme peaks under $(\sqrt{\frac{t \cdot 5}{2\pi}} - \lfloor \sqrt{\frac{t \cdot 5}{2\pi}} \rfloor)$ transformation

The lefthand column in Figure 13 presents the $N \bmod 5$ $(\sqrt{\frac{t \cdot 5}{2\pi}} - \lfloor \sqrt{\frac{t \cdot 5}{2\pi}} \rfloor)$ behaviour of the distribution of the relative position of extreme Riemann Siegel peaks from every piecewise interval $[N^2 \cdot \frac{2\pi}{5}, (N+1)^2 \cdot \frac{2\pi}{5}]$ obtained for $N=\{0,3000\}$ for $f_1(s)$, on the critical line. The estimates were obtained using equations (21), (32), (36) and (51).

Rows 1-5 presents the extreme peaks data for 3001 piecewise interval segmented by $N \bmod 5 = \{0, 1, 2, 3, 4\}$ respectively.

The righthand column in Figure 13 presents the growth in the absolute magnitude of the extreme Riemann Siegel Z function peak height on the critical line as a function of $\log(t)$ for $N \bmod 5 = \{0, 1, 2, 3, 4\}$ (shown in black, red, green, blue, cyan) overlayed on the total dataset (shown in gray).

In the lefthand column it can be seen that there is some evidence of a higher density of extreme peaks at particular relative positions depending on $N \bmod 5$ for $f_1(s)$.

In the righthand column there is weaker evidence that $N \bmod 5 = 2$ peaks (second and fourth rows in red and blue respectively) for $f_1(s)$ may tend to have slightly higher extreme peaks than the other $N \bmod 5$ values.

Table 3 gives a snapshot of the numerical comparison between the absolute magnitude of peak heights obtained at the highest t investigated via (i) spectrally filtered finite Euler Product estimates truncated at the first quiescent region equation (51) and (ii) tapered Dirichlet Series estimates with truncation at the first quiescent region equation (36). Also included is the grid point of the peak, the value of grid point in the interval $[N, N+1]$ and the relative position of the peak in the interval $[0, 1]$. The grid point spacing was $\Delta t = 0.05$ starting from $t = N^2 \cdot \frac{2\pi}{5}$ for each successive piecewise interval $N=\{0,3000\}$.

Table 3: Grid search results $f_1(s)$ for $N=2995-3000$. A comparison of fourier transform filtered Euler Product estimate and 128 point tapered Dirchlet Series estimate based peak heights both using truncation at the first quiescent region $N_1 = \left\lfloor \sqrt{\frac{t}{2\pi} \cdot 5} \right\rfloor$

t value of peak	$\sqrt{\frac{t}{2\pi} \cdot 5}$	$\sqrt{\frac{t}{2\pi} \cdot 5} - \left\lfloor \sqrt{\frac{t}{2\pi} \cdot 5} \right\rfloor$	filtered Euler Product estimate	tapered Dirichlet series estimate
11279428.369541 2995.978		0.9779541	24.98782	24.98585
11285347.619641 2996.764		0.7639698	27.16637	27.17009
11290863.745550 2997.496		0.4962693	28.11350	28.11372
11296365.934734 2998.227		0.2265404	27.37248	27.37673
11307801.287191 2999.744		0.7437144	28.12553	28.12361
11314341.152923 3000.611		0.6110397	24.48103	24.48167

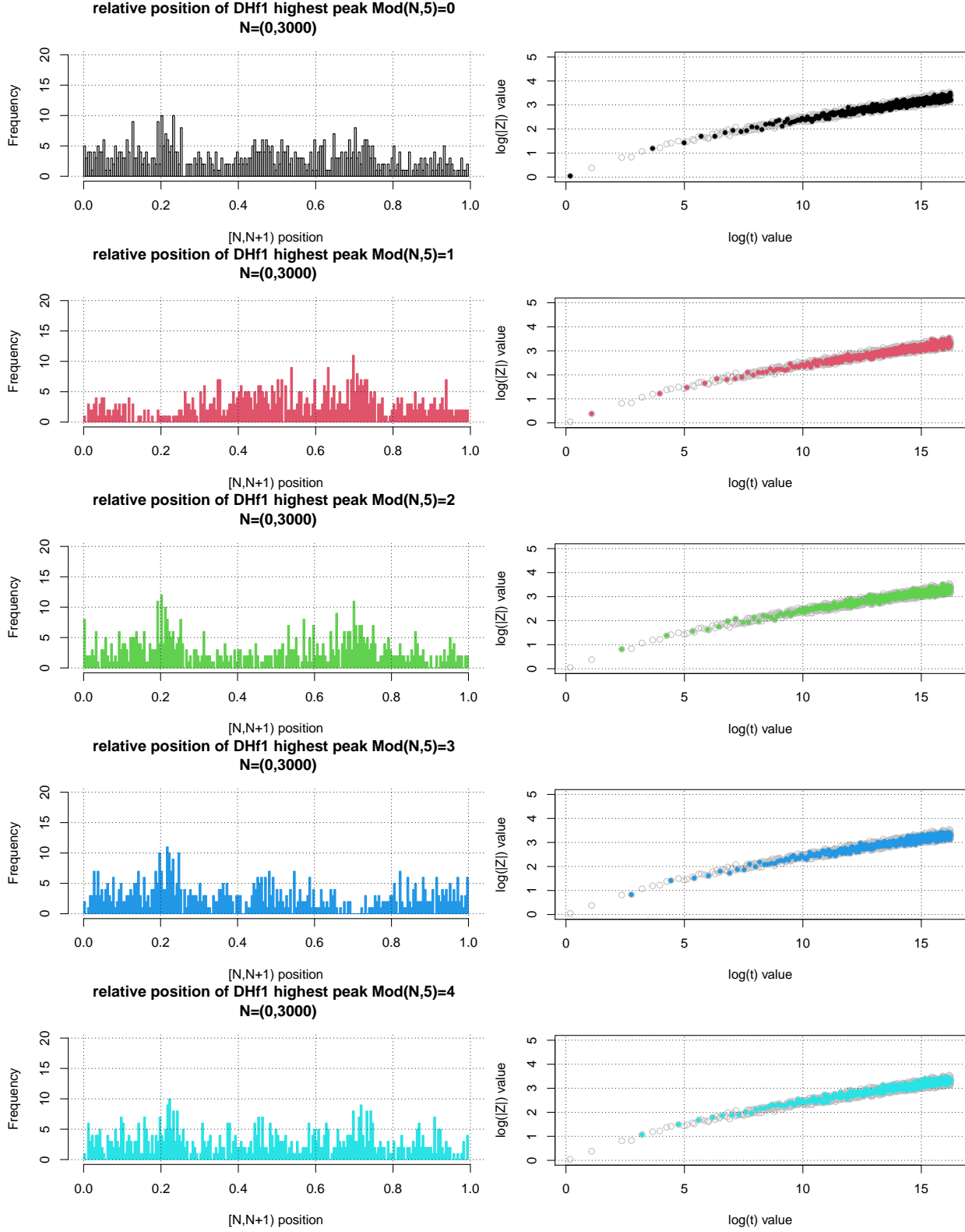


Figure 13: **Lefthand column** - Distribution of highest peaks of the Riemann Siegel Z function analogue of DHf1 and its approximations within each $[N^2 \cdot 2 \cdot \pi/5, (N + 1)^2 \cdot 2 \cdot \pi/5]$ piecewise interval segmented according to $N \bmod 5 = \{0, 1, 2, 3, 4\}$ (top row to bottom row) for $N=\{0-3000\}$ using their normalised positions $\sqrt{\frac{t-5}{2\pi}} - \lfloor \sqrt{\frac{t-5}{2\pi}} \rfloor$. **Righthand column** - Overlay of growth of largest Riemann Siegel Z function peaks from each given Mod(N,5) intervals compared to all $[N^2 \cdot 2 \cdot \pi/5, (N + 1)^2 \cdot 2 \cdot \pi/5]$ intervals.

Accuracy performance of dirichlet series based approximations I, II and III for the Riemann Siegel Z function analogue of $f_1(s)$

Figures 14 and 15 provide an accuracy assessment of equations (32,36,40) in approximating the Riemann Siegel Z function for $f_1(s)$ on the critical line, for the two intervals $t=(46,126)$ and $t=(5800,5820)$ respectively.

The left column of Figure 14 shows an overlay of the real (green) and imaginary (black) parts of equations (32) (top row) and (40) (bottom row) respectively with the real (red) and imaginary (blue) parts of the true Riemann Siegel Z function for $f_1(s)$. The right column of Figure 14 shows the real and imaginary parts (shown in red and green respectively) of the differences with the true Riemann Siegel Z function – top row numerical($\frac{d}{ds}$ (equation (32)) $-e^{I\theta_{f_1}(t)} \cdot f_1(1/2+I \cdot t)$), – bottom row numerical ($\frac{d}{ds}$ (equation (40)) $-e^{I\theta_{f_1}(t)} \cdot f_1(1/2+I \cdot t)$).

The left column of Figure 15 shows an overlay of the real (green) and imaginary (black) parts of equations (32) (top row), (36) (middle row) and (40) (bottom row) respectively with the real (red) and imaginary (blue) parts of the true Riemann Siegel Z function for $f_1(s)$. The right column of Figure 15 shows the real and imaginary parts (shown in red and green respectively) of the differences with the true Riemann Siegel Z function – top row numerical($\frac{d}{ds}$ (equation (32)) $-e^{I\theta_{f_1}(t)} \cdot f_1(1/2+I \cdot t)$), – middle row numerical ($\frac{d}{ds}$ (equation (36)) $-e^{I\theta_{f_1}(t)} \cdot f_1(1/2+I \cdot t)$), – bottom row numerical ($\frac{d}{ds}$ (equation (40)) $-e^{I\theta_{f_1}(t)} \cdot f_1(1/2+I \cdot t)$). At $t=(5800,5820)$, the high precision $f_1(s)$ Pari-GP functions the required runtime exceeded 20 hours to complete 1000 data points on a single thread.

From the two figures,

- equation (32) has excellent multi decimal place agreement with $e^{I\theta_{f_1}(t)} \cdot f_1(1/2+I \cdot t)$ with an oscillating residual error contribution monotonically decreasing with t except for nuisance higher error spikes at $\sqrt{(\frac{t}{2\pi} \cdot 5)} = \left\lfloor \sqrt{(\frac{t}{2\pi} \cdot 5)} \right\rfloor$
- equation (40) has small visible systematic deviations from $e^{I\theta_{f_1}(t)} \cdot f_1(1/2+I \cdot t)$. The visible systematic difference, in principle, will be analogous to the first order Riemann Siegel formula (catenary shaped) correction for $\zeta(s)$ however figure 2 indicates that such a first order Riemann Siegel formula correction for $f_1(s)$ has an $N \bmod 5$ behaviour with jump discontinuities at $\sqrt{(\frac{t}{2\pi} \cdot 5)} = \left\lfloor \sqrt{(\frac{t}{2\pi} \cdot 5)} \right\rfloor$ and varying correction lineshape dependence where $N = \left\lfloor \sqrt{(\frac{t}{2\pi} \cdot 5)} \right\rfloor$.
- equation (36) has smaller but still systematic deviations than equation (40) because equation (36) includes tapering which should introduce higher order corrections to equation (40).

Thus equations (32,36,40) on the critical line provide good performance in approximating $e^{I\theta_{f_1}(t)} \cdot f_1(1/2+I \cdot t)$ the Riemann Siegel Z function for $f_1(s)$ on the critical line.

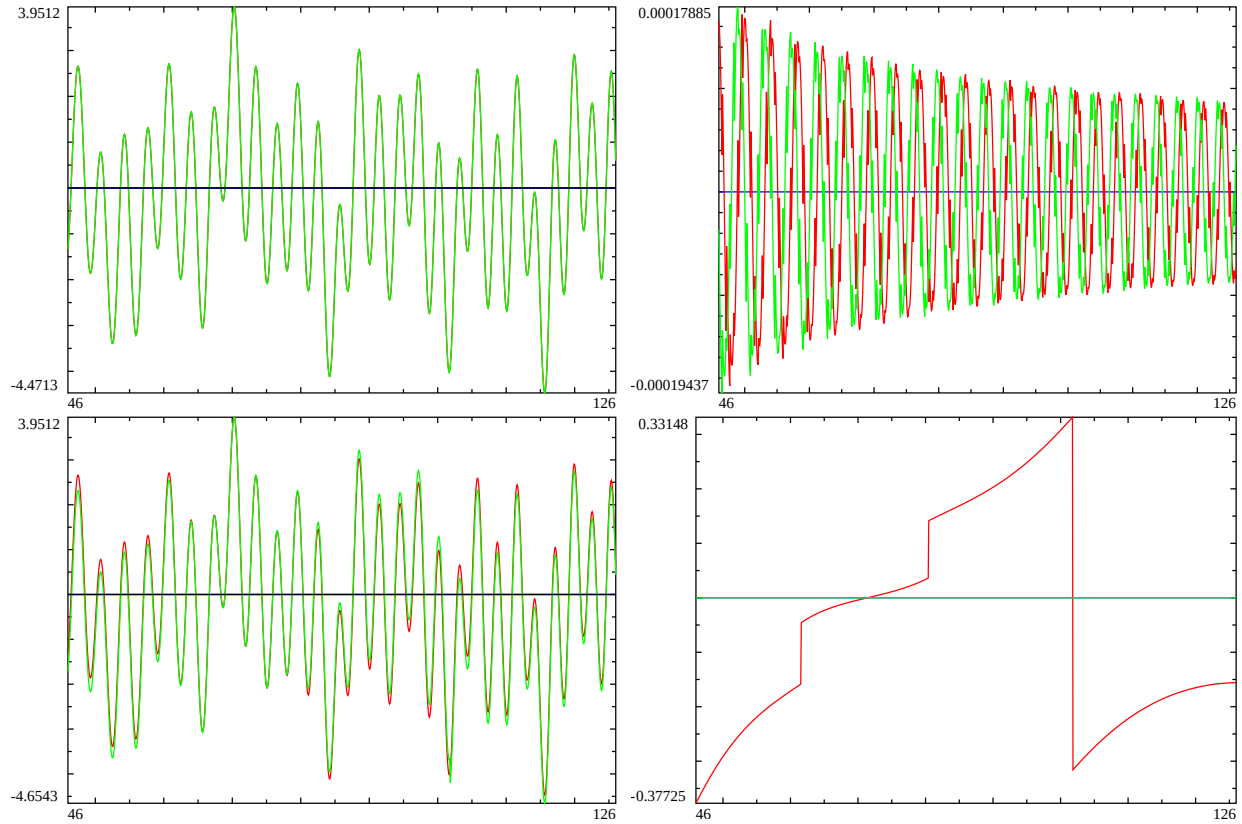


Figure 14: On the critical line, for the interval $t=(46,126)$. Left column - A overlay of real and imaginary components of Riemann Siegel Z function of DHf1 (red and blue) and and equations (32), (40) (green and black) in top (bottom row). Right column - the difference in the real (red) and imaginary (green) components of approximations I and III and the true Riemann Siegel Z function for DHf1.

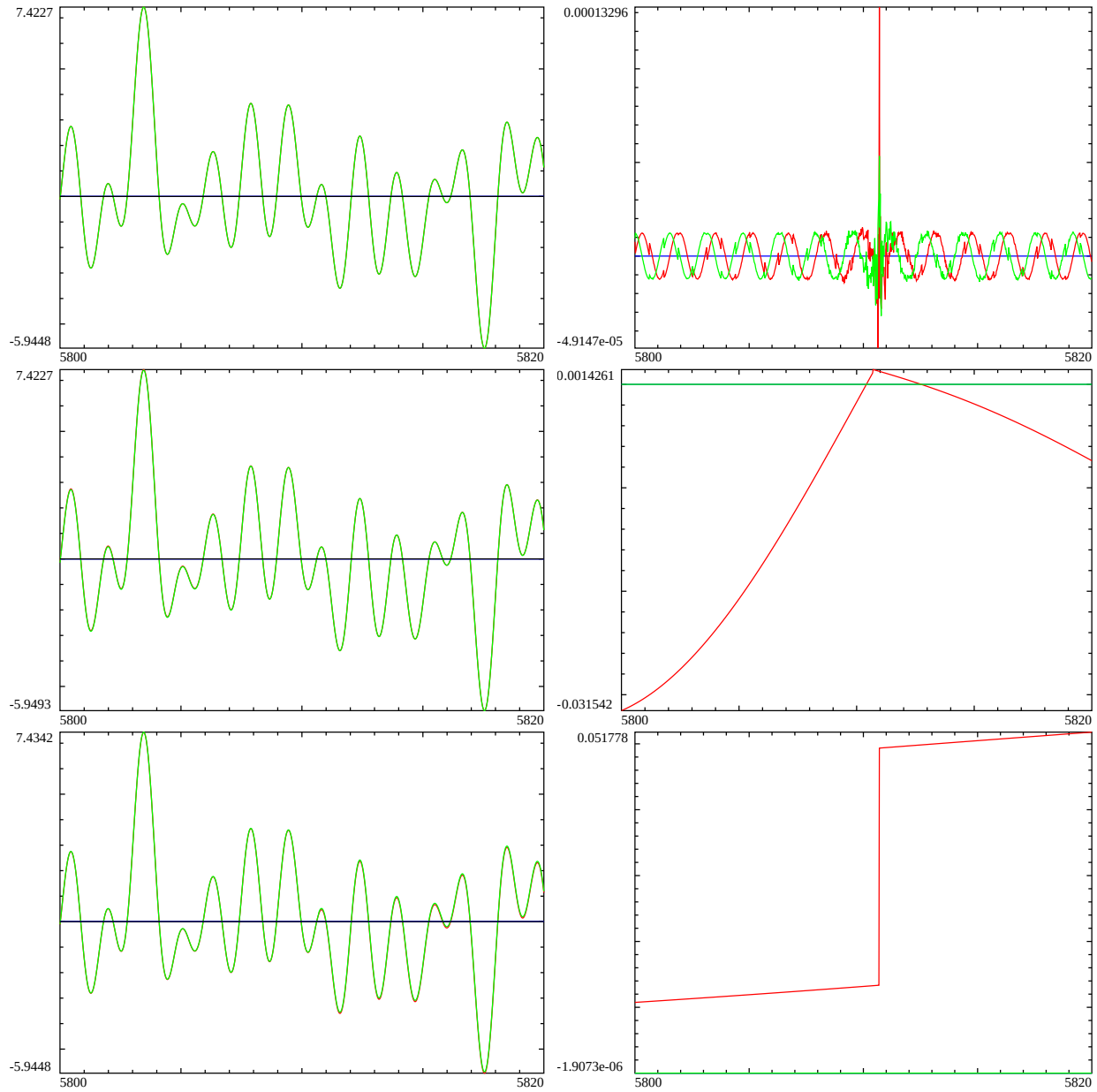


Figure 15: On the critical line, for the interval $t=(5800,5820)$. Left column - A overlay of real and imaginary components of Riemann Siegel Z function of DHf1 (red and blue) and equations (32), (36) and (40) (green and black) in top, middle and bottom row. Right column - the difference in the real (red) and imaginary (green) components of approximations I, II, III and the true Riemann Siegel Z function for DHf1.

A heuristic approximation for the indefinite integrals of the Riemann Siegel Z function analogue of tapered and untapered finite $f_1(s)$ function Dirichlet Series truncated at the second and first quiescent regions

Following [13] a possible approach to investigating insights into the $\sqrt{\frac{t}{2\pi}} - \left\lfloor \sqrt{\frac{t}{2\pi}} \right\rfloor$ behaviour of Riemann Siegel Z function peak height of $f_1(s)$ would be to investigate approximations for the first principles calculation of the indefinite integral of the Riemann Siegel Z function.

Therefore in this paper, co-opting [13] the following three critical line heuristic approximations of the indefinite integral of the Riemann Siegel Z function of $f_1(s)$ are attempted

(i) tapered truncation at the second quiescent region for $f_1(s)$ Dirichlet Series $\left\lfloor \frac{t}{\pi} \cdot 5 \right\rfloor$

$$\begin{aligned} & \left(\int e^{-\frac{1}{2} \log \chi(f_1(s))} f_1(s) ds \right)_{s=1/2+I \cdot t, \left\lfloor \frac{t}{\pi} \cdot 5 \right\rfloor, \text{tapered}} \\ & \approx e^{I \cdot \theta_{f_1}(t)} \cdot \left[\sum_{n=1}^{\left(\left\lfloor \frac{t}{\pi} \cdot 5 \right\rfloor - p \right)} \left(\frac{\chi_{f_1}(n)}{\left[\Re \left(\frac{d}{ds} \left[-\frac{1}{2} \log \{\chi(f_1(s))\} \right]_{s=(1/2+I \cdot t)} \right) - \log(n) \right] \cdot n^{(1/2+I \cdot t)}} \right) \right. \\ & \quad \left. + \sum_{i=(-p+1)}^p \frac{\frac{1}{2^{2p}} \left(2^{2p} - \sum_{k=1}^{i+p} \binom{2p}{2p-k} \right) \cdot \chi_{f_1}(\left\lfloor \frac{t}{\pi} \cdot 5 \right\rfloor + i)}{\left(\left[\Re \left(\frac{d}{ds} \left[-\frac{1}{2} \log \{\chi(f_1(s))\} \right]_{s=(1/2+I \cdot t)} \right) - \log(\left\lfloor \frac{t}{\pi} \cdot 5 \right\rfloor + i) \right] \cdot (\left\lfloor \frac{t}{\pi} \cdot 5 \right\rfloor + i)^{(1/2+I \cdot t)}} \right], t \rightarrow \infty \right] \end{aligned} \quad (137)$$

(ii) tapered truncation at the first quiescent region $N_2 = \left\lfloor \sqrt{\frac{t}{2\pi} \cdot 5} \right\rfloor$ for $f_1(s)$ Dirichlet Series

$$\begin{aligned} & \left(\int e^{-\frac{1}{2} \log \chi(f_1(s))} f_1(s) ds \right)_{s=1/2+I \cdot t, \left\lfloor \sqrt{\frac{t}{2\pi} \cdot 5} \right\rfloor, \text{tapered}} \\ & \approx e^{I \cdot \theta_{f_1}(t)} \cdot \left[\sum_{n=1}^{\left(\left\lfloor \sqrt{\frac{t}{2\pi} \cdot 5} \right\rfloor - p \right)} \left(\frac{\chi_{f_1}(n)}{\left[\Re \left(\frac{d}{ds} \left[-\frac{1}{2} \log \{\chi(f_1(s))\} \right]_{s=(1/2+I \cdot t)} \right) - \log(n) \right] \cdot n^{(1/2+I \cdot t)}} \right) \right. \\ & \quad \left. + \sum_{i=(-p+1)}^p \frac{\frac{1}{2^{2p}} \left(2^{2p} - \sum_{k=1}^{i+p} \binom{2p}{2p-k} \right) \cdot \chi_{f_1}(\left\lfloor \sqrt{\frac{t}{2\pi} \cdot 5} \right\rfloor + i)}{\left(\left[\Re \left(\frac{d}{ds} \left[-\frac{1}{2} \log \{\chi(f_1(s))\} \right]_{s=(1/2+I \cdot t)} \right) - \log(\left\lfloor \sqrt{\frac{t}{2\pi} \cdot 5} \right\rfloor + i) \right] \cdot (\left\lfloor \sqrt{\frac{t}{2\pi} \cdot 5} \right\rfloor + i)^{(1/2+I \cdot t)}} \right. \\ & \quad \left. + \chi_{f_1}(1/2 + I \cdot t) \cdot \left(\sum_{n=1}^{\left(\left\lfloor \sqrt{\frac{t}{2\pi} \cdot 5} \right\rfloor - p \right)} \left(\frac{\chi_{f_1}(n)}{\left[-\Re \left(\frac{d}{ds} \left[-\frac{1}{2} \log \{\chi(f_1(s))\} \right]_{s=(1/2+I \cdot t)} \right) + \log(n) \right] \cdot n^{(1-(1/2+I \cdot t))}} \right) \right. \right. \\ & \quad \left. \left. + \sum_{i=(-p+1)}^p \frac{\frac{1}{2^{2p}} \left(2^{2p} - \sum_{k=1}^{i+p} \binom{2p}{2p-k} \right) \cdot \chi_{f_1}(\left\lfloor \sqrt{\frac{t}{2\pi} \cdot 5} \right\rfloor + i)}{\left(\left[-\Re \left(\frac{d}{ds} \left[-\frac{1}{2} \log \{\chi(f_1(s))\} \right]_{s=(1/2+I \cdot t)} \right) + \log(\left\lfloor \sqrt{\frac{t}{2\pi} \cdot 5} \right\rfloor + i) \right] \cdot (\left\lfloor \sqrt{\frac{t}{2\pi} \cdot 5} \right\rfloor + i)^{(1-(1/2+I \cdot t))}} \right) \right], t \rightarrow \infty \right] \end{aligned} \quad (138)$$

(ii) truncation at the first quiescent region $N_1 = \left\lfloor \sqrt{\frac{t}{2\pi} \cdot 5} \right\rfloor$ for $f_1(s)$ Dirichlet Series

$$\begin{aligned}
& \left(\int e^{-\frac{1}{2} \log \chi(f_1(s))} f_1(s) ds \right)_{s=1/2+I \cdot t, \lfloor \sqrt{\frac{t}{2\pi} \cdot 5} \rfloor, \text{tapered}} \\
& \approx e^{I \cdot \theta_{f_1}(t)} \cdot \left[\sum_{n=1}^{\lfloor \sqrt{\frac{t}{2\pi} \cdot 5} \rfloor} \left(\frac{\chi_{f_1}(n)}{\left[\Re \left(\frac{d}{ds} \left[-\frac{1}{2} \log \{\chi(f_1(s))\} \right]_{s=(1/2+I \cdot t)} \right] - \log(n) \right] \cdot n^{(1/2+I \cdot t)}} \right) \right. \\
& \quad \left. + \chi_{f_1}(1/2 + I \cdot t) \cdot \left(\sum_{n=1}^{\lfloor \sqrt{\frac{t}{2\pi} \cdot 5} \rfloor} \left(\frac{\chi_{f_1}(n)}{\left[-\Re \left(\frac{d}{ds} \left[-\frac{1}{2} \log \{\chi(f_1(s))\} \right]_{s=(1/2+I \cdot t)} \right] + \log(n) \right] \cdot n^{(1-(1/2+I \cdot t))}} \right) \right), t \rightarrow \infty \right. \\
& \quad \left. \right) \tag{139}
\end{aligned}$$

where

1. $\Re \left(\frac{d}{ds} \left[-\frac{1}{2} \log \{\chi(f_1(s))\} \right]_{s=(1/2+I \cdot t)} \right) \equiv \frac{\partial}{\partial t} [\theta_{f_1}(t)]$ on the critical line and
2. the nomenclature $e^{-\frac{1}{2} \log \chi(f_1(s))}$ is used to avoid confusion with the real valued Riemann Siegel Theta function ($\theta_{f_1}(t) = -\frac{1}{2} \cdot \text{imag} \left[\log \left(\chi(f_1(1/2 + I \cdot t)) \right) \right]$) see equation (25) which applies only to the critical line.
3. $-\frac{1}{2} \log \{\chi(f_1(s))\}$ appears as "vthetaf1(z)" in the code snippet presented earlier in the paper.

As shown in figure 17, the across the horizontal axis for the real part of equation (137) has symmetry in magnitude and the real parts of equations (138) & (139) on the critical line are zero. Therefore the integration constant(s) explicitly required for the indefinite integral approximations given by equations (137,138,139) have all been set to zero.

As discussed below, a crucial part of the approximation prescription is explicitly using only $\Re \left(\frac{d}{ds} \left[-\frac{1}{2} \log \{\chi(f_1(s))\} \right] \right)$ and its role in terms of delivering a total derivative estimation that is equivalent to the approximations I (II and III) for the Riemann Siegel Z function of the $f_1(s)$ is examined.

Total derivative behaviour of individual terms of equations (137,138,139) on the critical line

To be useful heuristic approximations of the indefinite integral of the Riemann Siegel Z function for the 1st degree 5-periodic function $f_1(s)$ the total derivatives $\frac{d}{ds}$ (equations(137, 138, 139)) must result in useful approximations of the $f_1(s)$ Riemann Siegel Z function and ideally be equivalent to equations (32), (36) and (40).

In the following discussion, it is demonstrated that there is a term by term agreement **on the critical line** between $\frac{d}{ds}$ (equations(137, 138, 139)) and approximations I,II,III.

Firstly a single term of the dirichlet terms of equation (137) and half the terms of equations (138) and (139) can be presented in the generic form

$$e^{I \cdot \theta_{f_1}(t)} \cdot \left(\frac{\chi_{f_1}(n)}{\left[\Re \left(\frac{d}{ds} \left[-\frac{1}{2} \log \{\chi(f_1(s))\} \right]_{s=(1/2+I \cdot t)} \right] - \log(n) \right] \cdot n^{(1/2+I \cdot t)}} \right) \cdot w(n) \tag{140}$$

and the other half of the terms of equations (138) and (139) can be presented in the second generic form

$$e^{-I \cdot \theta_{f1}(t)} \cdot \left(\frac{\chi_{f1}(n)}{\left[-\Re \left(\frac{d}{ds} \left[-\frac{1}{2} \log \{ \chi(f_1(s)) \} \right]_{s=(1/2+I \cdot t)} \right) + \log(n) \right] \cdot n^{(1-(1/2+I \cdot t))}} \right) \cdot w(n) \quad (141)$$

where $w(n)$ describes that each term provides a weighted contribution $w(n) \leq 1$, in particular the $w(n)=1$ below where tapering of the endpoints occurs and $w(n)=0$ above the tapered endpoints and (ii) the second generic form arises from equations (7) and (23)

$$e^{I \cdot \theta_{f1}(t)} \cdot \chi(f_1(1/2 + I \cdot t)) = e^{I \cdot \theta_{f1}(t)} \cdot e^{-I \cdot 2 \cdot \theta_{f1}(t)} = e^{-I \cdot \theta_{f1}(t)} \iff s = 1/2 + I \cdot t \quad (142)$$

In practice, while the overall length of non-zero weighted terms of the truncated Dirichlet series in equations (137,138,139) is dependent on t being piecewise functions, the individual n , $w(n)$ and $\chi_{f1}(n)$ values are constants with respect to **infinitesimal changes** in t .

Hence, each single term of the dirichlet terms of equations (137,138,139) can be re-written as a triple product

$$\left\{ \frac{1}{\left[\Re \left(\frac{d}{ds} \left[-\frac{1}{2} \log \{ \chi(f_1(s)) \} \right] \right) - \log(n) \right]} \right\} \cdot \left\{ \frac{e^{I \cdot \theta_{f1}(t)}}{n^{(1/2+I \cdot t)}} \right\} \cdot \{w(n) \cdot \chi_{f1}(n)\} \equiv A(s) \cdot B(s) \cdot C_{f1}(n) \quad (143)$$

$$\left\{ \frac{1}{\left[-\Re \left(\frac{d}{ds} \left[-\frac{1}{2} \log \{ \chi(f_1(s)) \} \right] \right) + \log(n) \right]} \right\} \cdot \left\{ \frac{e^{-I \cdot \theta_{f1}(t)}}{n^{(1-(1/2+I \cdot t))}} \right\} \cdot \{w(n) \cdot \chi_{f1}(n)\} \equiv -A(s) \cdot D(s) \cdot C_{f1}(n) \quad (144)$$

Using the chain rule, one obtains the generic form of the total derivative $\frac{d}{ds}$ for each dirichlet term of equations (137,138,139)

$$\frac{d}{ds} [A(s) \cdot B(s) \cdot C_{f1}(n)] = \left\{ \frac{dA(s)}{ds} \cdot B(s) + A(s) \cdot \frac{dB(s)}{ds} \right\} \cdot C_{f1}(n) \quad (145)$$

or

$$\frac{d}{ds} [-A(s) \cdot D(s) \cdot C_{f1}(n)] = - \left\{ \frac{dA(s)}{ds} \cdot D(s) + A(s) \cdot \frac{dB(s)}{ds} \right\} \cdot C_{f1}(n) \quad (146)$$

Since $A(s)$ in equations (145) and (146) for $f_1(s)$ is the same $A(s)$ in equations (68) and (69) for $L(\chi_5(3,.), s)$ therefore, $f_1(s)$ shares the same $\frac{dA(s)}{ds}$ behaviour on the critical line as $L(\chi_5(3,.), s)$. Equation (89) therefore applies to $f_1(s)$

$$\therefore \frac{d}{ds} \Re \left(\frac{d}{ds} \left[-\frac{1}{2} \log \{ \chi(f_1(s)) \} \right] \right)_{s=1/2+I \cdot t} = 0 \quad \forall \quad t \quad (147)$$

and hence

Which implies for equations (114-146) that the generic form of the total derivative $\frac{d}{ds}$ for each dirichlet term of equations (137,138,139) when calculated for $s = 1/2 + I \cdot t$ reduces to either

$$\frac{d}{ds} [A(s) \cdot B(s) \cdot C_{f1}(n)]_{s=1/2+I \cdot t} \Rightarrow \left\{ \underbrace{\frac{dA(s)}{ds}}_{=0, s=1/2+I \cdot t} \cdot B(s) + A(s) \cdot \frac{dB(s)}{ds} \right\} \cdot C_{f1}(n) \quad (148)$$

$$= A(s) \cdot \frac{dB(s)}{ds} \cdot C_{f1}(n)_{s=1/2+I \cdot t} \quad (149)$$

$$(150)$$

or

$$\frac{d}{ds} [-A(s) \cdot D(s) \cdot C_{f1}(n)]_{s=1/2+I \cdot t} \Rightarrow - \left\{ \underbrace{\frac{dA(s)}{ds}}_{=0, s=1/2+I \cdot t} \cdot D(s) + A(s) \cdot \frac{dD(s)}{ds} \right\} \cdot C_{f1}(n) \quad (151)$$

$$= -A(s) \cdot \frac{dD(s)}{ds} \cdot C_{f1}(n)_{s=1/2+I \cdot t} \quad (152)$$

$$(153)$$

and given that $B(s)$ and $D(s)$ in equations (145) and (146) for $f_1(s)$ is the same $B(s)$ in equations (68) and (69) for $L(\chi_5(3, .), s)$

$$A(s) \cdot \frac{dB(s)}{ds} \Big|_{s=1/2+I \cdot t} = \left[\frac{1}{\left[\Re \left(\frac{d}{ds} \left[-\frac{1}{2} \log \{ \chi(f_1(s)) \} \right] \right) - \log(n) \right]} \cdot \frac{d}{ds} \left\{ \frac{e^{I \cdot \theta_{f1}(t)}}{n^{(1/2+I \cdot t)}} \right\} \right]_{s=1/2+I \cdot t} \quad (154)$$

$$= \left[\frac{1}{\left[\Re \left(\frac{d}{ds} \left[-\frac{1}{2} \log \{ \chi(f_1(s)) \} \right] \right) - \log(n) \right]} \cdot \frac{d}{ds} \left\{ e^{-\frac{1}{2} \log \{ \chi(f_1(s)) \}} \cdot e^{-s \cdot \log(n)} \right\} \right]_{s=1/2+I \cdot t} \quad (155)$$

$$= \left[\frac{\frac{d}{ds} \left[-\frac{1}{2} \log \{ \chi(f_1(s)) \} \right] - \log(n)}{\left[\Re \left(\frac{d}{ds} \left[-\frac{1}{2} \log \{ \chi(f_1(s)) \} \right] \right) - \log(n) \right]} \cdot \left(e^{-\frac{1}{2} \log \{ \chi(f_1(s)) \}} \cdot e^{-s \cdot \log(n)} \right) \right]_{s=1/2+I \cdot t} \quad (156)$$

$$= \frac{e^{I \cdot \theta_{f1}(t)}}{n^{(1/2+I \cdot t)}} \Big|_{s=1/2+I \cdot t} \quad (157)$$

$$-A(s) \cdot \frac{dD(s)}{ds} \Big|_{s=1/2+I \cdot t} = - \left[\frac{1}{\left[\Re \left(\frac{d}{ds} \left[-\frac{1}{2} \log \{\chi(f_1(s))\} \right] \right) - \log(n) \right]} \cdot \frac{d}{ds} \left\{ \frac{e^{-I \cdot \theta_{f_1}(t)}}{n^{(1-(1/2+I \cdot t))}} \right\} \right]_{s=1/2+I \cdot t} \quad (158)$$

$$= - \left[\frac{1}{\left[\Re \left(\frac{d}{ds} \left[-\frac{1}{2} \log \{\chi(f_1(s))\} \right] \right) - \log(n) \right]} \cdot \frac{d}{ds} \left\{ e^{\frac{1}{2} \log \{\chi(f_1(s))\}} \cdot e^{s \cdot \log(n)} \right\} \right]_{s=1/2+I \cdot t} \quad (159)$$

$$= - \left[\underbrace{\frac{d}{ds} \left[\frac{1}{2} \log \{\chi(f_1(s))\} \right] + \log(n)}_{=-1, s=1/2+I \cdot t} \cdot \left(e^{\frac{1}{2} \log \{\chi(f_1(s))\}} \cdot e^{s \cdot \log(n)} \right) \right]_{s=1/2+I \cdot t} \quad (160)$$

$$= \frac{e^{-I \cdot \theta_{f_1}(t)}}{n^{(1-(1/2+I \cdot t))}} \Big|_{s=1/2+I \cdot t} \quad (161)$$

Therefore

$$\frac{d}{ds} \left[\left\{ \frac{1}{\left[\Re \left(\frac{d}{ds} \left[-\frac{1}{2} \log \{\chi(f_1(s))\} \right] \right) - \log(n) \right]} \right\} \cdot \left\{ \frac{e^{I \cdot \theta_{f_1}(t)}}{n^{(1/2+I \cdot t)}} \right\} \cdot \{w(n) \cdot \chi_{f_1}(n)\} \right]_{s=1/2+I \cdot t} \quad (162)$$

$$\equiv \left[e^{I \cdot \theta_{f_1}(t)} \cdot \frac{\chi_{f_1}(n)}{n^{(1/2+I \cdot t)}} \cdot w(n) \right]_{s=1/2+I \cdot t} \quad (163)$$

$$\frac{d}{ds} \left[\left\{ \frac{1}{\left[-\Re \left(\frac{d}{ds} \left[-\frac{1}{2} \log \{\chi(f_1(s))\} \right] \right) + \log(n) \right]} \right\} \cdot \left\{ \frac{e^{-I \cdot \theta_{f_1}(t)}}{n^{(1-(1/2+I \cdot t))}} \right\} \cdot \{w(n) \cdot \chi_{f_1}(n)\} \right]_{s=1/2+I \cdot t} \quad (164)$$

$$\equiv \left[e^{-I \cdot \theta_{f_1}(t)} \cdot \frac{\chi_{f_1}(n)}{n^{(1-(1/2+I \cdot t))}} \cdot w(n) \right]_{s=1/2+I \cdot t} \quad (165)$$

which together covers all the dirichlet terms of equations (32,36,40) when $s = 1/2 + I \cdot t$.

That is, **on the critical line**, the total derivative of equations (137-139) produces a term by term agreement with approximations I, II and III (equations (32,36,40)) respectively for $f_1(s)$.

It can observed numerically that $\frac{dA(s)}{ds} \neq 0$ when $s \neq 1/2 + I \cdot t$ and so equations (137-139) are not sufficiently accurate away from the critical line.

The $N \bmod 5$ piecewise nature of the indefinite integral approximation equation (137)

In order to show the piecewise nature of the heuristic approximation equation (137) and its total derivative on the same graph with enough resolution of its approximation of the $f_1(s)$ non-trivial zero positions, the lowest t interval for 128 point tapering Dirichlet Series truncation at the second quiescent region approximations

of the $f_1(s)$ function its Riemann Siegel Z function. Figure 16 displays along $s = 0.5 + I \cdot t$ in the lowest possible interval $t = (41, 181)$ for 128 point tapering at the second quiescent region, the behaviour of (i) the **numerical total derivative** of equation (137) –imaginary part in violetred, real part in black–, (ii) the approximate indefinite integral equation (137) itself –imaginary part in red, real part in blue– and (iii) the high precision Pari-GP calculation of $\frac{e^{I\theta f_1(t)}}{\sqrt{\epsilon}} f_1(1/2 + I \cdot t)$ the true Riemann Siegel Z function –imaginary part in gray, real part in green–. In practice, at the resolution of the graph, the **numerical total derivative** of equation (137) results (black and violetred) are completely overlayed by the true Riemann Siegel Z function (green and gray) since the difference between the two functions is very small.

The top row of figure 16 displays the approximate indefinite integral function, its numerical total derivative and the true Riemann Siegel Z function using the regular t scale, while the bottom row displays the functions using a $\sqrt{(\frac{t}{2\pi} \cdot 5)}$ transformed scale. Thus quasi-discontinuities in the indefinite integral at $\sqrt{(\frac{t}{2\pi} \cdot 5)} = \{6, 7, 8, 9, 10, 11, 12\}$ can be observed there are clearly mesoscale features, on the critical line, that are common (but not exactly the same) across the piecewise segments.

The real(indefinite integral equation (137)) shown in blue is smooth, hyperbolic in nature and changes character for each piecewise segment sequentially. Furthermore while the real(indefinite integral) shown in blue has curvature with respect to t , its total derivative (not the partial derivative with respect to t) numerically computed along the critical line and coinciding with the $\text{imag}(\text{Riemann Siegel Z function approximation})$ shown in violetred hidden behind the gray line of the true imaginary part of the Riemann Siegel Z function (on the critical line) is zero. This behaviour for the imaginary part of the **total derivative** of the indefinite integral implies that the $\text{imag}(\text{total derivative of the approximate indefinite integral equation (137)})$ has a $(\sigma - 1/2)$ multiplicative factor on the critical line. A similar behaviour (a $(\sigma - 1/2)$ multiplicative factor) was also interpreted for the numerical total derivative of the approximate indefinite integral of the $\zeta(1/2 + I \cdot t)$ Riemann Siegel Z function in [13].

The $\text{imag}(\text{indefinite integral equation (137)})$ shown in red has mesoscale features eg. the hyperbolic component changes behaviour each piecewise segment and contains fine scale features which dominate the contribution to its total derivative being (an approximation) of the $f_1(s)$ Riemann Siegel Z function.

To aid in highlighting the $\sqrt{\frac{t}{2\pi} \cdot 5} - \lfloor \sqrt{\frac{t}{2\pi} \cdot 5} \rfloor$ behaviour of the indefinite integral and the potential for a varying density of the relative position of the highest Riemann Siegel Z function peaks the bottom row of the figure 16 uses $\sqrt{\frac{t}{2\pi} \cdot 5} - \lfloor \sqrt{\frac{t}{2\pi} \cdot 5} \rfloor$ scaling of the t coordinate axis. This results in two widths of piecewise intervals of the approximate indefinite integral equation (137). Numerically, the height of the function at $(N)^2 \cdot \frac{2\pi}{5}$ while large does not appear to be infinity so the piecewise intervals are described as having quasi-discontinuities driven by the contribution of the Dirichlet Series term with $k \approx \sqrt{(\frac{t}{2\pi} \cdot 5)}$. On the bottom row it can be seen that the piecewise intervals for $N=[6,7],[7,8],[8,9],[11,12]$ have width $\Delta N = 1$ while the piecewise interval for $N[9,11]$ has width $\Delta N = 2$. On remembering that the dirichlet characters for $N \bmod 5 = 0$ are zero immediately suggests that the mesoscale quasi-discontinuities features are reflecting whether the dirichlet characters are zero or non-zero.

Following [13], with respect to interpeting the relative position of higher density of extreme peaks in figure 13, it is of interest whether at increasing t the mesoscale features of $\text{imag}(\text{indefinite integral equation (137)})$ settle down to particular relative positions.

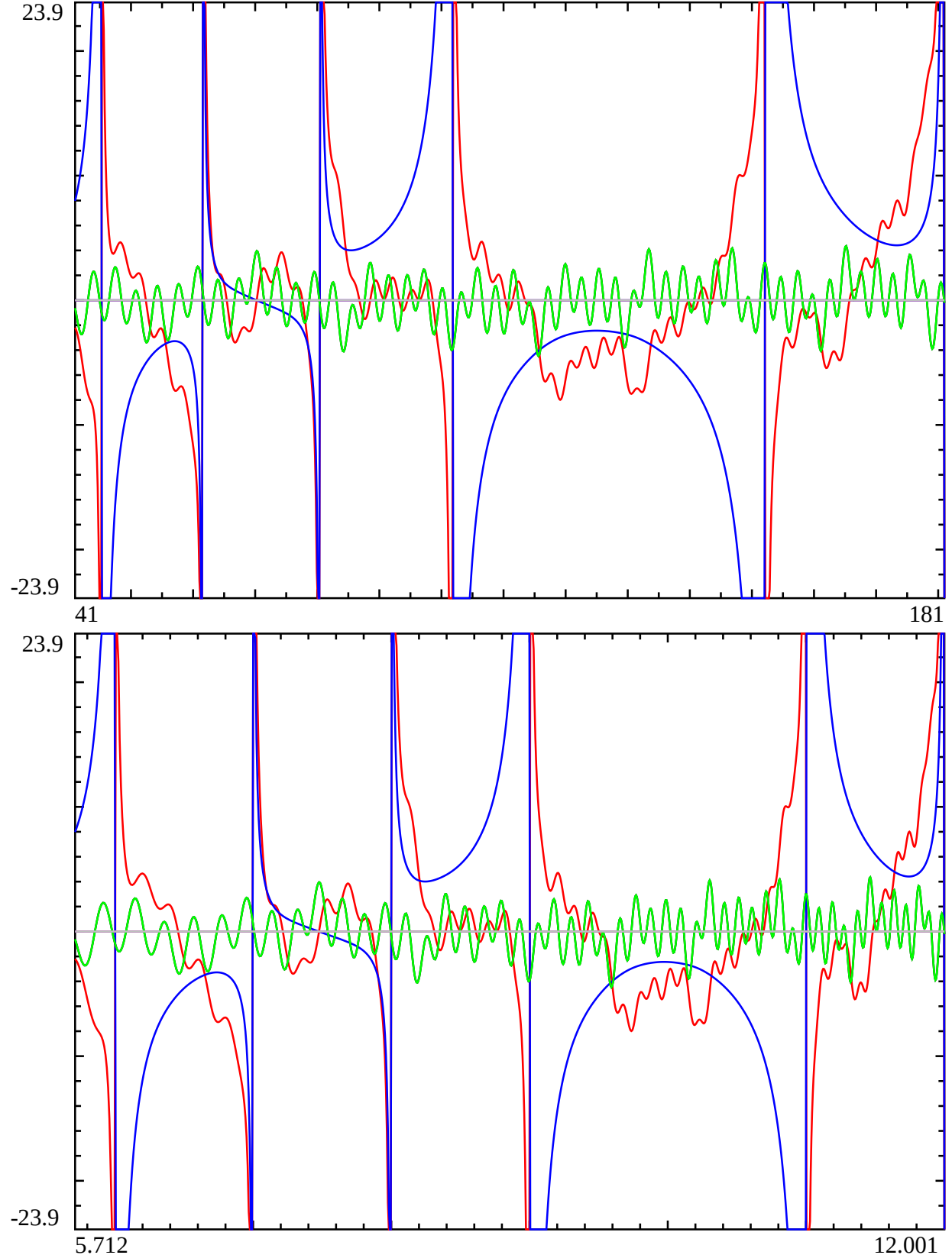


Figure 16: The behaviour of a heuristic approximation of the indefinite integral of the Riemann Siegel Z function for DHf1 **imag part in red, real part in blue**, its numerical derivative (approximating the Riemann Siegel Z function itself) real (imag) part shown in black (violet-red) based on **128 point end tapered** finite DHf1 Dirichlet Series sum (truncated at the second quiescent region) and the true DHf1 function (real (imag) part shown in green (gray)) along the critical line $s = 0.5 + I * t$ in the interval $t = (41, 181)$. The black, and violet-red lines of the real (imag) parts of the numerical total derivative of equation (4) are overlayed by the green, gray lines respectively of the true L53 L-function. From $t > 40.212$ ($64 \cdot \frac{5}{6}$), **128 point end tapered** finite DHf1 Dirichlet Series sums provide an excellent approximation of the DHf1 function to many decimal places. First row displays the functions using regular t scale, while the second row displays the functions using $\sqrt{\frac{t-5}{2\pi}}$ scale. Thus 59 quasi-discontinuities in the indefinite integral at $\sqrt{\frac{t-5}{2\pi}} = \{6, 7, 8, 9, 11\}$ can be observed and the mesoscale structure across each piecewise domain has a 5-periodic behaviour. There is no discontinuity at $\sqrt{\frac{t-5}{2\pi}} = \{10, 15, 20, \dots\}$ which is a mesoscale reflection of the zero Dirichlet character value for $\text{Mod}(N,5)=0$ for DHf1. The **real(Riemann Siegel Z function approximation for DHf1)** zeroes are turning points at the co-ordinates of $\text{imag}(\text{indefinite integral})$. While the **real(indefinite integral)** has curvature with respect to t, the **real(total derivative $\frac{d}{ds}$)** (not $\frac{\partial}{\partial t}$) numerically computed along the critical line and coinciding with the **imag(Riemann Siegel Z function approximation for DHf1)** is zero!

Differences in the piecewise nature of the indefinite integral approximations equations (137), (138) and (139) for the $f_1(s)$ Riemann Siegel Z function on the critical line.

Similar to [13], Figure 17 presents the normalised magnitude of the heuristic approximations equations (137,138,139) of the indefinite integral of the Riemann Siegel Z function of $f_1(s)$ **imag part in red, real part in blue** based on the finite Riemann Zeta Dirichlet Series sum truncated at the tapered second (lefthand column equation (137)), tapered first (middle column equation (138)) and first (righthand column equation (139)) quiescent regions along the critical line $s = 0.5 + I * t$ in various intervals $t = (41, 181)$, $t = (5148, 13858)$, $t = (50266, 53327)$, $t = (1256637, 12717139)$ and $t = (125663706, 125814548)$. The x axis is standardised by the transformation $\sqrt{\frac{t}{2\pi} \cdot 5}$. Importantly, very similar to [13] figure 17 shows that the y axis can be normalised to compare the heuristic approximation calculated values of the indefinite integral Riemann Siegel Z function for vastly different t values using a scaling factor of $(\frac{t}{2\pi} \cdot 5)^{0.25}$.

With respect to the piecewise nature of the indefinite integral approximations equations (137), (138) and (139) for the $f_1(s)$ Riemann Siegel Z function on the critical line, the normalised y scale shows that

1. there is little evolution of the real(equation(137)) shown in blue (lefthand column) with smooth hyperbolic lineshapes on each $[N, N+1]$ interval while the real(equations(138,139)) remain zero (on the critical line) as t increases. In comparison to real(equation(60)), real(equation(108)) in figures 5 and 11 from indefinite integrals approximations of $L(\chi_5(3, .), 1/2 + I \cdot t)$ and $L(\chi_5(2, .), 1/2 + I \cdot t)$ on the critical line for $N \bmod 5 = \{1, 3\}$ the real(equation(137)) remains asymmetric within the $[N, N+1]$ interval.
2. the evolution of the imag(equations(137,138,139)) shown in red can clearly be seen with the sharpening of mesoscale features that vary across the $[N, N+1]$ piecewise intervals. The imag(equation(138)) (middle column) behaviour is close to the imag(equation(137)) (lefthand column) behaviour but imag(equation(139)) (righthand column) clearly displays large differences at the righthand end of the $[N, N+1]$ piecewise intervals. (On careful examination there are also differences at the lefthand end of the $[N, N+1]$ piecewise intervals of the imag(equation(139)) (righthand column) behaviour compared to the other two indefinite integral approximations.)

In [13] the mesoscale features of the approximate indefinite integrals of the Riemann Siegel Z function of the ζ function on the critical line changed sign every piecewise interval $[N, N+1]$. For $f_1(s)$ the rate of sign change is observed to occur every tenth piecewise interval.

Figure 18 attempts to juxtapose (i) the mesoscale features of imag(equation(138)) for $N=\{10000-10004\}$ top row, (ii) the mesoscale features of imag(equation(138)) for $N=\{3000-3004\}$ second row, (iii) the $N \bmod 5$ behaviour of the extreme peaks for $N=\{0-3000\}$ under $\sqrt{\frac{t}{2\pi} \cdot 5} - \left\lfloor \sqrt{\frac{t}{2\pi} \cdot 5} \right\rfloor$ transformation middle row, (ii) the mesoscale features of imag(equation(138)) for $N=\{3005-3009\}$ second row and (ii) the mesoscale features of imag(equation(138)) for $N=\{10005-10009\}$ bottom row. Such a vertical juxtaposition helps clearly display the $N \bmod 10$ change in sign of the mesoscale features of the approximate indefinite integral of $f_1(s)$ Riemann Siegel Z function on the critical line. The vertical juxtaposition also indicates that the higher density in the relative position of the extreme peaks in the $f_1(s)$ Riemann Siegel Z function on the critical line (middle row) align well with regions of higher curvature in the approximate indefinite integral of $f_1(s)$ Riemann Siegel Z function on the critical line that occur with $N \bmod 5$ periodicity.

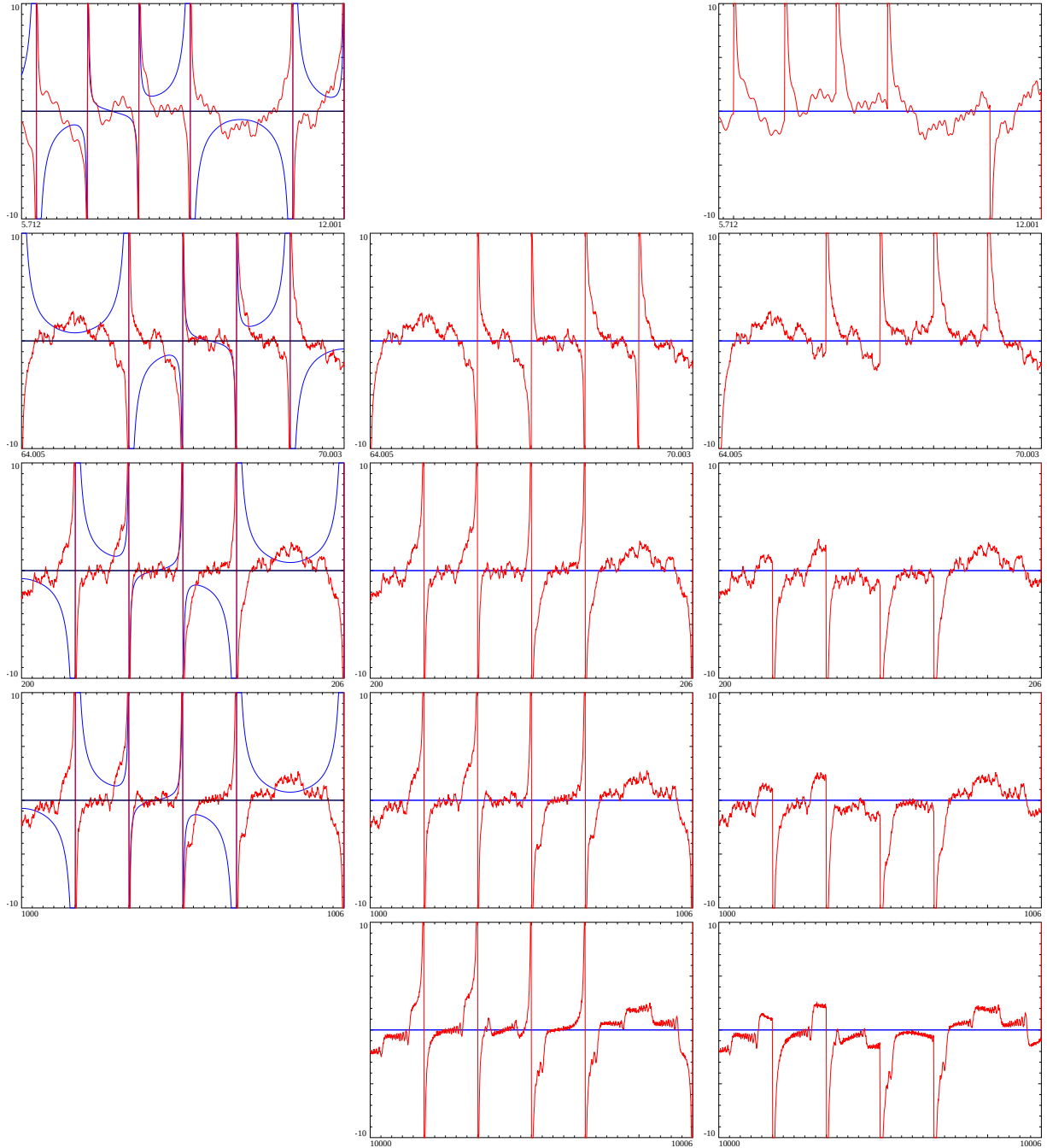


Figure 17: The normalised magnitude of the heuristic approximations equations (137,138,139) (using $\left(\frac{t \cdot 5}{2\pi}\right)^{0.25}$ scaling) of the indefinite integral of the Riemann Siegel Z function of DHf1 **imag part in red, real part in blue** based on the finite DHf1 Dirichlet Series sum truncated at the tapered second (lefthand column), tapered first (middle column) and first (righthand) quiescent region along the critical line $s = 0.5 + I * t$ in various intervals $t = (41, 181)$ top row, $t = (5148, 6158)$ second row, $t = (50266, 53327)$ third row, $t = (1256637, 1271762)$ fourth row and $t = (125663706, 125814548)$ bottom row where the horizontal axis uses a $\sqrt{\left(\frac{t \cdot 5}{2\pi}\right)}$ transformed scale. Mesoscale features are observed to evolve as t increases for the three approximations. The real component of equation (4) shown in blue (i) has a minimum absolute magnitude that depends on $\text{Mod}(N,5)$ and (ii) $\text{Mod}(N,10)$ behaviour for the sign of the mesoscale features but (iii) the magnitude scales as $\left(\frac{t \cdot 5}{2\pi}\right)^{0.25}$. The gaps in the grid of graphs occur where an approximation is infeasible (below the tapering limit) or calculationally much slower to obtain.

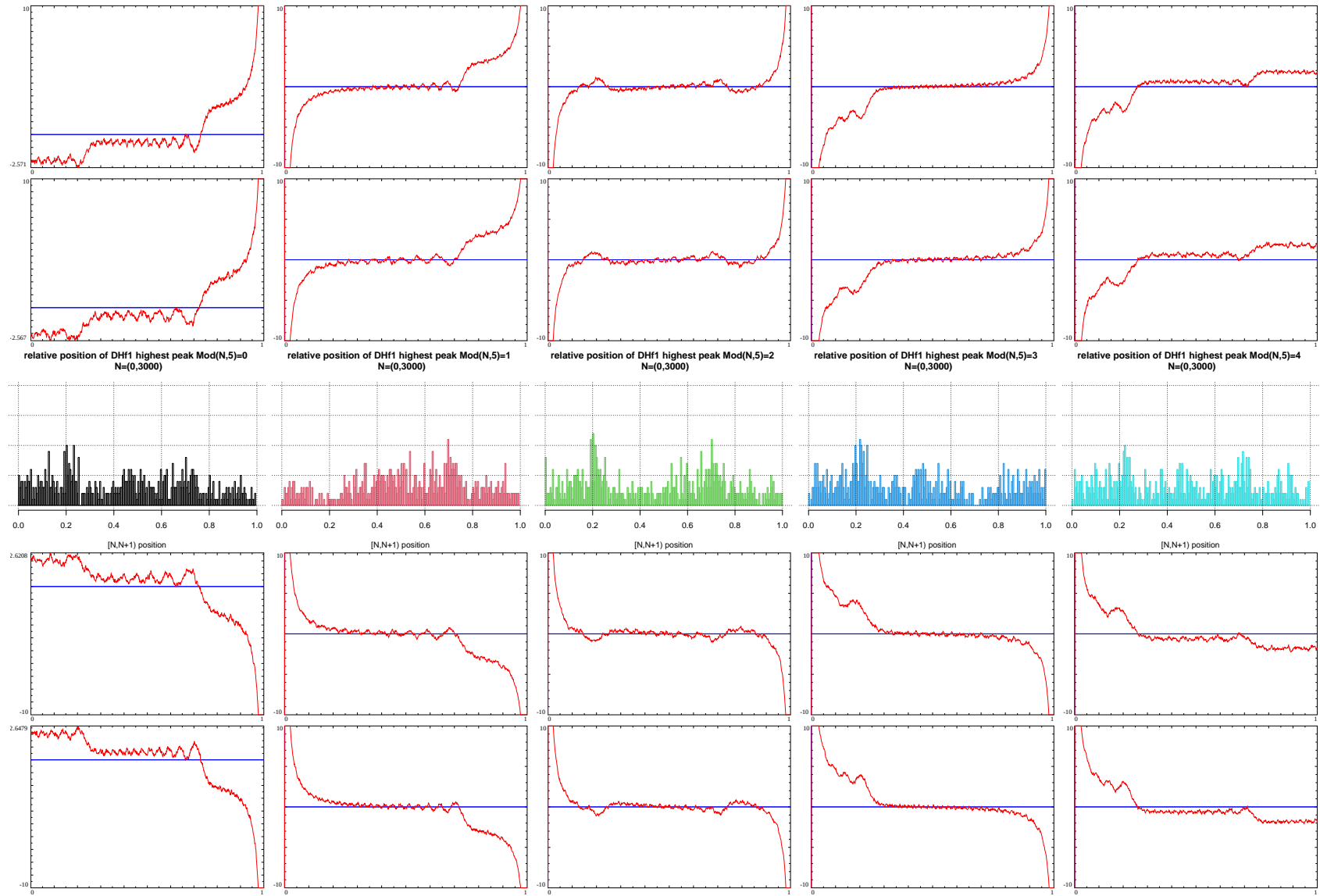


Figure 18: A vertical comparison of the distribution of the highest peaks (absolute magnitude) in $[N, N + 1]$ intervals on the critical line $s = 1/2 + I \cdot t$ where $N = \{0,..,3000\}$ for DHf1 and $t = N^2 \cdot \frac{2\pi}{5}$ segmented by $N \bmod 5 = \{0, 1, 2, 3, 4\}$ (middle row) with the mesoscale structure features clearly visible at higher t in a heuristic approximation of the imaginary component of the indefinite integral of the Riemann Siegel Z function of DHf1 along the critical line arranged in order by the intervals $[N, N + 1] \bmod 10$ where $N =$ (i) top row - $\{10000, 10001, 10002, 10003, 10004\}$, (ii) second row - $\{3000, 3001, 3002, 3003, 3004\}$, (iii) fourth row - $\{3005, 3006, 3007, 3008, 3009\}$ and (iv) bottom row - $\{10005, 10006, 10007, 10008, 10009\}$

Relative position of $f_2(1/2 + I \cdot t)$ extreme peaks under $(\sqrt{\frac{t \cdot 5}{2\pi}} - \lfloor \sqrt{\frac{t \cdot 5}{2\pi}} \rfloor)$ transformation

The lefthand column in Figure 19 presents the $N \bmod 5$ $(\sqrt{\frac{t \cdot 5}{2\pi}} - \lfloor \sqrt{\frac{t \cdot 5}{2\pi}} \rfloor)$ behaviour of the distribution of the relative position of extreme Riemann Siegel peaks from every piecewise interval $[N^2 \cdot \frac{2\pi}{5}, (N+1)^2 \cdot \frac{2\pi}{5}]$ obtained for $N=\{0,3000\}$ for $f_2(1/2 + I \cdot t)$, on the critical line. The estimates were obtained using equations (22), (33), (37) and (55).

Rows 1-5 presents the extreme peaks data for 3001 piecewise interval segmented by $N \bmod 5 = \{0, 1, 2, 3, 4\}$ respectively.

The righthand column in Figure 19 presents the growth in the absolute magnitude of the extreme Riemann Siegel Z function peak height on the critical line as a function of $\log(t)$ for $N \bmod 5 = \{0, 1, 2, 3, 4\}$ (shown in black, red, green, blue, cyan) overlayed on the total dataset (shown in gray).

Table 4 gives a snapshot of the numerical comparison between the absolute magnitude of peak heights obtained at the highest t investigated via (i) spectrally filtered finite Euler Product estimates truncated at the first quiescent region equation (55) and (ii) tapered Dirichlet Series estimates with truncation at the first quiescent region equation (37). Also included is the grid point of the peak, the value of grid point in the interval $[N, N+1]$ and the relative position of the peak in the interval $[0, 1]$. The grid point spacing was $\Delta t = 0.05$ starting from $t = N^2 \cdot \frac{2\pi}{5}$ for each successive piecewise interval $N=\{0,3000\}$.

Table 4: Grid search results $f_2(1/2 + I \cdot t)$ for $N=2994-3000$. A comparison of fourier transform filtered Euler Product estimate and 128 point tapered Dirchlet Series estimate based peak heights both using truncation at the first quiescent region $N_1 = \lfloor \sqrt{\frac{t}{2\pi} \cdot 5} \rfloor$

t value of peak	$\sqrt{\frac{t}{2\pi} \cdot 5}$	$\sqrt{\frac{t}{2\pi} \cdot 5} - \lfloor \sqrt{\frac{t}{2\pi} \cdot 5} \rfloor$	filtered Euler Product estimate	tapered Dirichlet series estimate
11270068.957645 2994.735		0.7346991	96.76932	96.75734
11279428.369541 2995.978		0.9779541	87.70807	87.70801
11285347.619641 2996.764		0.7639698	91.83551	91.82827
11290863.745550 2997.496		0.4962693	97.26973	97.27008
11296365.934734 2998.227		0.2265404	96.55066	96.54286
11307801.287191 2999.744		0.7437144	97.44273	97.42944
11314341.152923 3000.611		0.6110397	84.59533	84.59519

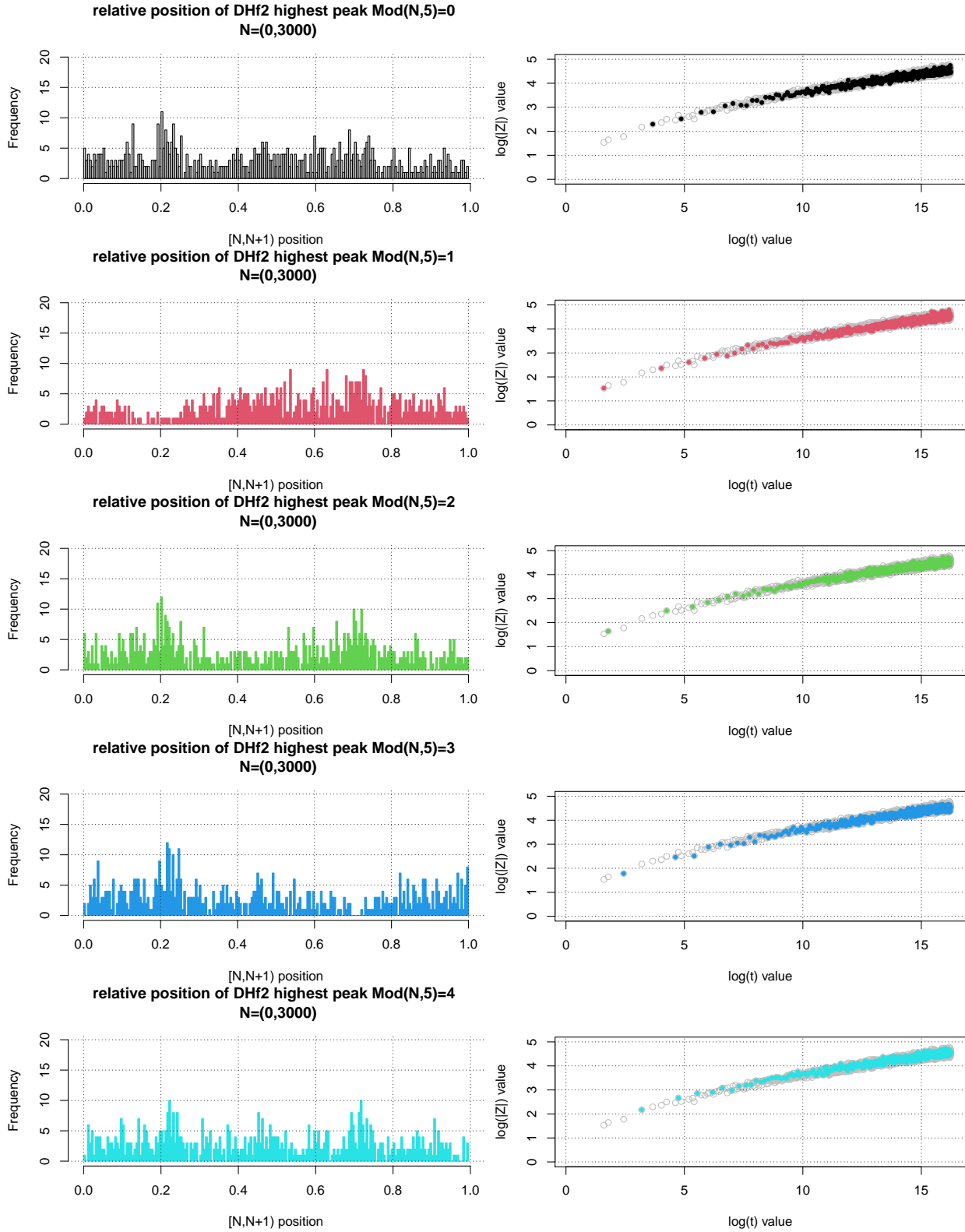


Figure 19: **Lefthand column** - Distribution of highest peaks of the Riemann Siegel Z function analogue of DHf2 and its approximations within each $[N^2 \cdot 2 \cdot \pi/5, (N + 1)^2 \cdot 2 \cdot \pi/5]$ piecewise interval segmented according to $N \bmod 5 = \{0, 1, 2, 3, 4\}$ (top row to bottom row) for $N=\{0-3000\}$ using their normalised positions $\sqrt{\frac{t-5}{2\pi}} - \lfloor \sqrt{\frac{t-5}{2\pi}} \rfloor$. **Righthand column** - Overlay of growth of largest Riemann Siegel Z function peaks from each given $\text{Mod}(N,5)$ intervals compared to all $[N^2 \cdot 2 \cdot \pi/5, (N + 1)^2 \cdot 2 \cdot \pi/5]$ intervals.

Accuracy performance of dirichlet series based approximations I, II and III for the Riemann Siegel Z function analogue of $f_2(s)$

Figures 20 and 21 provide an accuracy assessment of equations (33,37,41) in approximating the Riemann Siegel Z function for $f_2(s)$ on the critical line, for the two intervals $t=(46,126)$ and $t=(5800,5820)$ respectively.

The left column of Figure 20 shows an overlay of the real (green) and imaginary (black) parts of equations (33) (top row) and (41) (bottom row) respectively with the real (red) and imaginary (blue) parts of the true Riemann Siegel Z function for $f_2(s)$. The right column of Figure 20 shows the real and imaginary parts (shown in red and green respectively) of the differences with the true Riemann Siegel Z function – top row numerical($\frac{d}{ds}$ (equation (33)) $-e^{I\theta_{f_2}(t)} \cdot f_2(1/2+I \cdot t)$), – bottom row numerical($\frac{d}{ds}$ (equation (41)) $-e^{I\theta_{f_2}(t)} \cdot f_2(1/2+I \cdot t)$).

The left column of Figure 21 shows an overlay of the real (green) and imaginary (black) parts of equations (33) (top row), (37) (middle row) and (41) (bottom row) respectively with the real (red) and imaginary (blue) parts of the true Riemann Siegel Z function for $f_2(s)$. The right column of Figure 21 shows the real and imaginary parts (shown in red and green respectively) of the differences with the true Riemann Siegel Z function – top row numerical($\frac{d}{ds}$ (equation (33)) $-e^{I\theta_{f_2}(t)} \cdot f_2(1/2+I \cdot t)$), – middle row numerical($\frac{d}{ds}$ (equation (37)) $-e^{I\theta_{f_2}(t)} \cdot f_2(1/2+I \cdot t)$), – bottom row numerical($\frac{d}{ds}$ (equation (41)) $-e^{I\theta_{f_2}(t)} \cdot f_2(1/2+I \cdot t)$). At $t=(5800,5820)$, the high precision $f_2(s)$ Pari-GP functions required runtime exceeded 20 hours to complete 1000 data points on a single thread.

From the two figures,

- equation (33) has excellent multi decimal place agreement with $e^{I\theta_{f_2}(t)} \cdot f_2(1/2+I \cdot t)$ with an oscillating residual error contribution monotonically decreasing with t except for nuisance higher error spikes at $\sqrt{(\frac{t}{2\pi} \cdot 5)} = \left\lfloor \sqrt{(\frac{t}{2\pi} \cdot 5)} \right\rfloor$
- equation (41) has small visible systematic deviations from $e^{I\theta_{f_2}(t)} \cdot f_2(1/2+I \cdot t)$. The visible systematic difference, in principle, will be analogous to the first order Riemann Siegel formula (catenary shaped) correction for $\zeta(s)$ however figure 20 indicates that such a first order Riemann Siegel formula correction for $f_2(s)$ has an $N \bmod 5$ behaviour with jump discontinuities at $\sqrt{(\frac{t}{2\pi} \cdot 5)} = \left\lfloor \sqrt{(\frac{t}{2\pi} \cdot 5)} \right\rfloor$ and varying correction lineshape dependence where $N = \left\lfloor \sqrt{(\frac{t}{2\pi} \cdot 5)} \right\rfloor$.
- equation (37) has smaller but still systematic deviations than equation (41) because equation (37) includes tapering which should introduce higher order corrections to equation (41).

Thus equations (33,37,41) on the critical line provide good performance in approximating $e^{I\theta_{f_2}(t)} \cdot f_2(1/2+I \cdot t)$ the Riemann Siegel Z function for $f_2(s)$ on the critical line.

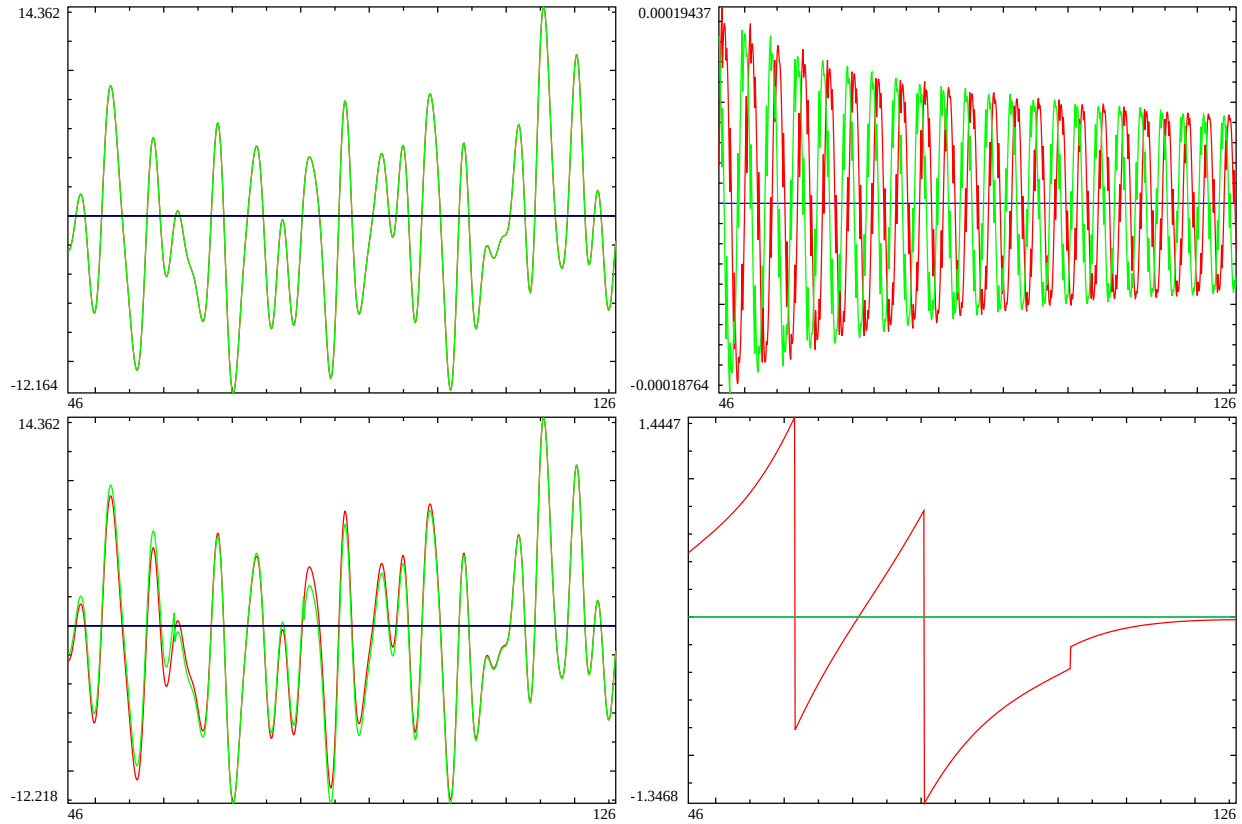


Figure 20: On the critical line, for the interval $t=(46,126)$. Left column - A overlay of real and imaginary components of Riemann Siegel Z function of DHf2 (red and blue) and and equations (33), (41) (green and black) in top (bottom row). Right column - the difference in the real (red) and imaginary (green) components of approximations I and III and the true Riemann Siegel Z function for L53.

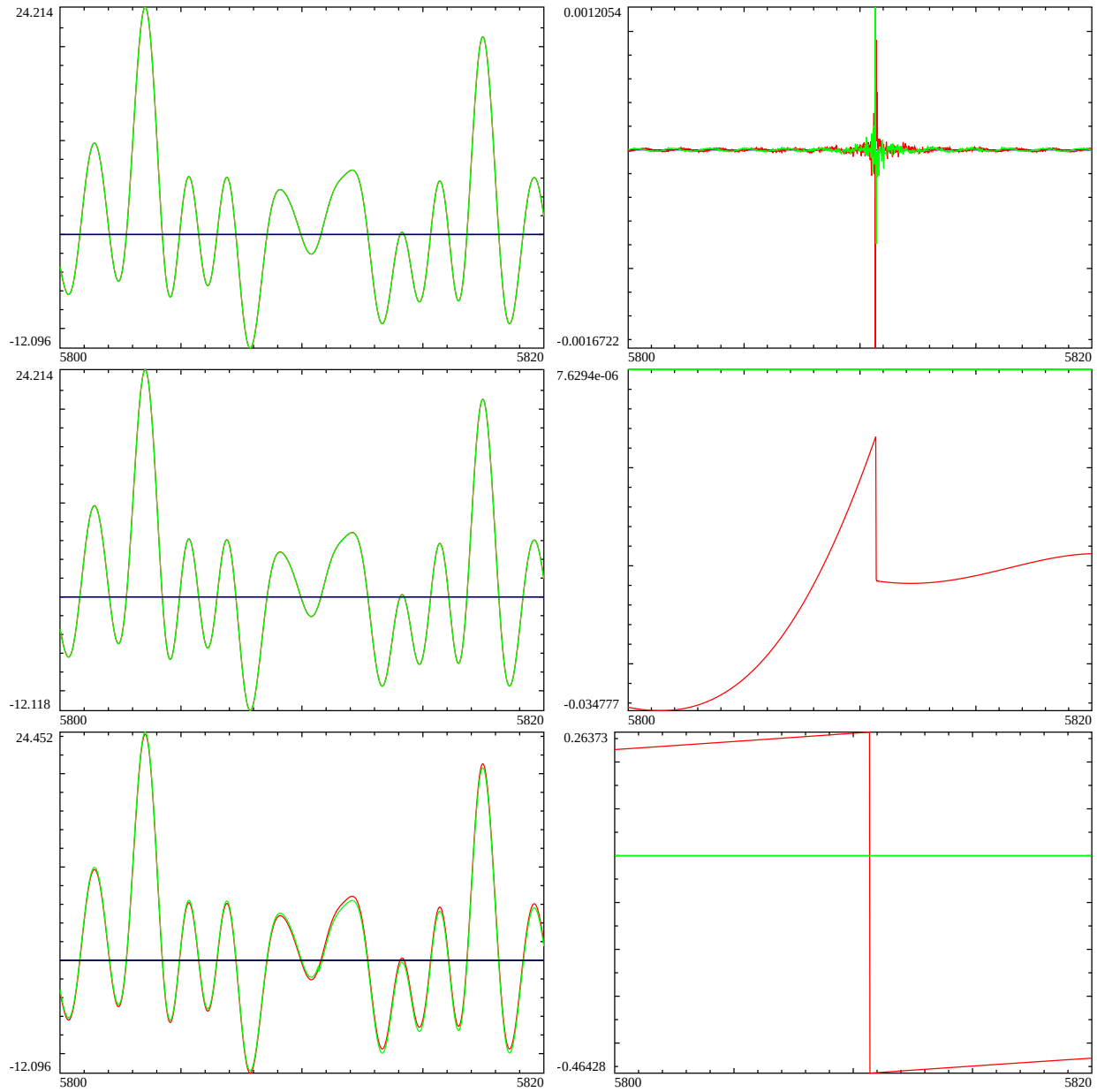


Figure 21: On the critical line, for the interval $t=(5800,5820)$. Left column - A overlay of real and imaginary components of Riemann Siegel Z function of DHf2 (red and blue) and equations (33), (37) and (41) (green and black) in top, middle and bottom row. Right column - the difference in the real (red) and imaginary (green) components of approximations I, II, III and the true Riemann Siegel Z function for DHf2.

A heuristic approximation for the indefinite integrals of the Riemann Siegel Z function analogue of tapered and untapered finite $f_2(s)$ function Dirichlet Series truncated at the second and first quiescent regions

Following [13] a possible approach to investigating insights into the $\sqrt{\frac{t}{2\pi}} - \left\lfloor \sqrt{\frac{t}{2\pi}} \right\rfloor$ behaviour of Riemann Siegel Z function peak height of $f_2(s)$ would be to investigate approximations for the first principles calculation of the indefinite integral of the Riemann Siegel Z function.

Therefore in this paper, co-opting [13] the following three critical line heuristic approximations of the indefinite integral of the Riemann Siegel Z function of $f_2(s)$ are attempted

(i) tapered truncation at the second quiescent region for $f_2(s)$ Dirichlet Series $\left\lfloor \frac{t}{\pi} \cdot 5 \right\rfloor$

$$\begin{aligned} & \left(\int e^{-\frac{1}{2} \log \chi(f_2(s))} f_2(s) ds \right)_{s=1/2+I \cdot t, \left\lfloor \frac{t}{\pi} \cdot 5 \right\rfloor, \text{tapered}} \\ & \approx e^{I \cdot \theta_{f_2}(t)} \cdot \left[\sum_{n=1}^{\left(\left\lfloor \frac{t}{\pi} \cdot 5 \right\rfloor - p \right)} \left(\frac{\chi_{f_2}(n)}{\left[\Re \left(\frac{d}{ds} \left[-\frac{1}{2} \log \{\chi(f_2(s))\} \right]_{s=(1/2+I \cdot t)} \right) - \log(n) \right] \cdot n^{(1/2+I \cdot t)}} \right) \right. \\ & \quad \left. + \sum_{i=(-p+1)}^p \frac{\frac{1}{2^{2p}} \left(2^{2p} - \sum_{k=1}^{i+p} \binom{2p}{2p-k} \right) \cdot \chi_{f_2}(\left\lfloor \frac{t}{\pi} \cdot 5 \right\rfloor + i)}{\left(\left[\Re \left(\frac{d}{ds} \left[-\frac{1}{2} \log \{\chi(f_2(s))\} \right]_{s=(1/2+I \cdot t)} \right) - \log(\left\lfloor \frac{t}{\pi} \cdot 5 \right\rfloor + i) \right] \cdot (\left\lfloor \frac{t}{\pi} \cdot 5 \right\rfloor + i)^{(1/2+I \cdot t)}} \right], t \rightarrow \infty \right. \end{aligned} \quad (166)$$

(ii) tapered truncation at the first quiescent region $N_2 = \left\lfloor \sqrt{\frac{t}{2\pi} \cdot 5} \right\rfloor$ for $f_2(s)$ Dirichlet Series

$$\begin{aligned} & \left(\int e^{-\frac{1}{2} \log \chi(f_2(s))} f_2(s) ds \right)_{s=1/2+I \cdot t, \left\lfloor \sqrt{\frac{t}{2\pi} \cdot 5} \right\rfloor, \text{tapered}} \\ & \approx e^{I \cdot \theta_{f_2}(t)} \cdot \left[\sum_{n=1}^{\left(\left\lfloor \sqrt{\frac{t}{2\pi} \cdot 5} \right\rfloor - p \right)} \left(\frac{\chi_{f_2}(n)}{\left[\Re \left(\frac{d}{ds} \left[-\frac{1}{2} \log \{\chi(f_2(s))\} \right]_{s=(1/2+I \cdot t)} \right) - \log(n) \right] \cdot n^{(1/2+I \cdot t)}} \right) \right. \\ & \quad \left. + \sum_{i=(-p+1)}^p \frac{\frac{1}{2^{2p}} \left(2^{2p} - \sum_{k=1}^{i+p} \binom{2p}{2p-k} \right) \cdot \chi_{f_2}(\left\lfloor \sqrt{\frac{t}{2\pi} \cdot 5} \right\rfloor + i)}{\left(\left[\Re \left(\frac{d}{ds} \left[-\frac{1}{2} \log \{\chi(f_2(s))\} \right]_{s=(1/2+I \cdot t)} \right) - \log(\left\lfloor \sqrt{\frac{t}{2\pi} \cdot 5} \right\rfloor + i) \right] \cdot (\left\lfloor \sqrt{\frac{t}{2\pi} \cdot 5} \right\rfloor + i)^{(1/2+I \cdot t)}} \right. \\ & \quad \left. + \chi_{f_2}(1/2 + I \cdot t) \cdot \left(\sum_{n=1}^{\left(\left\lfloor \sqrt{\frac{t}{2\pi} \cdot 5} \right\rfloor - p \right)} \left(\frac{\chi_{f_2}(n)}{\left[-\Re \left(\frac{d}{ds} \left[-\frac{1}{2} \log \{\chi(f_2(s))\} \right]_{s=(1/2+I \cdot t)} \right) + \log(n) \right] \cdot n^{(1-(1/2+I \cdot t))}} \right) \right. \right. \\ & \quad \left. \left. + \sum_{i=(-p+1)}^p \frac{\frac{1}{2^{2p}} \left(2^{2p} - \sum_{k=1}^{i+p} \binom{2p}{2p-k} \right) \cdot \chi_{f_2}(\left\lfloor \sqrt{\frac{t}{2\pi} \cdot 5} \right\rfloor + i)}{\left(\left[-\Re \left(\frac{d}{ds} \left[-\frac{1}{2} \log \{\chi(f_2(s))\} \right]_{s=(1/2+I \cdot t)} \right) + \log(\left\lfloor \sqrt{\frac{t}{2\pi} \cdot 5} \right\rfloor + i) \right] \cdot (\left\lfloor \sqrt{\frac{t}{2\pi} \cdot 5} \right\rfloor + i)^{(1-(1/2+I \cdot t))}} \right) \right], t \rightarrow \infty \right. \end{aligned} \quad (167)$$

(ii) truncation at the first quiescent region $N_1 = \left\lfloor \sqrt{\frac{t}{2\pi} \cdot 5} \right\rfloor$ for $f_2(s)$ Dirichlet Series

$$\begin{aligned}
& \left(\int e^{-\frac{1}{2} \log \chi(f_2(s))} f_2(s) ds \right)_{s=1/2+I \cdot t, \left| \sqrt{\frac{t}{2\pi}} \cdot 5 \right|, \text{tapered}} \\
& \approx e^{I \cdot \theta_{f_2}(t)} \cdot \left[\sum_{n=1}^{\left(\lfloor \sqrt{\frac{t}{2\pi}} \cdot 5 \rfloor \right)} \left(\frac{\chi_{f_2}(n)}{\left[\Re \left(\frac{d}{ds} \left[-\frac{1}{2} \log \{ \chi(f_2(s)) \} \right]_{s=(1/2+I \cdot t)} \right] - \log(n) \right] \cdot n^{(1/2+I \cdot t)}} \right) \right. \\
& \left. + \chi_{f_2}(1/2 + I \cdot t) \cdot \left(\sum_{n=1}^{\left(\lfloor \sqrt{\frac{t}{2\pi}} \cdot 5 \rfloor \right)} \left(\frac{\chi_{f_2}(n)}{\left[-\Re \left(\frac{d}{ds} \left[-\frac{1}{2} \log \{ \chi(f_2(s)) \} \right]_{s=(1/2+I \cdot t)} \right] + \log(n) \right] \cdot n^{(1-(1/2+I \cdot t))}} \right) \right), t \rightarrow \infty \right. \\
& \left. \quad (168) \right]
\end{aligned}$$

where

1. $\Re \left(\frac{d}{ds} \left[-\frac{1}{2} \log \{ \chi(f_2(s)) \} \right]_{s=(1/2+I \cdot t)} \right) \equiv \frac{\partial}{\partial t} [\theta_{f_2}(t)]$ on the critical line and
2. the nomenclature $e^{-\frac{1}{2} \log \chi(f_2(s))}$ is used to avoid confusion with the real valued Riemann Siegel Theta function ($\theta_{f_2}(t) = -\frac{1}{2} \cdot \text{imag} \left[\log \left(\chi(f_2(1/2 + I \cdot t)) \right) \right]$) see equation (28) which applies only to the critical line.

As shown in figure 23, the magnitude across the horizontal axis for the real part of equation (166) has symmetry and the real parts of equations (167) & (168) on the critical line are zero. Therefore the integration constant(s) explicitly required for the indefinite integral approximations given by equations (166,167,168) have all been set to zero.

As discussed below, a crucial part of the approximation prescription is explicitly using only $\Re \left(\frac{d}{ds} \left[-\frac{1}{2} \log \{ \chi(f_2(s)) \} \right] \right)$ and its role in terms of delivering a total derivative estimation that is equivalent to the approximations I (II and III) for the Riemann Siegel Z function of the $f_2(s)$ is examined.

Total derivative behaviour of individual terms of equations (166,167,168) on the critical line

To be useful heuristic approximations of the indefinite integral of the Riemann Siegel Z function for the 1st degree 5-periodic function $f_2(s)$ the total derivatives $\frac{d}{ds}$ (equations(166, 167, 168)) must result in useful approximations of the $f_2(s)$ Riemann Siegel Z function and ideally be equivalent to equations (33), (37) and (41).

In the following discussion, it is demonstrated that there is a term by term agreement **on the critical line** between $\frac{d}{ds}$ (equations(166, 167, 168)) and approximations I,II,III.

Firstly a single term of the dirichlet terms of equation (166) and half the terms of equations (167) and (168) can be presented in the generic form

$$e^{I \cdot \theta_{f_2}(t)} \cdot \left(\frac{\chi_{f_2}(n)}{\left[\Re \left(\frac{d}{ds} \left[-\frac{1}{2} \log \{ \chi(f_2(s)) \} \right]_{s=(1/2+I \cdot t)} \right] - \log(n) \right] \cdot n^{(1/2+I \cdot t)}} \right) \cdot w(n) \quad (169)$$

and the other half of the terms of equations (167) and (168) can be presented in the second generic form

$$e^{-I \cdot \theta_{f2}(t)} \cdot \left(\frac{\chi_{f2}(n)}{\left[-\Re \left(\frac{d}{ds} \left[-\frac{1}{2} \log \{ \chi(f_2(s)) \} \right] \right]_{s=(1/2+I \cdot t)} + \log(n) \right] \cdot n^{(1-(1/2+I \cdot t))}} \right) \cdot w(n) \quad (170)$$

where $w(n)$ describes that each term provides a weighted contribution $w(n) \leq 1$, in particular the $w(n)=1$ below where tapering of the endpoints occurs and $w(n)=0$ above the tapered endpoints and (ii) the second generic form arises from equations (17) and (23)

$$e^{I \cdot \theta_{f2}(t)} \cdot \chi(f_2(1/2 + I \cdot t)) = e^{I \cdot \theta_{f2}(t)} \cdot e^{-I \cdot 2 \cdot \theta_{f2}(t)} = e^{-I \cdot \theta_{f2}(t)} \iff s = 1/2 + I \cdot t \quad (171)$$

In practice, while the overall length of non-zero weighted terms of the truncated Dirichlet series in equations (166,167,168) is dependent on t being piecewise functions, the individual n , $w(n)$ and $\chi_{f2}(n)$ values are constants with respect to **infinitesimal changes** in t .

Hence, each single term of the dirichlet terms of equations (166,167,168) can be re-written as a triple product

$$\left\{ \frac{1}{\left[\Re \left(\frac{d}{ds} \left[-\frac{1}{2} \log \{ \chi(f_2(s)) \} \right] \right) - \log(n) \right]} \right\} \cdot \left\{ \frac{e^{I \cdot \theta_{f2}(t)}}{n^{(1/2+I \cdot t)}} \right\} \cdot \{w(n) \cdot \chi_{f2}(n)\} \equiv A_{f2}(s) \cdot B_{f2}(s) \cdot C_{f2}(n) \quad (172)$$

$$\left\{ \frac{1}{\left[-\Re \left(\frac{d}{ds} \left[-\frac{1}{2} \log \{ \chi(f_2(s)) \} \right] \right) + \log(n) \right]} \right\} \cdot \left\{ \frac{e^{-I \cdot \theta_{f2}(t)}}{n^{(1-(1/2+I \cdot t))}} \right\} \cdot \{w(n) \cdot \chi_{f2}(n)\} \equiv -A_{f2}(s) \cdot D_{f2}(s) \cdot C_{f2}(n). \quad (173)$$

Using the chain rule, one obtains the generic form of the total derivative $\frac{d}{ds}$ for each dirichlet term of equations (166,167,168)

$$\frac{d}{ds} [A_{f2}(s) \cdot B_{f2}(s) \cdot C_{f2}(n)] = \left\{ \frac{dA_{f2}(s)}{ds} \cdot B_{f2}(s) + A_{f2}(s) \cdot \frac{dB_{f2}(s)}{ds} \right\} \cdot C_{f2}(n) \quad (174)$$

or

$$\frac{d}{ds} [-A_{f2}(s) \cdot D_{f2}(s) \cdot C_{f2}(n)] = - \left\{ \frac{dA_{f2}(s)}{ds} \cdot D_{f2}(s) + A_{f2}(s) \cdot \frac{dD_{f2}(s)}{ds} \right\} \cdot C_{f2}(n). \quad (175)$$

Examining $\frac{dA_{f2}(s)}{ds}$ explicitly

$$\frac{dA_{f2}(s)}{ds} = \frac{d}{ds} \left\{ \frac{1}{\left[\Re \left(\frac{d}{ds} \left[-\frac{1}{2} \log \{ \chi(f_2(s)) \} \right] \right) - \log(n) \right]} \right\} \quad (176)$$

$$= \frac{1}{\left[\Re \left(\frac{d}{ds} \left[-\frac{1}{2} \log \{ \chi(f_2(s)) \} \right] \right) - \log(n) \right]^2} \cdot \frac{d}{ds} \Re \left(\frac{d}{ds} \left[-\frac{1}{2} \log \{ \chi(f_2(s)) \} \right] \right) \quad (177)$$

Secondly, to make further progress it is simpler to (i) inspect the second total derivative of $\left[-\frac{1}{2} \log\{\chi(f_2(s))\}\right]$ rather than $\Re\left(\frac{d}{ds} \left[-\frac{1}{2} \log\{\chi(f_2(s))\}\right]\right)$ i.e. ignore the $\Re()$ operation for the moment in equation (177),

$$\frac{d}{ds} \left(\frac{d}{ds} \left[-\frac{1}{2} \log\{\chi(f_2(s))\} \right] \right) \quad (178)$$

(ii) and instead of equation (13) use the following alternative functional equation multiplicative factor representation (see [1])

$$f_2(s) = -5^{\left(\frac{1}{2}-s\right)} \pi^{\left(s-\frac{1}{2}\right)} \cdot \frac{\Gamma\left[\frac{(2-s)}{2}\right]}{\Gamma\left[\frac{(1+s)}{2}\right]} \cdot f_2(1-s) \quad (179)$$

$$= \chi(f_2(s)) \cdot f_2(s) \quad \left[\equiv -\chi(f_1(s)) \cdot f_2(s) \right] \quad (180)$$

$$\therefore \chi(f_2(s)) \equiv -5^{\left(\frac{1}{2}-s\right)} \pi^{\left(s-\frac{1}{2}\right)} \cdot \frac{\Gamma\left[\frac{(2-s)}{2}\right]}{\Gamma\left[\frac{(1+s)}{2}\right]} \quad (181)$$

and (iii) use the $\log(\Gamma(s))$ identity [14,15] obtained from the Weierstrass product form of the $\Gamma(s)$ function

$$\log(\Gamma(s)) = -\gamma \cdot s - \log(s) + \sum_{k=1}^{\infty} \left[\frac{s}{k} - \log\left(1 + \frac{s}{k}\right) \right] \quad (182)$$

to obtain the following $-\frac{1}{2} \cdot \log(\chi(f_2(s)))$ expansion

$$\begin{aligned} -\frac{1}{2} \cdot \log(\chi(f_2(s))) &= -\frac{1}{2} \left\{ \log(-1) + \left(\frac{1}{2} - s\right) \cdot \log(5) + \left(s - \frac{1}{2}\right) \cdot \log(\pi) \right. \\ &\quad - \gamma \cdot \left[\frac{(2-s)}{2} \right] - \log \left[\frac{(2-s)}{2} \right] + \sum_{k=1}^{\infty} \left[\frac{\left[\frac{(2-s)}{2}\right]}{k} - \log\left(1 + \frac{\left[\frac{(2-s)}{2}\right]}{k}\right) \right] \\ &\quad \left. - \left(-\gamma \cdot \left[\frac{(1+s)}{2} \right] - \log \left[\frac{(1+s)}{2} \right] + \sum_{k=1}^{\infty} \left[\frac{\left[\frac{(1+s)}{2}\right]}{k} - \log\left(1 + \frac{\left[\frac{(1+s)}{2}\right]}{k}\right) \right] \right) \right\} \end{aligned} \quad (183)$$

from which the following first total derivative is obtained

$$\begin{aligned} \frac{d}{ds} \left[-\frac{1}{2} \log\{\chi(f_2(s))\} \right] &= -\frac{1}{2} \left\{ -\log(5) + \log(\pi) + \frac{\gamma}{2} + \frac{1}{(2-s)} + \sum_{k=1}^{\infty} \left[-\frac{1}{2k} + \frac{1}{(2k+2-s)} \right] \right. \\ &\quad \left. - \left(-\frac{\gamma}{2} - \frac{1}{(1+s)} + \sum_{k=1}^{\infty} \left[\frac{1}{2k} - \frac{1}{(2k+1+s)} \right] \right) \right\} \end{aligned} \quad (184)$$

$$= -\frac{1}{2} \left\{ -\log(5) + \log(\pi) + \gamma + \frac{1}{(2-s)} + \frac{1}{(1+s)} - \sum_{k=1}^{\infty} \left[\frac{1}{k} - \frac{1}{(2k+2-s)} - \frac{1}{(2k+1+s)} \right] \right\} \quad (185)$$

and the second total derivative is then iteratively obtained from $\frac{d}{ds}$ [equation(185)]

$$\frac{d^2}{ds^2} \left[-\frac{1}{2} \log\{\chi(f_2(s))\} \right] = -\frac{1}{2} \left\{ \frac{1}{(2-s)^2} - \frac{1}{(1+s)^2} - \sum_{k=1}^{\infty} \left[-\frac{1}{(2k+2-s)^2} + \frac{1}{(2k+1+s)^2} \right] \right\} \quad (186)$$

Looking at the values of the first and second total derivative of $-\frac{1}{2} \log\{\chi(f_2(s))\}$ on the critical line $s = 1/2 + I \cdot t$

$$\begin{aligned} \frac{d}{ds} \left[-\frac{1}{2} \log\{\chi(f_2(s))\} \right]_{s=1/2+I \cdot t} &= -\frac{1}{2} \left\{ -\log(5) + \log(\pi) + \gamma + \frac{1}{(3/2 - I \cdot t)} + \frac{1}{(3/2 + I \cdot t)} \right. \\ &\quad \left. - \sum_{k=1}^{\infty} \left[\frac{1}{k} - \frac{1}{(2k+3/2 - I \cdot t)} - \frac{1}{(2k+3/2 + I \cdot t)} \right] \right\} \end{aligned} \quad (187)$$

$$\begin{aligned} &= -\frac{1}{2} \left\{ -\log(5) + \log(\pi) + \gamma + \frac{3/2 + I \cdot t + (3/2 - I \cdot t)}{(3/2 - I \cdot t)(3/2 + I \cdot t)} \right. \\ &\quad \left. - \sum_{k=1}^{\infty} \left[\frac{1}{k} - \frac{(2k+3/2 + I \cdot t) + (2k+3/2 - I \cdot t)}{(2k+3/2 - I \cdot t)(2k+3/2 + I \cdot t)} \right] \right\} \end{aligned} \quad (188)$$

$$= -\frac{1}{2} \left\{ -\log(5) + \log(\pi) + \gamma + \frac{3}{(9/4 + t^2)} - \sum_{k=1}^{\infty} \left[\frac{1}{k} - \frac{(4k+3)}{[(2k+3/2)^2 + t^2]} \right] \right\} \quad (189)$$

$$\therefore \frac{d}{ds} \left[-\frac{1}{2} \log\{\chi(f_2(s))\} \right]_{s=1/2+I \cdot t} \in \mathbb{R} \quad (190)$$

$$\begin{aligned} \frac{d^2}{ds^2} \left[-\frac{1}{2} \log\{\chi(f_2(s))\} \right]_{s=1/2+I \cdot t} &= -\frac{1}{2} \left\{ \frac{1}{(3/2 - I \cdot t)^2} - \frac{1}{(3/2 + I \cdot t)^2} \right. \\ &\quad \left. - \sum_{k=1}^{\infty} \left[-\frac{1}{(2k+3/2 - I \cdot t)^2} + \frac{1}{(2k+3/2 + I \cdot t)^2} \right] \right\} \end{aligned} \quad (191)$$

$$\begin{aligned} &= -\frac{1}{2} \left\{ \frac{(9/4 + I \cdot 3 \cdot t + t^2) - (9/4 - I \cdot 3 \cdot t + t^2)^2}{(3/2 - I \cdot t)^2 \cdot (3/2 + I \cdot t)^2} \right. \\ &\quad \left. - \sum_{k=1}^{\infty} \left[-\frac{(2k+3/2 + I \cdot t)^2 - (2k+3/2 - I \cdot t)^2}{(2k+3/2 - I \cdot t)^2 \cdot (2k+3/2 + I \cdot t)^2} \right] \right\} \end{aligned} \quad (192)$$

$$= -\frac{1}{2} \left\{ \frac{I \cdot 6 \cdot t}{(9/4 + t^2)^2} - \sum_{k=1}^{\infty} \left[-\frac{I \cdot (4k+3) \cdot t}{[(2k+3/2)^2 + t^2]^2} \right] \right\} \quad (193)$$

$$\therefore \frac{d^2}{ds^2} \left[-\frac{1}{2} \log\{\chi(f_2(s))\} \right]_{s=1/2+I \cdot t} \in \mathbb{C} - \mathbb{R} \quad \text{i.e., purely imaginary} \quad (194)$$

The relationship

- $\left[-\frac{1}{2} \log\{\chi(f_2(s))\} \right]_{s=1/2+I \cdot t} \in \text{pure imaginary},$
- $\frac{d}{ds} \left[-\frac{1}{2} \log\{\chi(f_2(s))\} \right]_{s=1/2+I \cdot t} \in \mathbb{R},$
- $\frac{d^2}{ds^2} \left[-\frac{1}{2} \log\{\chi(f_2(s))\} \right]_{s=1/2+I \cdot t} \in \text{pure imaginary}$

is a demonstration of an analytic complex function ($\left[-\frac{1}{2} \log\{\chi(f_2(s))\} \right]_{s=1/2+I \cdot t}$) following the Cauchy Riemann conditions.

Since differentiation of a **real valued** function (e.g. $\frac{d}{ds} \left[\Re \left(\frac{d}{ds} \left[-\frac{1}{2} \log\{\chi(f_2(s))\} \right] \right) \right]_{s=1/2+I \cdot t}$) must result in a **real valued** result but $\frac{d^2}{ds^2} \left[-\frac{1}{2} \log\{\chi(f_2(s))\} \right]_{s=1/2+I \cdot t} \in \text{pure imaginary}$

$$\therefore \frac{d}{ds} \Re \left(\frac{d}{ds} \left[-\frac{1}{2} \log\{\chi(f_2(s))\} \right] \right)_{s=1/2+I \cdot t} = 0 \quad \forall t \quad (195)$$

Which implies going back to equations (172-175) that the generic form of the total derivative $\frac{d}{ds}$ for each dirichlet term of equations (166,167,168) when calculated for $s = 1/2 + I \cdot t$ reduces to

$$\frac{d}{ds} [A_{f2}(s) \cdot B_{f2}(s) \cdot C_{f2}(n)]_{s=1/2+I \cdot t} \Rightarrow \left\{ \underbrace{\frac{dA_{f2}(s)}{ds}}_{=0, s=1/2+I \cdot t} \cdot B_{f2}(s) + A_{f2}(s) \cdot \frac{dB_{f2}(s)}{ds} \right\} \cdot C_{f2}(n) \quad (196)$$

$$= A_{f2}(s) \cdot \frac{dB_{f2}(s)}{ds} \cdot C_{f2}(n)_{s=1/2+I \cdot t} \quad (197)$$

(198)

$$\frac{d}{ds} [-A_{f2}(s) \cdot D_{f2}(s) \cdot C_{f2}(n)]_{s=1/2+I \cdot t} \Rightarrow - \left\{ \underbrace{\frac{dA_{f2}(s)}{ds}}_{=0, s=1/2+I \cdot t} \cdot D_{f2}(s) + A_{f2}(s) \cdot \frac{dD_{f2}(s)}{ds} \right\} \cdot C_{f2}(n) \quad (199)$$

$$= -A_{f2}(s) \cdot \frac{dD_{f2}(s)}{ds} \cdot C_{f2}(n) \cdot \underset{s=1/2+I \cdot t}{\dots} \quad (200)$$

(201)

However

$$A_{f2}(s) \cdot \frac{dB_{f2}(s)}{ds} \underset{s=1/2+I \cdot t}{=} \left[\frac{1}{\left[\Re \left(\frac{d}{ds} \left[-\frac{1}{2} \log\{\chi(f_2(s))\} \right] \right) - \log(n) \right]} \cdot \frac{d}{ds} \left\{ \frac{e^{I \cdot \theta_{f2}(t)}}{n^{(1/2+I \cdot t)}} \right\} \right]_{s=1/2+I \cdot t} \quad (202)$$

$$= \left[\frac{1}{\left[\Re \left(\frac{d}{ds} \left[-\frac{1}{2} \log\{\chi(f_2(s))\} \right] \right) - \log(n) \right]} \cdot \frac{d}{ds} \left\{ e^{-\frac{1}{2} \log\{\chi(f_2(s))\}} \cdot e^{-s \cdot \log(n)} \right\} \right]_{s=1/2+I \cdot t} \quad (203)$$

$$= \left[\underbrace{\frac{\frac{d}{ds} \left[-\frac{1}{2} \log\{\chi(f_2(s))\} \right] - \log(n)}{\left[\Re \left(\frac{d}{ds} \left[-\frac{1}{2} \log\{\chi(f_2(s))\} \right] \right) - \log(n) \right]} \cdot \left(e^{-\frac{1}{2} \log\{\chi(f_2(s))\}} \cdot e^{-s \cdot \log(n)} \right)}_{=1, s=1/2+I \cdot t} \right]_{s=1/2+I \cdot t} \quad (204)$$

$$= \frac{e^{I \cdot \theta_{f2}(t)}}{n^{(1/2+I \cdot t)}} \underset{s=1/2+I \cdot t}{=} \quad (205)$$

$$\begin{aligned}
-A_{f2}(s) \cdot \frac{dD_{f2}(s)}{ds} \Big|_{s=1/2+I \cdot t} &= - \left[\frac{1}{\left[\Re \left(\frac{d}{ds} \left[-\frac{1}{2} \log \{\chi(f_2(s))\} \right] \right) - \log(n) \right]} \cdot \frac{d}{ds} \left\{ \frac{e^{-I \cdot \theta_{f2}(t)}}{n^{(1-(1/2+I \cdot t))}} \right\} \right]_{s=1/2+I \cdot t} \\
&= - \left[\frac{1}{\left[\Re \left(\frac{d}{ds} \left[-\frac{1}{2} \log \{\chi(f_2(s))\} \right] \right) - \log(n) \right]} \cdot \frac{d}{ds} \left\{ e^{\frac{1}{2} \log \{\chi(f_2(s))\}} \cdot e^{s \cdot \log(n)} \right\} \right]_{s=1/2+I \cdot t} \tag{206}
\end{aligned}$$

$$\begin{aligned}
&= - \left[\underbrace{\frac{\frac{d}{ds} \left[\frac{1}{2} \log \{\chi(f_2(s))\} \right] + \log(n)}{\left[\Re \left(\frac{d}{ds} \left[-\frac{1}{2} \log \{\chi(f_2(s))\} \right] \right) - \log(n) \right]} \cdot \left(e^{\frac{1}{2} \log \{\chi(f_2(s))\}} \cdot e^{s \cdot \log(n)} \right)}_{=-1, s=1/2+I \cdot t} \right]_{s=1/2+I \cdot t} \tag{207}
\end{aligned}$$

$$= \frac{e^{-I \cdot \theta_{f2}(t)}}{n^{(1-(1/2+I \cdot t))}} \Big|_{s=1/2+I \cdot t} \tag{208}$$

Therefore

$$\frac{d}{ds} \left[\left\{ \frac{1}{\left[\Re \left(\frac{d}{ds} \left[-\frac{1}{2} \log \{\chi(f_2(s))\} \right] \right) - \log(n) \right]} \right\} \cdot \left\{ \frac{e^{I \cdot \theta_{f2}(t)}}{n^{(1/2+I \cdot t)}} \right\} \cdot \{w(n) \cdot \chi_{f2}(n)\} \right]_{s=1/2+I \cdot t} \tag{210}$$

$$\equiv \left[e^{I \cdot \theta_{f2}(t)} \cdot \frac{\chi_{f2}(n)}{n^{(1/2+I \cdot t)}} \cdot w(n) \right]_{s=1/2+I \cdot t} \tag{211}$$

$$\frac{d}{ds} \left[\left\{ \frac{1}{\left[-\Re \left(\frac{d}{ds} \left[-\frac{1}{2} \log \{\chi(f_2(s))\} \right] \right) + \log(n) \right]} \right\} \cdot \left\{ \frac{e^{-I \cdot \theta_{f2}(t)}}{n^{(1-(1/2+I \cdot t))}} \right\} \cdot \{w(n) \cdot \chi_{f2}(n)\} \right]_{s=1/2+I \cdot t} \tag{212}$$

$$\equiv \left[e^{-I \cdot \theta_{f2}(t)} \cdot \frac{\chi_{f2}(n)}{n^{(1-(1/2+I \cdot t))}} \cdot w(n) \right]_{s=1/2+I \cdot t} \tag{213}$$

which together covers all the dirichlet terms of equations (33,37,41) when $s = 1/2 + I \cdot t$.

That is, **on the critical line**, the total derivative of equations (166-168) produces a term by term agreement with approximations I, II and III (equations (33,37,41)) respectively for $f_2(s)$.

It can be observed numerically that $\frac{dA_{f2}(s)}{ds} \neq 0$ when $s \neq 1/2 + I \cdot t$ and so equations (166-168) are not sufficiently accurate away from the critical line.

The $N \bmod 5$ piecewise nature of the indefinite integral approximation equation (166)

In order to show the piecewise nature of the heuristic approximation equation (166) and its total derivative on the same graph with enough resolution of its approximation of the $f_2(s)$ non-trivial zero positions, the lowest t interval for 128 point tapering Dirichlet Series truncation at the second quiescent region approximations of the $f_2(s)$ function its Riemann Siegel Z function. Figure 22 displays along $s = 0.5 + I * t$ in the lowest possible interval $t = (41, 181)$ for 128 point tapering at the second quiescent region, the behaviour of (i) the **numerical total derivative** of equation (166) –imaginary part in violetred, real part in black–, (ii) the approximate indefinite integral equation (166) itself –imaginary part in red, real part in blue– and (iii) the high precision Pari-GP calculation of $\frac{e^{I\theta f_2(t)}}{\sqrt{f_2(1/2 + I \cdot t)}}$ the true Riemann Siegel Z function –imaginary part in gray, real part in green–. In practice, at the resolution of the graph, the **numerical total derivative** of equation (166) results (black and violetred) are completely overlayed by the true Riemann Siegel Z function (green and gray) since the difference between the two functions is very small.

The top row of figure 22 displays the approximate indefinite integral function, its numerical total derivative and the true Riemann Siegel Z function using the regular t scale, while the bottom row displays the functions using a $\sqrt{(\frac{t}{2\pi} \cdot 5)}$ transformed scale. Thus quasi-discontinuities in the indefinite integral at $\sqrt{(\frac{t}{2\pi} \cdot 5)} = \{6, 7, 8, 9, 10, 11, 12\}$ can be observed there are clearly mesoscale features, on the critical line, that are common (but not exactly the same) across the piecewise segments.

The real(indefinite integral equation (166)) shown in blue is smooth, hyperbolic in nature and changes character for each piecewise segment sequentially. Furthermore while the real(indefinite integral) shown in blue has curvature with respect to t, its total derivative (not the partial derivative with respect to t) numerically computed along the critical line and coinciding with the imag(Riemann Siegel Z function approximation) shown in violetred hidden behind the gray line of the true imaginary part of the Riemann Siegel Z function (on the critical line) is zero! This behaviour for the imaginary part of the **total derivative** of the indefinite integral implies that the imag(total derivative of the approximate indefinite integral equation (166)) has a $(\sigma - 1/2)$ multiplicative factor on the critical line. A similar behaviour (a $(\sigma - 1/2)$ multiplicative factor) was also interpreted for the numerical total derivative of the approximate indefinite integral of the $\zeta(1/2 + I \cdot t)$ Riemann Siegel Z function in [13].

The imag(indefinite integral equation (166)) shown in red has mesoscale features eg. the hyperbolic component changes behaviour each piecewise segment and contains fine scale features which dominate the contribution to its total derivative being (an approximation) of the $f_2(s)$ Riemann Siegel Z function.

To aid in highlighting the $\sqrt{\frac{t}{2\pi} \cdot 5} - \left\lfloor \sqrt{\frac{t}{2\pi} \cdot 5} \right\rfloor$ behaviour of the indefinite integral and the potential for a varying density of the relative position of the highest Riemann Siegel Z function peaks the bottom row of the figure 22 uses $\sqrt{\frac{t}{2\pi} \cdot 5} - \left\lfloor \sqrt{\frac{t}{2\pi} \cdot 5} \right\rfloor$ scaling of the t coordinate axis. This results in two widths of piecewise intervals of the approximate indefinite integral equation (166). Numerically, the height of the function at $(N)^2 \cdot \frac{2\pi}{5}$ while large does not appear to be infinity so the piecewise intervals are described as having quasi-discontinuities driven by the contribution of the Dirichlet Series term with $k \approx \sqrt{(\frac{t}{2\pi} \cdot 5)}$. On the bottom row it can be seen that the piecewise intervals for $N=[6,7],[7,8],[8,9],[11,12]$ have width $\Delta N = 1$ while the piecewise interval for $N[9,11]$ has width $\Delta N = 2$. On remembering that the dirichlet characters for $N \bmod 5 = 0$ are zero immediately suggests that the mesoscale quasi-discontinuities features are reflecting whether the dirichlet characters are zero or non-zero.

Following [13], with respect to interpeting the relative position of higher density of extreme peaks in figure 19, it is of interest whether at increasing t the mesoscale features of imag(indefinite integral equation (166)) settle down to particular relative positions.

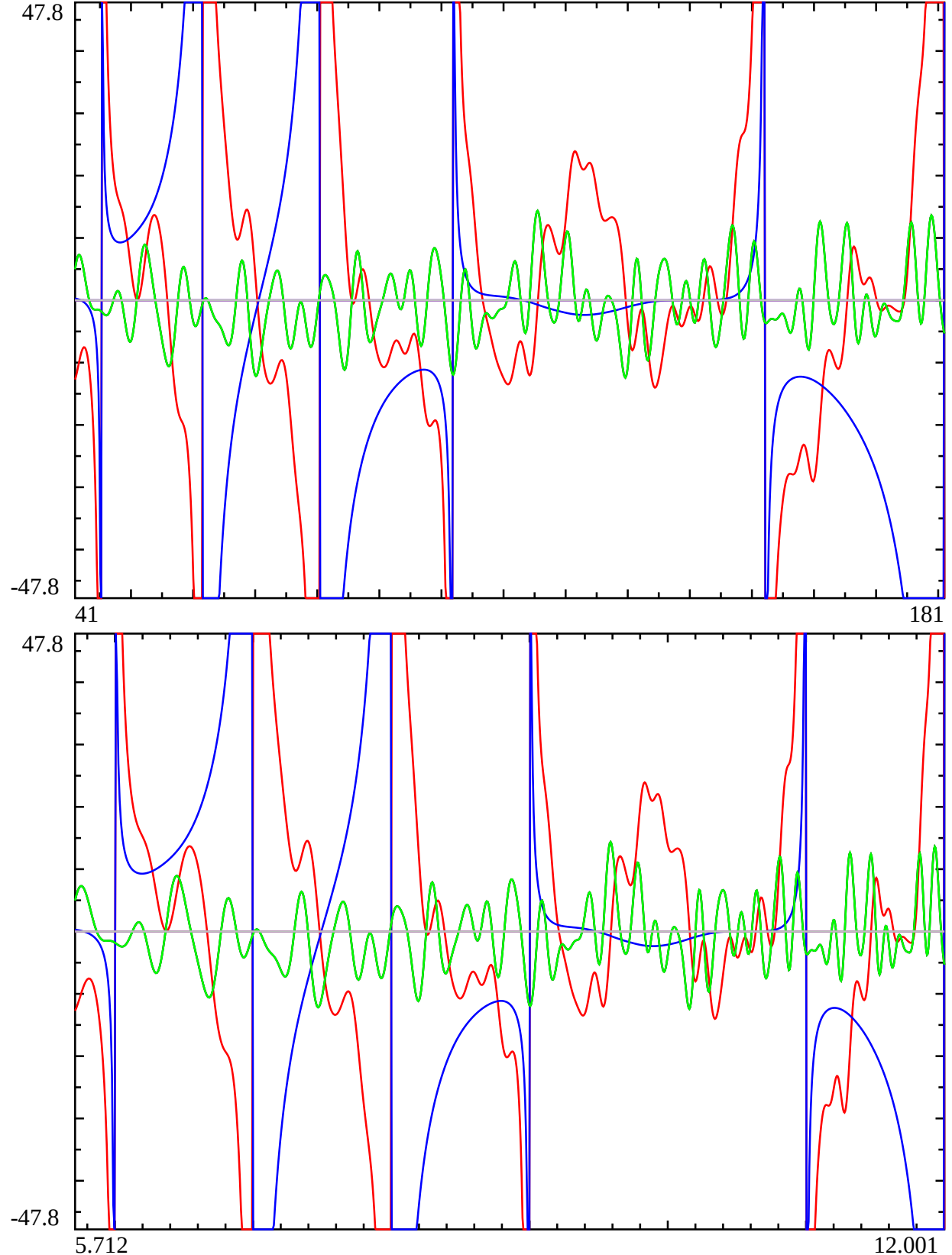


Figure 22: The behaviour of a heuristic approximation of the indefinite integral of the Riemann Siegel Z function for DHf2 **imag part in red, real part in blue**, its numerical derivative (approximating the Riemann Siegel Z function itself) real (imag) part shown in black (violet-red) based on **128 point end tapered** finite DHf2 Dirichlet Series sum (truncated at the second quiescent region) and the true DHf2 function (real (imag) part shown in green (gray)) along the critical line $s = 0.5 + I * t$ in the interval $t = (41, 181)$. The black, and violet-red lines of the real (imag) parts of the numerical total derivative of equation (4) are overlayed by the green, gray lines respectively of the true L53 L-function. From $t > 40.212$ ($64 \cdot \frac{5}{6}$), **128 point end tapered** finite DHf2 Dirichlet Series sums provide an excellent approximation of the DHf2 function to many decimal places. First row displays the functions using regular t scale, while the second row displays the functions using $\sqrt{\frac{t-5}{2\pi}}$ scale. Thus 76 quasi-discontinuities in the indefinite integral at $\sqrt{\frac{t-5}{2\pi}} = \{6, 7, 8, 9, 11\}$ can be observed and the mesoscale structure across each piecewise domain has a 5-periodic behaviour. There is no discontinuity at $\sqrt{\frac{t-5}{2\pi}} = \{10, 15, 20, \dots\}$ which is a mesoscale reflection of the zero Dirichlet character value for $\text{Mod}(N, 5) = 0$ for DHf2. The **real(Riemann Siegel Z function approximation for DHf2)** zeroes are turning points at the co-ordinates of $\text{imag}(\text{indefinite integral})$. While the **real(indefinite integral)** has curvature with respect to t, the **real(total derivative $\frac{d}{ds}$)** (not $\frac{\partial}{\partial t}$) numerically computed along the critical line and coinciding with the **imag(Riemann Siegel Z function approximation for DHf2)** is zero!

Differences in the piecewise nature of the indefinite integral approximations equations (166), (167) and (168) for the $f_2(s)$ Riemann Siegel Z function on the critical line.

Similar to [13], Figure 23 presents the normalised magnitude of the heuristic approximations equations (166,167,168) of the indefinite integral of the Riemann Siegel Z function of $f_2(s)$ **imag part in red, real part in blue** based on the finite Riemann Zeta Dirichlet Series sum truncated at the tapered second (lefthand column equation (166)), tapered first (middle column equation (167)) and first (righthand column equation (168)) quiescent regions along the critical line $s = 0.5 + I * t$ in various intervals $t = (46, 181)$, $t = (5148, 16758)$, $t = (50266, 53327)$, $t = (1256637, 12717168)$ and $t = (125663706, 125814548)$. The x axis is standardised by the transformation $\sqrt{\frac{t}{2\pi} \cdot 5}$. Importantly, very similar to [13] figure 23 shows that the y axis can be normalised to compare the heuristic approximation calculated values of the indefinite integral Riemann Siegel Z function for vastly different t values using a scaling factor of $(\frac{t}{2\pi} \cdot 5)^{0.25}$.

With respect to the piecewise nature of the indefinite integral approximations equations (166), (167) and (168) for the $f_2(s)$ Riemann Siegel Z function on the critical line, the normalised y scale shows that

1. there is little evolution of the real(equation(166)) shown in blue (lefthand column) with smooth hyperbolic lineshapes on each $[N, N+1]$ interval while the real(equations(167,168)) remain zero (on the critical line) as t increases. In comparison to real(equation(60)), real(equation(108)) in figures 5 and 11 from indefinite integrals approximations of $L(\chi_5(3, .), 1/2 + I \cdot t)$ and $L(\chi_5(2, .), 1/2 + I \cdot t)$ on the critical line for $N \bmod 5 = \{1, 3\}$ the real(equation(166)) remains asymmetric within the $[N, N+1]$ interval.
2. the evolution of the imag(equations(166,167,168)) shown in red can clearly be seen with the sharpening of mesoscale features that vary across the $[N, N+1]$ piecewise intervals. The imag(equation(167)) (middle column) behaviour is close to the imag(equation(166)) (lefthand column) behaviour but imag(equation(168)) (righthand column) clearly displays large differences at the righthand end of the $[N, N+1]$ piecewise intervals. (On careful examination there are also differences at the lefthand end of the $[N, N+1]$ piecewise intervals of the imag(equation(168)) (righthand column) behaviour compared to the other two indefinite integral approximations.)

In [13] the mesoscale features of the approximate indefinite integrals of the Riemann Siegel Z function of the ζ function on the critical line changed sign every piecewise interval $[N, N+1]$. For $f_2(s)$ the rate of sign change is observed to occur every tenth piecewise interval.

Figure 24 attempts to juxtapose (i) the mesoscale features of imag(equation(167)) for $N=\{10000-10004\}$ top row, (ii) the mesoscale features of imag(equation(167)) for $N=\{3000-3004\}$ second row, (iii) the $N \bmod 5$ behaviour of the extreme peaks for $N=\{0-3000\}$ under $\sqrt{\frac{t}{2\pi} \cdot 5} - \left\lfloor \sqrt{\frac{t}{2\pi} \cdot 5} \right\rfloor$ transformation middle row, (ii) the mesoscale features of imag(equation(167)) for $N=\{3005-3009\}$ second row and (ii) the mesoscale features of imag(equation(167)) for $N=\{10005-10009\}$ bottom row. Such a vertical juxtaposition helps clearly display the $N \bmod 10$ change in sign of the mesoscale features of the approximate indefinite integral of $f_2(s)$ Riemann Siegel Z function on the critical line. The vertical juxtaposition also indicates that the higher density in the relative position of the extreme peaks in the $f_2(s)$ Riemann Siegel Z function on the critical line (middle row) align well with regions of higher curvature in the approximate indefinite integral of $f_2(s)$ Riemann Siegel Z function on the critical line that occur with $N \bmod 5$ periodicity.

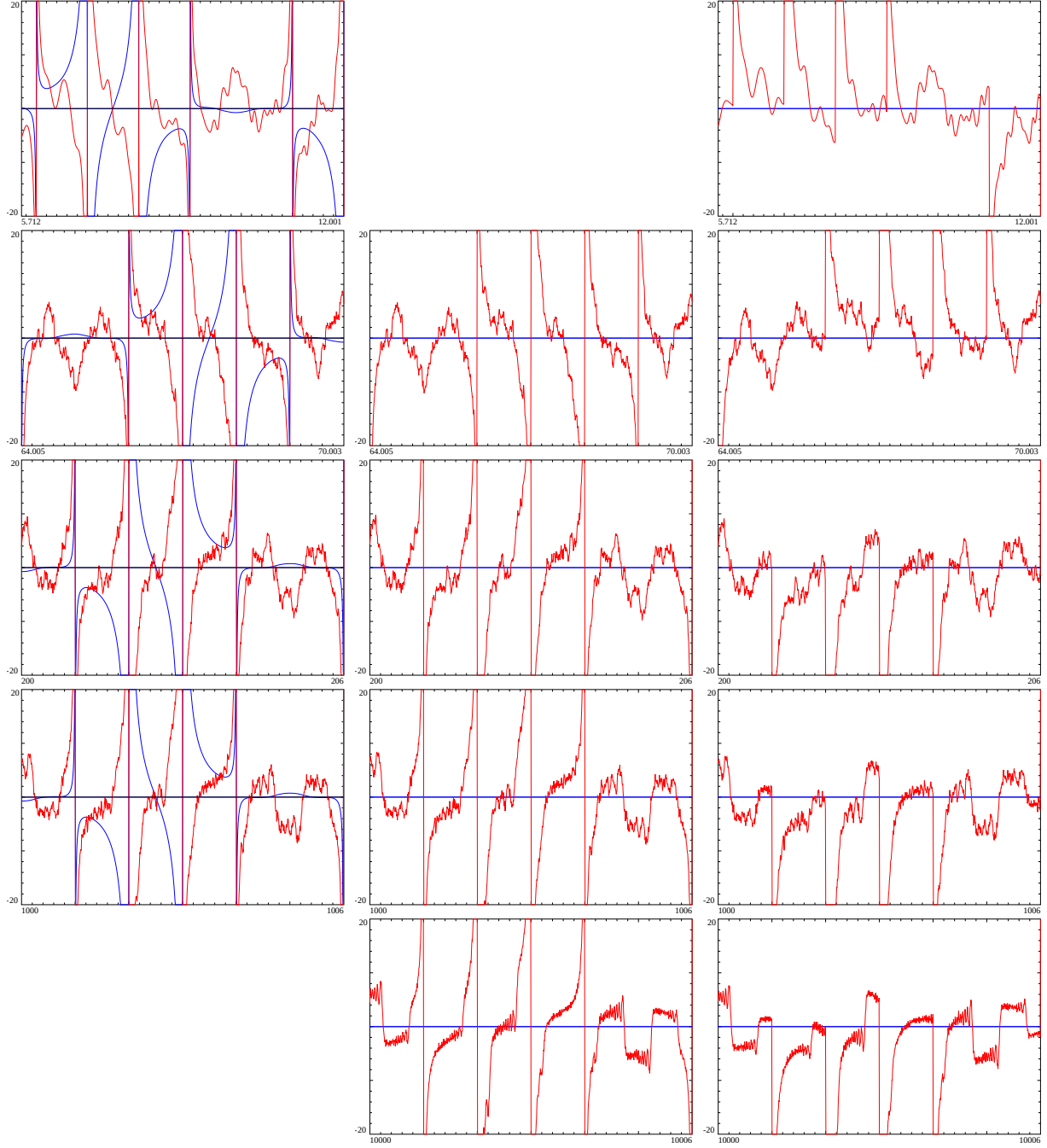


Figure 23: The normalised magnitude of the heuristic approximations equations (166,167,168) (using $\left(\frac{t-5}{2\pi}\right)^{0.25}$ scaling) of the indefinite integral of the Riemann Siegel Z function of DHf2 **imag part in red, real part in blue** based on the finite DHf2 Dirichlet Series sum truncated at the tapered second (lefthand column), tapered first (middle column) and first (righthand) quiescent region along the critical line $s = 0.5 + I * t$ in various intervals $t = (46, 181)$ top row, $t = (5148, 6158)$ second row, $t = (50266, 53327)$ third row, $t = (1256637, 1271762)$ fourth row and $t = (125663706, 125814548)$ bottom row where the horizontal axis uses a $\sqrt{\left(\frac{t-5}{2\pi}\right)}$ transformed scale. Mesoscale features are observed to evolve as t increases for the three approximations. The real component equation (4) shown in blue (i) has a minimum absolute magnitude that depends on $\text{Mod}(N,5)$ and (ii) $\text{Mod}(N,10)$ behaviour for the sign of the mesoscale features but (iii) the magnitude scales as $\left(\frac{t-5}{2\pi}\right)^{0.25}$. The gaps in the grid of graphs occur where an approximation is infeasible (below the tapering limit) or calculationally much slower to obtain.

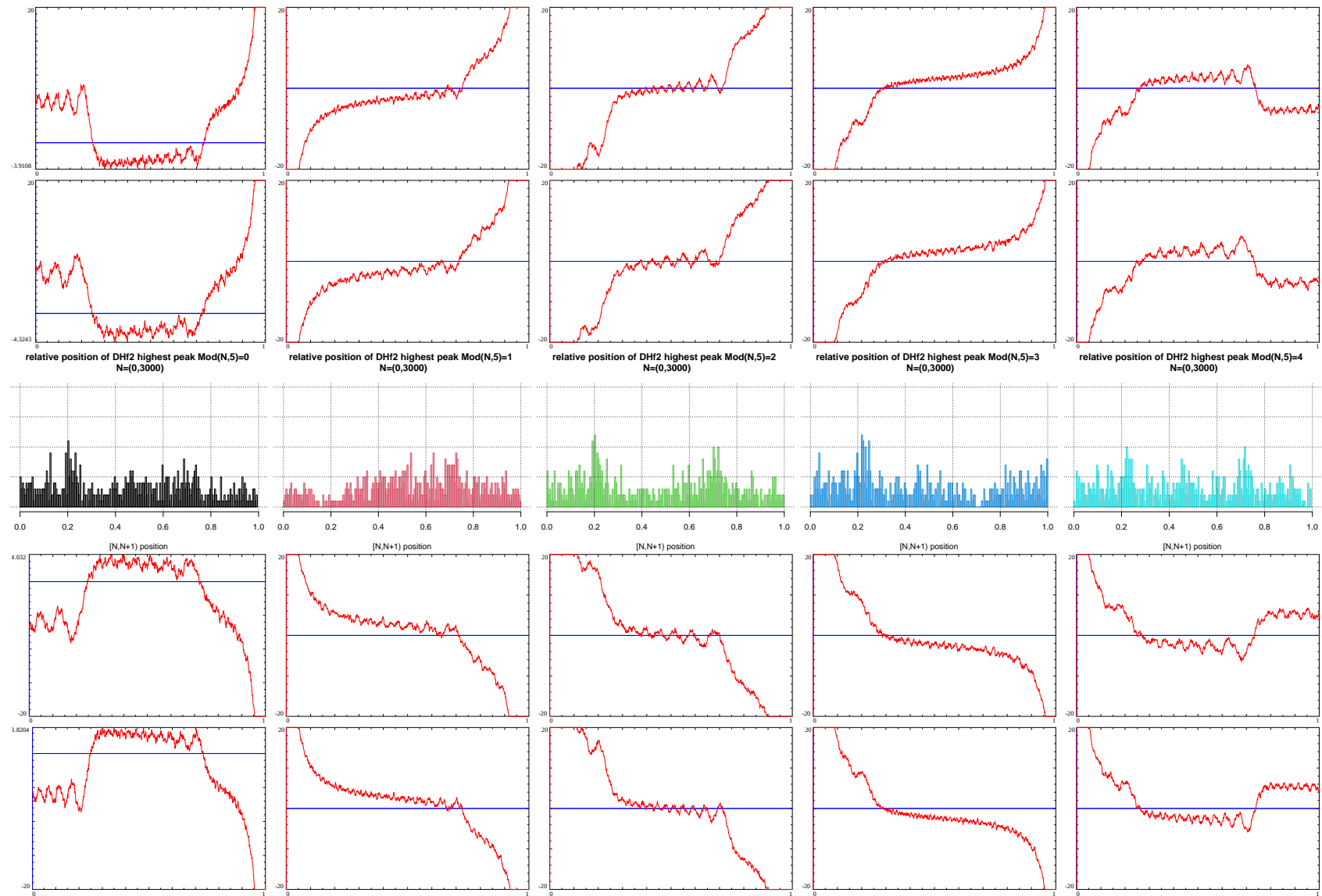


Figure 24: A vertical comparison of the distribution of the highest peaks (absolute magnitude) in $[N, N + 1]$ intervals on the critical line $s = 1/2 + I \cdot t$ where $N = \{0,..,3000\}$ for DHf2 and $t = N^2 \cdot \frac{2\pi}{5}$ segmented by $N \bmod 5 = \{0, 1, 2, 3, 4\}$ (middle row) with the mesoscale structure features clearly visible at higher t in a heuristic approximation of the imaginary component of the indefinite integral of the Riemann Siegel Z function of DHf2 along the critical line arranged in order by the intervals $[N, N + 1] \bmod 10$ where $N =$ (i) top row - $\{10000, 10001, 10002, 10003, 10004\}$, (ii) second row - $\{3000, 3001, 3002, 3003, 3004\}$, (iii) fourth row - $\{3005, 3006, 3007, 3008, 3009\}$ and (iv) bottom row - $\{10005, 10006, 10007, 10008, 10009\}$

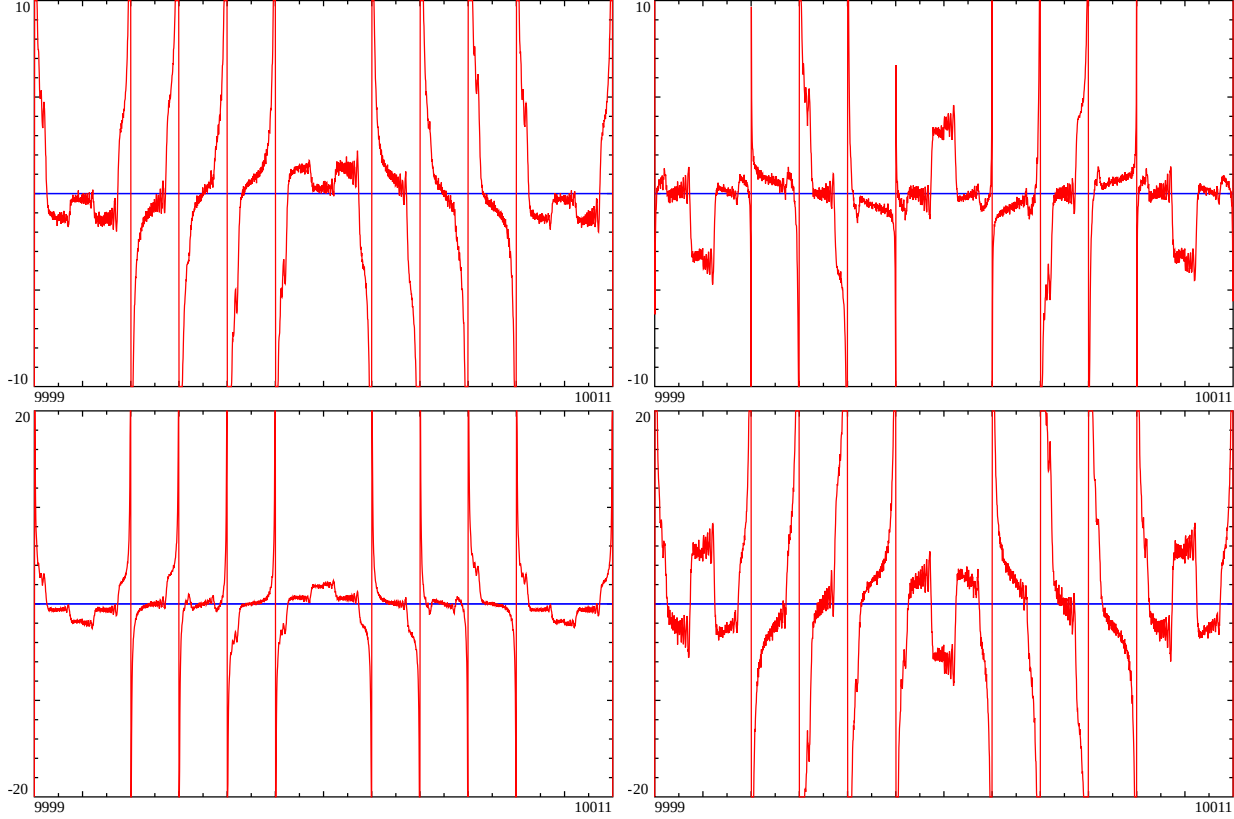


Figure 25: Universal scaling comparison of the 10-periodic behaviour of a tapered Dirichlet Series approximation of the imaginary part of indefinite integral of different 5-periodic L-functions. In the top row, L52 (lefthand panel, equation (109)), L53 (righthand panel, equation (61)), in the bottom row DHf1 (lefthand panel, equation (138)), and DHf2 (righthand panel, equation (167)). The y axis magnitude in the bottom row is twice as large as the top row scale. Given the contributing L-functions are of first degree with conductor value 5, their first quiescent region is at $N_1 = \sqrt{\left(\frac{t}{2\pi}\right)^1 \cdot 5} = \sqrt{\left(\frac{t}{2\pi}\right)^d \cdot N_C}$, the x axis is scaled by $\sqrt{\left(\frac{t-5}{2\pi}\right)}$ to produce uniform spaced intervals and the growth for all four 5-periodic functions is empirically found to be reasonably scaled by $\left(\frac{t-5}{2\pi}\right)^{0.25}$.

A comparison of the $N \bmod 10$ behaviour across the four 5-periodic function on the critical line $s = 1/2 + I \cdot t$

Figure 25 illustrates the $N \bmod 10$ behaviour of the imaginary part of the four 5-periodic functions on the critical line across the imaginary axis interval $t = (125638574, 125940319)$ corresponding to $N = \{9999 - 10009\}$, i.e. $N \bmod 10 = \{9, 0, 1, 2, 3, 4, 5, 6, 7, 8, 9, 0\}$. In the lefthand column are **approximations** equations (109) and (138) in the top (bottom) row for $\text{imag} \left(\frac{e^{-\frac{1}{2} \log \chi(f_1(s))}}{\sqrt{\epsilon}} L(\chi_5(2, .), s) ds \right)_{s=1/2+I \cdot t}$ and $\text{imag} \left(e^{-\frac{1}{2} \log \chi(f_1(s))} f_1(s) ds \right)_{s=1/2+I \cdot t}$ respectively. In the righthand column are **approximations** equations (61) and (167) in the top (bottom) row for $\text{imag} \left(\frac{e^{-\frac{1}{2} \log \chi(f_1(s))}}{\sqrt{\epsilon}} L(\chi_5(2, .), s) ds \right)_{s=1/2+I \cdot t}$ and $\text{imag} \left(e^{-\frac{1}{2} \log \chi(f_2(s))} f_2(s) ds \right)_{s=1/2+I \cdot t}$. It can be seen that the mesoscale features (which sharpen as $t \rightarrow \infty$) of these four functions for the investigated intervals on the critical line have a periodicity of $N \bmod 10$.

Conclusion

On the critical line, a higher density of the extreme Riemann Siegel Z function peaks from each scaled $[N, N+1]$ interval of the two 5-periodic 1st degree Dirichlet L-functions $L(\chi_5(3, .), s)$, $L(\chi_5(2, .), s)$ and their Davenport-Heilbronn function counterparts $f_1(s)$ and $f_2(s)$ is observed to occur when analysed by a $\sqrt{\frac{t \cdot 5}{2\pi}} - \left\lfloor \sqrt{\frac{t \cdot 5}{2\pi}} \right\rfloor$ transformation of the t co-ordinate split into $N \bmod 5$ groups where $N = \left\lfloor \sqrt{\frac{t \cdot 5}{2\pi}} \right\rfloor$.

A heuristic approximation of the indefinite integral of the Riemann Siegel Z function analogues for the four 5-periodic functions (currently only valid on the critical line) exhibits interesting piecewise interval mesoscale features that may help explain this observed higher density of the extreme Riemann Siegel Z function peaks under $\sqrt{\frac{t \cdot 5}{2\pi}} - \left\lfloor \sqrt{\frac{t \cdot 5}{2\pi}} \right\rfloor$ transformation of the t co-ordinate.

The growth rate of these heuristic approximations of the indefinite integral of the Riemann Siegel Z function analogues for the four 5-periodic functions scales as $(\frac{t}{2\pi} \cdot 5)^{0.25}$ on the critical line, which is similar but slightly different from the analogous heuristic approximation behaviour of the indefinite integral of the Riemann Siegel Z function of $\zeta(0.5 + I \cdot t)$ which empirically has a growth rate of $(\frac{t}{2\pi})^{0.25}$. The factor 5 above arises from $N_C = 5$ for $L(\chi_5(3, .), s)$ and $L(\chi_5(2, .), s)$.

References

1. The LMFDB Collaboration, The L-functions and Modular Forms Database, <http://www.lmfdb.org>, 2019, [Online; accessed January 2020].
2. Spira, R. Mathematics of Computation, Volume 63, Number 208, October 1994, Pages 747-748
3. Balanzario, E.P. and Sanchez-Ortiz, J. Mathematics of Computation, Volume 76, Number 260, October 2007, Pages 2045–2049
4. E. Bombieri, A. Ghosh, “Around the Davenport–Heilbronn function”, Uspekhi Mat. Nauk, 66:2(398) (2011), 15–66; Russian Math. Surveys, 66:2 (2011), 221–270 <https://doi.org/10.4213/rm9410> IAS lecture https://www.youtube.com/watch?v=-JUHypc2_9A
5. The PARI~Group, PARI/GP version 2.12.0, Univ. Bordeaux, 2018, <http://pari.math.u-bordeaux.fr/>.
6. Edwards, H.M. (1974). Riemann’s zeta function. Pure and Applied Mathematics 58. New York-London: Academic Press. ISBN 0-12-232750-0. Zbl 0315.10035.
7. Berry, M. V. “The Riemann-Siegel Expansion for the Zeta Function: High Orders and Remainders.” Proc. Roy. Soc. London A 450, 439-462, 1995.
8. J. Arias De Reyna, “High precision computation of Riemann’s Zeta function by the Riemann-Siegel formula”, Mathematics of Computation Vol 80, no. 274, 2011, Pages 995–1009
9. Martin, J.P.D. “Examples of spectrally filtered first quiescent region truncated partial Euler Product based approximations of Riemann Siegel Z functions for different L-functions and the two Davenport-Heilbronn 5-periodic functions on the critical line away from the real axis.” (2025) figshare. Preprint. <https://doi.org/10.6084/m9.figshare.29577545.v2>
10. R Core Team (2017). R: A language and environment for statistical computing. R Foundation for Statistical Computing, Vienna, Austria. <https://www.R-project.org/>.
11. Martin, J.P.D. “Examples of quiescent regions in the oscillatory divergence of several 1st degree L functions and their Davenport Heilbronn counterparts.” (2021) <https://dx.doi.org/10.6084/m9.figshare.14956053>
12. RStudio Team (2015). RStudio: Integrated Development for R. RStudio, Inc., Boston, MA <http://www.rstudio.com/>.
13. Martin, J.P.D. “Evidence of a sharp multi-modal distribution in the relative position of the highest Riemann Zeta peaks along the critical line in the piecewise intervals $[N^2 \cdot 2\pi, (N+1)^2 \cdot 2\pi]$, $N \in \mathbb{Z}$ and a possible explanation using a heuristic approximation on the critical line of the indefinite integral of the Riemann Siegel Z function.” (2025) <https://dx.doi.org/10.6084/m9.figshare.30740681>
14. <https://mathworld.wolfram.com/LogGammaFunction.html>
15. Boros, G. and Moll, V. “The Expansion of the Loggamma Function.” §10.6 in Irresistible Integrals: Symbolics, Analysis and Experiments in the Evaluation of Integrals. Cambridge, England: Cambridge University Press, pp. 201-203, 2004.

Appendix A: Revisiting the heuristic approximation for the indefinite integrals of the Riemann Siegel Z function analogue of tapered and untapered finite $\zeta(s)$ Dirichlet Series truncated at the second and first quiescent regions

Restating the three critical line heurisitic approximations of the indefinite integral of the Riemann Siegel Z function of $\zeta(s)$ reported in [13]

(i) tapered truncation at the second quiescent region for $\zeta(s)$ Dirichlet Series $\lfloor \frac{t}{\pi} \rfloor$

$$\begin{aligned} & \left(\int e^{-\frac{1}{2} \log \chi(\zeta(s))} \zeta(s) ds \right)_{s=1/2+I \cdot t, \lfloor \frac{t}{\pi} \rfloor, \text{tapered}} \\ & \approx e^{I \cdot \theta_\zeta(t)} \cdot \left[\sum_{n=1}^{\lfloor \frac{t}{\pi} \rfloor - p} \left(\frac{1}{\left[\Re \left(\frac{d}{ds} \left[-\frac{1}{2} \log \{\chi(\zeta(s))\} \right]_{s=(1/2+I \cdot t)} \right) - \log(n) \right] \cdot n^{(1/2+I \cdot t)}} \right) \right. \\ & + \left. \sum_{i=(-p+1)}^p \frac{\frac{1}{2^{2p}} \left(2^{2p} - \sum_{k=1}^{i+p} \binom{2p}{2p-k} \right)}{\left[\left[\Re \left(\frac{d}{ds} \left[-\frac{1}{2} \log \{\chi(\zeta(s))\} \right]_{s=(1/2+I \cdot t)} \right) - \log(\lfloor \frac{t}{\pi} \rfloor + i) \right] \cdot (\lfloor \frac{t}{\pi} \rfloor + i)^{(1/2+I \cdot t)}} \right], t \rightarrow \infty \end{aligned} \quad (214)$$

(ii) tapered truncation at the first quiescent region $N_2 = \left\lfloor \sqrt{\frac{t}{2\pi}} \right\rfloor$ for $\zeta(s)$ Dirichlet Series

$$\begin{aligned} & \left(\int e^{-\frac{1}{2} \log \chi(\zeta(s))} \zeta(s) ds \right)_{s=1/2+I \cdot t, \lfloor \sqrt{\frac{t}{2\pi}} \rfloor, \text{tapered}} \\ & \approx e^{I \cdot \theta_\zeta(t)} \cdot \left[\sum_{n=1}^{\lfloor \sqrt{\frac{t}{2\pi}} \rfloor - p} \left(\frac{1}{\left[\Re \left(\frac{d}{ds} \left[-\frac{1}{2} \log \{\chi(\zeta(s))\} \right]_{s=(1/2+I \cdot t)} \right) - \log(n) \right] \cdot n^{(1/2+I \cdot t)}} \right) \right. \\ & + \left. \sum_{i=(-p+1)}^p \frac{\frac{1}{2^{2p}} \left(2^{2p} - \sum_{k=1}^{i+p} \binom{2p}{2p-k} \right)}{\left[\left[\Re \left(\frac{d}{ds} \left[-\frac{1}{2} \log \{\chi(\zeta(s))\} \right]_{s=(1/2+I \cdot t)} \right) - \log(\lfloor \sqrt{\frac{t}{2\pi}} \rfloor + i) \right] \cdot (\lfloor \sqrt{\frac{t}{2\pi}} \rfloor + i)^{(1/2+I \cdot t)}} \right. \\ & + \left. \chi_{\zeta(s)}(1/2 + I \cdot t) \cdot \left(\sum_{n=1}^{\lfloor \sqrt{\frac{t}{2\pi}} \rfloor - p} \left(\frac{1}{\left[-\Re \left(\frac{d}{ds} \left[-\frac{1}{2} \log \{\chi(\zeta(s))\} \right]_{s=(1/2+I \cdot t)} \right) + \log(n) \right] \cdot n^{(1-(1/2+I \cdot t))}} \right) \right. \right. \\ & + \left. \left. \sum_{i=(-p+1)}^p \frac{\frac{1}{2^{2p}} \left(2^{2p} - \sum_{k=1}^{i+p} \binom{2p}{2p-k} \right)}{\left[-\Re \left(\frac{d}{ds} \left[-\frac{1}{2} \log \{\chi(\zeta(s))\} \right]_{s=(1/2+I \cdot t)} \right) + \log(\lfloor \sqrt{\frac{t}{2\pi}} \rfloor + i) \right] \cdot (\lfloor \sqrt{\frac{t}{2\pi}} \rfloor + i)^{(1-(1/2+I \cdot t))}} \right), t \rightarrow \infty \right. \end{aligned} \quad (215)$$

(ii) truncation at the first quiescent region $N_1 = \left\lfloor \sqrt{\frac{t}{2\pi}} \right\rfloor$ for $\zeta(s)$ Dirichlet Series

$$\begin{aligned}
& \left(\int e^{-\frac{1}{2} \log \chi(\zeta(s))} \zeta(s) ds \right)_{s=1/2+I \cdot t, \left| \sqrt{\frac{t}{2\pi}} \right|, \text{tapered}} \\
& \approx e^{I \cdot \theta_\zeta(t)} \cdot \left[\sum_{n=1}^{\left(\lfloor \sqrt{\frac{t}{2\pi}} \rfloor \right)} \left(\frac{1}{\left[\Re \left(\frac{d}{ds} \left[-\frac{1}{2} \log \{\chi(\zeta(s))\} \right]_{s=(1/2+I \cdot t)} \right] - \log(n) \right] \cdot n^{(1/2+I \cdot t)}} \right) \right. \\
& + \chi_\zeta(1/2 + I \cdot t) \cdot \left. \left(\sum_{n=1}^{\left(\lfloor \sqrt{\frac{t}{2\pi}} \rfloor \right)} \left(\frac{1}{\left[-\Re \left(\frac{d}{ds} \left[-\frac{1}{2} \log \{\chi(\zeta(s))\} \right]_{s=(1/2+I \cdot t)} \right] + \log(n) \right] \cdot n^{(1-(1/2+I \cdot t))}} \right) \right), t \rightarrow \infty \right. \tag{216}
\end{aligned}$$

and restating in general the Riemann Zeta functional equation

$$\zeta(s) = \chi(\zeta(s)) \cdot \zeta(1-s) \tag{217}$$

$$= e^{-\frac{1}{2} \cdot \log \chi(\zeta(s))} \cdot \zeta(1-s) \tag{218}$$

$$= \pi^{\left(\frac{(1-2s)}{2} \right)} \cdot \frac{\Gamma \left[\frac{(1-s)}{2} \right]}{\Gamma \left[\frac{(s)}{2} \right]} \cdot \zeta(1-s) \tag{219}$$

and in particular the Riemann Zeta functional equation, on the critical line

$$\zeta(1/2 + I \cdot t) = \chi(\zeta(1/2 + I \cdot t)) \cdot \zeta(1/2 - I \cdot t) \tag{220}$$

$$= e^{-I \cdot 2\theta_\zeta(t)} \cdot \zeta(1/2 - I \cdot t) \tag{221}$$

it can be seen that

1. $\Re \left(\frac{d}{ds} \left[-\frac{1}{2} \log \{\chi(\zeta(s))\} \right]_{s=(1/2+I \cdot t)} \right) \equiv \frac{\partial}{\partial t} [\theta_\zeta(t)]$ on the critical line and
2. the nomenclature $e^{-\frac{1}{2} \log \chi(\zeta(s))}$ (a complex valued function across the complex function) is used to avoid confusion with $e^{I \cdot \theta_\zeta(t)}$ where $\theta_\zeta(t)$ is the real valued Riemann Siegel Theta function ($\theta_\zeta(t) = -\frac{1}{2} \cdot \text{imag} [\log (\chi(\zeta(1/2 + I \cdot t)))]$) which applies only to the critical line.

As mentioned in [13], a crucial part of the above indefinite integral approximation prescription was explicitly using only $\Re \left(\frac{d}{ds} \left[-\frac{1}{2} \log \{\chi(\zeta(s))\} \right] \right)$ and [13] presented **numerical** evidence of the above approximation's first total derivative estimation that closely estimated the true Riemann Siegel Z function of $\zeta(s)$ behaviour for the intervals that were examined.

Following the derivation presented earlier in this paper for 5-periodic function with functional equations, the next section illustrates an **analytic** argument why equations (214), (215) and (216) are expected to produce total derivative estimates that will be useful approximations of the true Riemann Siegel Z function of $\zeta(s)$ behaviour away from the real axis on the critical line.

Total derivative behaviour of individual terms of equations (214), (215) and (216) on the critical line

To be useful heuristic approximations of the indefinite integral of the Riemann Siegel Z function for the Riemann Zeta function $\zeta(s)$ the total derivatives $\frac{d}{ds}$ (*equations(214), (215)and(216)*) must result in useful approximations of the $\zeta(s)$ Riemann Siegel Z function and ideally be equivalent respectively to

$$\left[e^{-\frac{1}{2} \log \chi(\zeta(s))} \zeta(s) \right]_{s=1/2+I \cdot t, \lfloor \frac{t}{\pi} \rfloor, \text{tapered}} \approx e^{I \cdot \theta_\zeta(t)} \cdot \left[\sum_{n=1}^{\lfloor \frac{t}{\pi} \rfloor - p} \left(\frac{1}{n^{(1/2+I \cdot t)}} \right) + \sum_{i=(-p+1)}^p \frac{\frac{1}{2^{2p}} \left(2^{2p} - \sum_{k=1}^{i+p} \binom{2p}{2p-k} \right)}{((\lfloor \frac{t}{\pi} \rfloor + i)^{(1/2+I \cdot t)})} \right], t \rightarrow \infty \quad (222)$$

$$\begin{aligned} & \left[e^{-\frac{1}{2} \log \chi(\zeta(s))} \zeta(s) \right]_{s=1/2+I \cdot t, \lfloor \sqrt{\frac{t}{2\pi}} \rfloor, \text{tapered}} \\ & \approx e^{I \cdot \theta_\zeta(t)} \cdot \left[\sum_{n=1}^{\lfloor \sqrt{\frac{t}{2\pi}} \rfloor - p} \left(\frac{1}{n^{(1/2+I \cdot t)}} \right) + \sum_{i=(-p+1)}^p \frac{\frac{1}{2^{2p}} \left(2^{2p} - \sum_{k=1}^{i+p} \binom{2p}{2p-k} \right)}{((\lfloor \sqrt{\frac{t}{2\pi}} \rfloor + i)^{(1/2+I \cdot t)})} \right. \\ & \quad \left. + \chi_{\zeta(s)}(1/2 + I \cdot t) \cdot \left(\sum_{n=1}^{\lfloor \sqrt{\frac{t}{2\pi}} \rfloor - p} \left(\frac{1}{n^{(1-(1/2+I \cdot t))}} \right) + \sum_{i=(-p+1)}^p \frac{\frac{1}{2^{2p}} \left(2^{2p} - \sum_{k=1}^{i+p} \binom{2p}{2p-k} \right)}{((\lfloor \sqrt{\frac{t}{2\pi}} \rfloor + i)^{(1-(1/2+I \cdot t))})} \right) \right], t \rightarrow \infty \end{aligned} \quad (223)$$

$$\begin{aligned} & \left[e^{-\frac{1}{2} \log \chi(\zeta(s))} \zeta(s) \right]_{s=1/2+I \cdot t, \lfloor \sqrt{\frac{t}{2\pi}} \rfloor, \text{tapered}} \\ & \approx e^{I \cdot \theta_\zeta(t)} \cdot \left[\sum_{n=1}^{\lfloor \sqrt{\frac{t}{2\pi}} \rfloor} \left(\frac{1}{n^{(1/2+I \cdot t)}} \right) + \chi_{\zeta(s)}(1/2 + I \cdot t) \cdot \left(\sum_{n=1}^{\lfloor \sqrt{\frac{t}{2\pi}} \rfloor} \left(\frac{1}{n^{(1-(1/2+I \cdot t))}} \right) \right) \right], t \rightarrow \infty \end{aligned} \quad (224)$$

In the following discussion, it is demonstrated that there is a term by term agreement **on the critical line** between $\frac{d}{ds}$ (*equations(214), (215)and(216)*) and Riemann Siegel Z function approximations (222), (223) and (224).

Firstly a single term of the dirichlet terms of equations (214) and half of the terms of (215) and (216) can be presented in the generic form

$$e^{I \cdot \theta_\zeta(t)} \cdot \left(\frac{1}{\left[\Re \left(\frac{d}{ds} \left[-\frac{1}{2} \log \{\chi(\zeta(s))\} \right]_{s=(1/2+I \cdot t)} \right) - \log(n) \right] \cdot n^{(1/2+I \cdot t)}} \right) \cdot w(n) \quad (225)$$

and the other half of the terms of (215) and (216) can be presented in the second generic form

$$e^{-I \cdot \theta_\zeta(t)} \cdot \left(\frac{1}{\left[-\Re \left(\frac{d}{ds} \left[-\frac{1}{2} \log \{\chi(\zeta(s))\} \right]_{s=(1/2+I \cdot t)} \right) + \log(n) \right] \cdot n^{(1-(1/2+I \cdot t))}} \right) \cdot w(n) \quad (226)$$

where (i) $w(n)$ describes that each term provides a weighted contribution $w(n) \leq 1$, in particular the $w(n)=1$ below where tapering of the endpoints occurs and $w(n)=0$ above the tapered endpoints and (ii) the second generic form arises from equation (221)

$$e^{I \cdot \theta_\zeta(t)} \cdot \chi(\zeta(1/2 + I \cdot t)) = e^{I \cdot \theta_\zeta(t)} \cdot e^{-I \cdot 2 \cdot \theta_\zeta(t)} = e^{-I \cdot \theta_\zeta(t)} \iff s = 1/2 + I \cdot t \quad (227)$$

In practice, while the overall length of non-zero weighted terms of the truncated Dirichlet series in equations (214), (215) and (216) is dependent on t being piecewise functions, the individual n , $w(n)$ and $\chi_{L52}(n)$ values are constants with respect to **infinitesimal changes** in t .

Hence, each single term of the dirichlet terms of equations (214), (215) and (216) can be re-written as either of two possible triple products

$$\left\{ \frac{1}{\left[\Re \left(\frac{d}{ds} \left[-\frac{1}{2} \log \{\chi(\zeta(s))\} \right] \right) - \log(n) \right]} \right\} \cdot \left\{ \frac{e^{I \cdot \theta_\zeta(t)}}{n^{(1/2+I \cdot t)}} \right\} \cdot \{w(n)\} \equiv A(s) \cdot B(s) \cdot C(n) \quad (228)$$

$$\left\{ \frac{1}{\left[-\Re \left(\frac{d}{ds} \left[-\frac{1}{2} \log \{\chi(\zeta(s))\} \right] \right) + \log(n) \right]} \right\} \cdot \left\{ \frac{e^{-I \cdot \theta_\zeta(t)}}{n^{(1-(1/2+I \cdot t))}} \right\} \cdot \{w(n)\} \equiv -A(s) \cdot D(s) \cdot C(n) \quad (229)$$

Using the chain rule, one obtains the generic form of the total derivative $\frac{d}{ds}$ for each dirichlet term of equations (214), (215) and (216)

$$\frac{d}{ds} [A(s) \cdot B(s) \cdot C(n)] = \left\{ \frac{dA(s)}{ds} \cdot B(s) + A(s) \cdot \frac{dB(s)}{ds} \right\} \cdot C(n) \quad (230)$$

or

$$\frac{d}{ds} [-A(s) \cdot D(s) \cdot C(n)] = - \left\{ \frac{dA(s)}{ds} \cdot D(s) + A(s) \cdot \frac{dD(s)}{ds} \right\} \cdot C(n) \quad (231)$$

Examining $\frac{dA(s)}{ds}$ explicitly

$$\frac{dA(s)}{ds} = \frac{d}{ds} \left\{ \frac{1}{\left[\Re \left(\frac{d}{ds} \left[-\frac{1}{2} \log \{\chi(\zeta(s))\} \right] \right) - \log(n) \right]} \right\} \quad (232)$$

$$= \frac{1}{\left[\Re \left(\frac{d}{ds} \left[-\frac{1}{2} \log \{\chi(\zeta(s))\} \right] \right) - \log(n) \right]^2} \cdot \frac{d}{ds} \Re \left(\frac{d}{ds} \left[-\frac{1}{2} \log \{\chi(\zeta(s))\} \right] \right) \quad (233)$$

Secondly, to make further progress it is simpler to (i) inspect the second total derivative of $\left[-\frac{1}{2} \log \{\chi(\zeta(s))\} \right]$ rather than $\Re \left(\frac{d}{ds} \left[-\frac{1}{2} \log \{\chi(\zeta(s))\} \right] \right)$ i.e. ignore the $\Re()$ operation for the moment in equation (233),

$$\frac{d}{ds} \left(\frac{d}{ds} \left[-\frac{1}{2} \log \{\chi(\zeta(s))\} \right] \right) \quad (234)$$

(ii) use the dual gamma function functional equation multiplicative factor representation equation (219)

$$\chi(\zeta(s)) \equiv \pi^{(\frac{(1-2s)}{2})} \cdot \frac{\Gamma\left[\frac{(1-s)}{2}\right]}{\Gamma\left[\frac{(s)}{2}\right]} \quad (235)$$

and (iii) use the $\log(\Gamma(s))$ identity [14,15] obtained from the Weierstrass product form of the $\Gamma(s)$ function

$$\log(\Gamma(s)) = -\gamma \cdot s - \log(s) + \sum_{k=1}^{\infty} \left[\frac{s}{k} - \log\left(1 + \frac{s}{k}\right) \right] \quad (236)$$

to obtain the following $-\frac{1}{2} \cdot \log(\chi(\zeta(s)))$ expansion

$$\begin{aligned} -\frac{1}{2} \cdot \log(\chi(f_1(s))) &= -\frac{1}{2} \left\{ \left(\frac{1}{2} - s \right) \cdot \log(\pi) \right. \\ &\quad - \gamma \cdot \left[\frac{(1-s)}{2} \right] - \log\left[\frac{(1-s)}{2} \right] + \sum_{k=1}^{\infty} \left[\frac{\left[\frac{(1-s)}{2} \right]}{k} - \log\left(1 + \frac{\left[\frac{(1-s)}{2} \right]}{k}\right) \right] \\ &\quad \left. - \left(-\gamma \cdot \left[\frac{(s)}{2} \right] - \log\left[\frac{(s)}{2} \right] + \sum_{k=1}^{\infty} \left[\frac{\left[\frac{(s)}{2} \right]}{k} - \log\left(1 + \frac{\left[\frac{(s)}{2} \right]}{k}\right) \right] \right) \right\} \end{aligned} \quad (237)$$

from which the following first total derivative is obtained

$$\begin{aligned} \frac{d}{ds} \left[-\frac{1}{2} \log\{\chi(f_1(s))\} \right] &= -\frac{1}{2} \left\{ -\log(\pi) \right. \\ &\quad + \frac{\gamma}{2} + \frac{1}{(1-s)} + \sum_{k=1}^{\infty} \left[-\frac{1}{2k} + \frac{1}{(2k+1-s)} \right] - \left(-\frac{\gamma}{2} - \frac{1}{(s)} + \sum_{k=1}^{\infty} \left[\frac{1}{2k} - \frac{1}{(2k+s)} \right] \right) \left. \right\} \\ &= -\frac{1}{2} \left\{ -\log(\pi) + \gamma + \frac{1}{(1-s)} + \frac{1}{(s)} + \sum_{k=1}^{\infty} \left[-\frac{1}{k} + \frac{1}{(2k+1-s)} + \frac{1}{(2k+s)} \right] \right\} \end{aligned} \quad (238)$$

and the second total derivative is then iteratively obtained from $\frac{d}{ds}$ [equation(239)]

$$\frac{d^2}{ds^2} \left[-\frac{1}{2} \log\{\chi(\zeta(s))\} \right] = -\frac{1}{2} \left\{ \frac{1}{(1-s)^2} - \frac{1}{(s)^2} + \sum_{k=1}^{\infty} \left[\frac{1}{(2k+1-s)^2} - \frac{1}{(2k+s)^2} \right] \right\} \quad (240)$$

Looking at the values of the first and second total derivative of $-\frac{1}{2} \log\{\chi(\zeta(s))\}$ on the critical line $s = 1/2 + I \cdot t$

$$\begin{aligned} \frac{d}{ds} \left[-\frac{1}{2} \log\{\chi(\zeta(s))\} \right]_{s=1/2+I \cdot t} &= -\frac{1}{2} \left\{ -\log(\pi) + \gamma + \frac{1}{(1/2 - I \cdot t)} + \frac{1}{(1/2 + I \cdot t)} \right. \\ &\quad \left. + \sum_{k=1}^{\infty} \left[-\frac{1}{k} + \frac{1}{(2k + 1/2 - I \cdot t)} + \frac{1}{(2k + 1/2 + I \cdot t)} \right] \right\} \end{aligned} \quad (241)$$

$$\begin{aligned} &= -\frac{1}{2} \left\{ -\log(\pi) + \gamma + \frac{1/2 + I \cdot t + (1/2 - I \cdot t)}{(1/2 - I \cdot t)(1/2 + I \cdot t)} \right. \\ &\quad \left. + \sum_{k=1}^{\infty} \left[-\frac{1}{k} + \frac{(2k + 1/2 + I \cdot t) + (2k + 1/2 - I \cdot t)}{(2k + 1/2 - I \cdot t)(2k + 1/2 + I \cdot t)} \right] \right\} \end{aligned} \quad (242)$$

$$\begin{aligned} &= -\frac{1}{2} \left\{ -\log(\pi) + \gamma + \frac{1}{(1/4 + t^2)} + \sum_{k=1}^{\infty} \left[-\frac{1}{k} - \frac{(4k + 1)}{[(2k + 1/2)^2 + t^2]} \right] \right\} \end{aligned} \quad (243)$$

$$\therefore \frac{d}{ds} \left[-\frac{1}{2} \log\{\chi(\zeta(s))\} \right]_{s=1/2+I \cdot t} \in \mathbb{R} \quad (244)$$

$$\begin{aligned} \frac{d^2}{ds^2} \left[-\frac{1}{2} \log\{\chi(\zeta(s))\} \right]_{s=1/2+I \cdot t} &= -\frac{1}{2} \left\{ \frac{1}{(1/2 - I \cdot t)^2} - \frac{1}{(1/2 + I \cdot t)^2} \right. \\ &\quad \left. + \sum_{k=1}^{\infty} \left[\frac{1}{(2k + 1/2 - I \cdot t)^2} - \frac{1}{(2k + 1/2 + I \cdot t)^2} \right] \right\} \end{aligned} \quad (245)$$

$$\begin{aligned} &= -\frac{1}{2} \left\{ \frac{(1/4 + I \cdot t + t^2) - (1/4 - I \cdot t + t^2)^2}{(1/2 - I \cdot t)^2 \cdot (1/2 + I \cdot t)^2} \right. \\ &\quad \left. + \sum_{k=1}^{\infty} \left[\frac{(2k + 1/2 + I \cdot t)^2 - (2k + 1/2 - I \cdot t)^2}{(2k + 1/2 - I \cdot t)^2 \cdot (2k + 1/2 + I \cdot t)^2} \right] \right\} \end{aligned} \quad (246)$$

$$= -\frac{1}{2} \left\{ \frac{I \cdot 2 \cdot t}{(1/4 + t^2)^2} + \sum_{k=1}^{\infty} \left[\frac{I \cdot (4k + 1) \cdot t}{[((2k + 1/2)^2 + t^2)^2]} \right] \right\} \quad (247)$$

$$\therefore \frac{d^2}{ds^2} \left[-\frac{1}{2} \log\{\chi(\zeta(s))\} \right]_{s=1/2+I \cdot t} \in \mathbb{C} - \mathbb{R} \quad \text{i.e., purely imaginary} \quad (248)$$

The relationship $* \left[-\frac{1}{2} \log\{\chi(\zeta(s))\} \right]_{s=1/2+I \cdot t} \in \text{pure imaginary}$, $* \frac{d}{ds} \left[-\frac{1}{2} \log\{\chi(\zeta(s))\} \right]_{s=1/2+I \cdot t} \in \mathbb{R}$, $* \frac{d^2}{ds^2} \left[-\frac{1}{2} \log\{\chi(\zeta(s))\} \right]_{s=1/2+I \cdot t} \in \text{pure imaginary}$ is a demonstration of a analytic complex function $(\left[-\frac{1}{2} \log\{\chi(\zeta(s))\} \right]_{s=1/2+I \cdot t})$ following the Cauchy Riemann conditions.

Since differentiation of a **real valued** function (e.g. $\frac{d}{ds} \left[\Re \left(\frac{d}{ds} \left[-\frac{1}{2} \log\{\chi(\zeta(s))\} \right] \right) \right]_{s=1/2+I \cdot t}$) must result in a **real valued** result but the wider complex valued function differentiation $\frac{d^2}{ds^2} \left[-\frac{1}{2} \log\{\chi(\zeta(s))\} \right]_{s=1/2+I \cdot t} \in \text{pure imaginary}$

$$\therefore \frac{d}{ds} \Re \left(\frac{d}{ds} \left[-\frac{1}{2} \log\{\chi(\zeta(s))\} \right] \right)_{s=1/2+I \cdot t} = 0 \quad \forall t \quad (249)$$

In particular, the mesoscale features are explicitly influenced by the which is backed by numerical confirmation for various examples of t . Which implies going back to equations (228), (229), (230) and (231) that the generic form of the total derivative $\frac{d}{ds}$ for each dirichlet term of equations (214), (215) and (216) when calculated for $s = 1/2 + I \cdot t$ reduces to

$$\frac{d}{ds} [A(s) \cdot B(s) \cdot C(n)]_{s=1/2+I \cdot t} \Rightarrow \left\{ \underbrace{\frac{dA(s)}{ds}}_{=0, s=1/2+I \cdot t} \cdot B(s) + A(s) \cdot \frac{dB(s)}{ds} \right\} \cdot C(n) \quad (250)$$

$$= A(s) \cdot \frac{dB(s)}{ds} \cdot C(n)_{s=1/2+I \cdot t} \quad (251)$$

$$\frac{d}{ds} [-A(s) \cdot D(s) \cdot C(n)]_{s=1/2+I \cdot t} \Rightarrow - \left\{ \underbrace{\frac{dA(s)}{ds}}_{=0, s=1/2+I \cdot t} \cdot D(s) + A(s) \cdot \frac{dD(s)}{ds} \right\} \cdot C(n) \quad (252)$$

$$= -A(s) \cdot \frac{dD(s)}{ds} \cdot C(n)_{s=1/2+I \cdot t} \quad (253)$$

However

$$A(s) \cdot \frac{dB(s)}{ds} \Big|_{s=1/2+I \cdot t} = \left[\frac{1}{\left[\Re \left(\frac{d}{ds} \left[-\frac{1}{2} \log\{\chi(\zeta(s))\} \right] \right) - \log(n) \right]} \cdot \frac{d}{ds} \left\{ \frac{e^{I \cdot \theta_\zeta(t)}}{n^{(1/2+I \cdot t)}} \right\} \right]_{s=1/2+I \cdot t} \quad (254)$$

$$= \left[\frac{1}{\left[\Re \left(\frac{d}{ds} \left[-\frac{1}{2} \log\{\chi(\zeta(s))\} \right] \right) - \log(n) \right]} \cdot \frac{d}{ds} \left\{ e^{-\frac{1}{2} \log\{\chi(\zeta(s))\}} \cdot e^{-s \cdot \log(n)} \right\} \right]_{s=1/2+I \cdot t} \quad (255)$$

$$= \left[\underbrace{\frac{d}{ds} \left[-\frac{1}{2} \log\{\chi(\zeta(s))\} \right] - \log(n)}_{=1, s=1/2+I \cdot t} \cdot \left(e^{-\frac{1}{2} \log\{\chi(\zeta(s))\}} \cdot e^{-s \cdot \log(n)} \right) \right]_{s=1/2+I \cdot t} \quad (256)$$

$$= \frac{e^{I \cdot \theta_\zeta(t)}}{n^{(1/2+I \cdot t)}} \Big|_{s=1/2+I \cdot t} \quad (257)$$

$$-A(s) \cdot \frac{dD(s)}{ds} \Big|_{s=1/2+I \cdot t} = - \left[\frac{1}{\left[\Re \left(\frac{d}{ds} \left[-\frac{1}{2} \log \{\chi(\zeta(s))\} \right] \right) - \log(n) \right]} \cdot \frac{d}{ds} \left\{ \frac{e^{-I \cdot \theta_\zeta(t)}}{n^{(1-(1/2+I \cdot t))}} \right\} \right]_{s=1/2+I \cdot t} \quad (258)$$

$$= - \left[\frac{1}{\left[\Re \left(\frac{d}{ds} \left[-\frac{1}{2} \log \{\chi(\zeta(s))\} \right] \right) - \log(n) \right]} \cdot \frac{d}{ds} \left\{ e^{\frac{1}{2} \log \{\chi(\zeta(s))\}} \cdot e^{s \cdot \log(n)} \right\} \right]_{s=1/2+I \cdot t} \quad (259)$$

$$= - \left[\frac{\frac{d}{ds} \left[\frac{1}{2} \log \{\chi(\zeta(s))\} \right] + \log(n)}{\underbrace{\left[\Re \left(\frac{d}{ds} \left[-\frac{1}{2} \log \{\chi(\zeta(s))\} \right] \right) - \log(n) \right]}_{=-1, s=1/2+I \cdot t}} \cdot \left(e^{\frac{1}{2} \log \{\chi(\zeta(s))\}} \cdot e^{s \cdot \log(n)} \right) \right]_{s=1/2+I \cdot t} \quad (260)$$

$$= \frac{e^{-I \cdot \theta_\zeta(t)}}{n^{(1-(1/2+I \cdot t))}} \Big|_{s=1/2+I \cdot t} \quad (261)$$

Therefore

$$\begin{aligned} & \frac{d}{ds} \left[\left\{ \frac{1}{\left[\Re \left(\frac{d}{ds} \left[-\frac{1}{2} \log \{\chi(\zeta(s))\} \right] \right) - \log(n) \right]} \right\} \cdot \left\{ \frac{e^{I \cdot \theta_\zeta(t)}}{n^{(1/2+I \cdot t)}} \right\} \cdot \{w(n)\} \right]_{s=1/2+I \cdot t} \\ & \equiv \left[e^{I \cdot \theta_\zeta(t)} \cdot \frac{1}{n^{(1/2+I \cdot t)}} \cdot w(n) \right]_{s=1/2+I \cdot t} \end{aligned} \quad (262)$$

(263)

and

$$\begin{aligned} & \frac{d}{ds} \left[\left\{ \frac{1}{\left[-\Re \left(\frac{d}{ds} \left[\frac{1}{2} \log \{\chi(\zeta(s))\} \right] \right) + \log(n) \right]} \right\} \cdot \left\{ \frac{e^{-I \cdot \theta_\zeta(t)}}{n^{(1-(1/2+I \cdot t))}} \right\} \cdot \{w(n)\} \right]_{s=1/2+I \cdot t} \\ & \equiv \left[e^{-I \cdot \theta_\zeta(t)} \cdot \frac{1}{n^{(1-(1/2+I \cdot t))}} \cdot w(n) \right]_{s=1/2+I \cdot t} \end{aligned} \quad (264)$$

(265)

which together covers all the dirichlet terms of equations (222), (223) and (224) when $s = 1/2 + I \cdot t$

That is, **on the critical line**, the total derivative of equations (214), (215) and (216) produces a term by term agreement with the finite dirichlet series based approximations (222), (223) and (224) respectively for the Riemann Siegel Z function of $\zeta(s)$.

It was observed numerically in [13] that when $s = 0.6 + I \cdot t$, i.e. away from the critical line, the total derivatives of equations (214), (215) and (216) are not numerically equivalent to equations (222), (223) and (224).